COPPE
Instituto Alberto Luiz Coimbra de Pós-Graduação e Pesquisa de Engenharia
UFRJ

MODELING, CONTROL AND OPTIMIZATION OF THE ENANTIOMERIC SEPARATION OF PRAZIQUANTEL IN SIMULATED MOVING BED

Ataíde Souza Andrade Neto

Dissertação de Mestrado apresentada ao Programa de Pós-graduação em Engenharia Química, COPPE, da Universidade Federal do Rio de Janeiro, como parte dos requisitos necessários à obtenção do título de Mestre em Engenharia Química.

Orientadores: Argimiro Resende Secchi
Maurício Bezerra de Souza Júnior

Rio de Janeiro
Setembro de 2015

MODELING, CONTROL AND OPTIMIZATION OF THE ENANTIOMERIC SEPARATION OF PRAZIQUANTEL IN SIMULATED MOVING BED

Ataíde Souza Andrade Neto

DISSERTAÇÃO SUBMETIDA AO CORPO DOCENTE DO INSTITUTO ALBERTO LUIZ COIMBRA DE PÓS-GRADUAÇÃO E PESQUISA DE ENGENHARIA (COPPE) DA UNIVERSIDADE FEDERAL DO RIO DE JANEIRO COMO PARTE DOS REQUISITOS NECESSÁRIOS PARA A OBTENÇÃO DO GRAU DE MESTRE EM CIÊNCIAS EM ENGENHARIA QUÍMICA.

Examinada por:

_____
Prof. Argimiro Resende Secchi, D.Sc.

_____
Prof. Maurício Bezerra de Souza Júnior, D.Sc.

_____
Prof. Príamo Albuquerque Melo Júnior , D.Sc.

_____
Prof. Amaro Gomes Barreto Júnior, D.Sc.

RIO DE JANEIRO, RJ – BRASIL
SETEMBRO DE 2015

Andrade Neto, Ataíde Souza

Modeling, Control and Optimization of the Enantiomeric Separation of Praziquantel in Simulated Moving Bed/Ataíde Souza Andrade Neto. – Rio de Janeiro: UFRJ/COPPE, 2015.

XXI, 91 p.: il.; 29,7cm.

Orientadores: Argimiro Resende Secchi

Maurício Bezerra de Souza Júnior

Dissertação (mestrado) – UFRJ/COPPE/Programa de Engenharia Química, 2015.

Referências Bibliográficas: p. 70 – 75.

1. Controle preditivo. 2. Leito móvel simulado. 3. Enantioseparação. 4. Praziquantel. I. Secchi, Argimiro Resende *et al.* II. Universidade Federal do Rio de Janeiro, COPPE, Programa de Engenharia Química. III. Título.

It is not that easy following a carrier in academic research, even more in turbulent times as we now live. For me, it was not a choice, but a discovery, a decision engraved in stone with no doubt or regrets. Because it is not an easy journey, sometimes fear takes over, but in those moments you just hold on and take comfort in your friends. Because it is not an easy journey, sometimes motivation goes away, but in those moments you just hold on and look up to your heroes.

I dedicate this work to my professors, that also happen to be my friends and my heroes.

Acknowledgments

As matter of justice, I'm paying my moral debts! The road so far has been of constant learning and of many achievements. For every single one, I have to thank several friends and colleagues.

First of all, I thank my family for all the support and respect. Especially my mother, Vera, for comprehension and dedication; my aunt, Rita, for the attention and source of inspiration; my father, Robson, and my siblings, Júlio and Letícia, for the admiration and affection; and my nephew, Bernardo, for being — without even realizing — source of happiness, love and union.

For all the shared moments, I thank my master's colleagues. Especially the ones who endured the so called "maddening" first trimester together: Tahyná, Débora, Fellipe, Pedro, Rafael, Afrânio, Letícia, Carol, Leandro and Mayara.

To the friends at LADES/LADES2/LASAP: Thiago, Sílvio, Leo, Pedro Nin, Jessi, Maurílio, Simone, Evandro and Caio, for the fellowship and casualness discussions, I am grateful.

To all the friends at G130: Alessandra, Maurício, Cauê, Tiago and Maurício, for the warm reception, I am also grateful.

To Gobério and Guilherme to whom I owe and admire so much, thank you for the fraternity.

To all the old friends, especially Idia, Déborah, Bárbara, Ricardo and Marcos for the fondness.

Professors Evaristo, Fred and Príamo, I must thank you for the friendship, for every teaching and for being so inspiring.

Professor Pedro Leite, for every word of encouragement, for being responsible to my formation and for showing me the love for science, I can't stop to thank you.

Professor Maurício, for the attention, the teachings, discussions and above

all the confidence in my potential, I am very grateful.

At last, but certainly not least, I am immensely grateful to Professor Argimiro for the guidance and dedication. Thank you for all of our discussions, for your help and for your patience. I've been learning with you not just how to be a better scientist, but also how to be a better person. You are one of my true idols and role models!

To the FAPERJ, for the financial aid, I am also thankful.

"Reality is that which exists; the unreal does not exist; the unreal is merely that negation of existence which is the content of a human consciousness when it attempts to abandon reason. Truth is the recognition of reality; reason, man's only means of knowledge, is his only standard of truth.

The most depraved sentence you can now utter is to ask: Whose reason? The answer is: Yours. No matter how vast your knowledge or how modest, it is your own mind that has to acquire it. It is only with your own knowledge that you can deal. It is only your own knowledge that you can claim to possess or ask others to consider. Your mind is your only judge of truth and if others dissent from your verdict, reality is the court of final appeal. Nothing but a man's mind can perform that complex, delicate, crucial process of identification which is thinking. Nothing can direct the process but his own judgment. Nothing can direct his judgment but his moral integrity."

(John Galt, from Ayn Rand's *"Atlas Shrugged"*)

This is a severe criticism to the lack of discernment. It is a criticism to those who live in ignorance, not for lack of knowledge, but for lack of critical thinking; to those who don't want to reflect upon the events and information that are delivered to them, constantly, on a daily basis. It is mostly a criticism to anyone who put beliefs above facts; to whom propagate ideas, without reason, only for the "sake" of replication. Those who live this way, in the shadows of reality, in a non-representative fragment of reality, take on the false as true and the true as false, thereby denying the truth by sheer choice. It is due to the existence of those who choose this path that, in Mrs. Rand's words, *"the truth is not for all men, but only for those who seek it"*, those who seek it not with the eyes, but with their mind, in order to have a reliable picture of what reality truly is — absolute and unchanging.

Resumo da Dissertação apresentada à COPPE/UFRJ como parte dos requisitos necessários para a obtenção do grau de Mestre em Ciências (M.Sc.)

MODELAGEM, CONTROLE E OTIMIZAÇÃO DA SEPARAÇÃO ENANTIOMÉRICA DE PRAZIQUANTEL EM LEITO MÓVEL SIMULADO

Ataíde Souza Andrade Neto

Setembro/2015

Orientadores: Argimiro Resende Secchi
Maurício Bezerra de Souza Júnior

Programa: Engenharia Química

A esquistossomose é a segunda doença parasitária de maior ocorrência no mundo, atrás apenas para a malária. Atualmente, o praziquantel é o medicamento mais empregado no tratamento da doença. Neste trabalho, conduziu-se um estudo sobre a separação enantiomérica de praziquantel por cromatografia em leito móvel simulado, abrangendo-se a modelagem, simulação, controle e otimização do processo. A abordagem direta foi empregada a fim de se obter um modelo de alta representatividade. Dois modelos, com diferentes níveis de descrição, foram explorados, a saber: o modelo de equilíbrio local e o modelo de força motriz linear. Um algoritmo NMPC *(Nonlinear Model Predictive Control)*, baseado em um modelo de primeiros princípios acoplado a um estimador de parâmetros foi desenvolvido. Vários cenários de controle, considerando-se falhas na instrumentação e erros de modelagem, foram simulados visando avaliar o esquema de controle proposto. Em todos os casos estudados, o controlador foi capaz de manter as variáveis controladas nos níveis desejados, com uma rápida resposta e ações de controle suaves, mostrando um bom desempenho. Adicionalmente, um pacote computacional generalizado para a modelagem, simulação otimização e controle de separação binária em leito móvel simulado foi desenvolvido.

Abstract of Dissertation presented to COPPE/UFRJ as a partial fulfillment of the requirements for the degree of Master of Science (M.Sc.)

MODELING, CONTROL AND OPTIMIZATION OF THE ENANTIOMERIC SEPARATION OF PRAZIQUANTEL IN SIMULATED MOVING BED

Ataíde Souza Andrade Neto

September/2015

Advisors: Argimiro Resende Secchi
Maurício Bezerra de Souza Júnior

Department: Chemical Engineering

Schistosomiasis is currently the second most occurring parasitical disease in the world, outnumbered only by malaria; nowadays, praziquantel is the main drug employed in its treatment. In this work, a modeling, optimization and control study of praziquantel enantioseparation by simulated moving bed chromatography was carried out. The direct approach was followed in order to create a representative model of the system and two models of different description levels were explored, namely, the local equilibrium and the linear driving force models. A nonlinear model predictive control based on first principles models, coupled to a parameter estimator, was developed. Several control scenarios concerning instrumentation malfunction and plant-model mismatch were simulated in order to evaluate the proposed control scheme. In every studied case, the controller was able to maintain the controlled variables on the desired levels, with a fast response and smooth actuation, resulting in an excellent performance. Additionally, a general software package for modeling, simulation, optimization and control of binary separations in simulated moving bed is presented.

Contents

List of Figures

List of Tables

List of Symbols

C (ML^{-3})	Fluid Phase Mass Concentration, p. 21
C_f (ML^{-3})	Feeding Stream Concentration, p. 22
D (L^2T^{-1})	Effective Coefficient of Dispersion, p. 21
H $(-)$	Henry Constant, p. 15
H_c $(-)$	Control Horizon, p. 11
H_p $(-)$	Prediction Horizon, p. 11
K (L^3M^{-1})	Adsorption Constant, p. 24
Q (L^3T^{-1})	SMB Fluid Flow Rate, p. 12
Q_d (L^3T^{-1})	Desorbent Flow Rate, p. 22
Q_f (L^3T^{-1})	Feeding Flow Rate, p. 22
Q_r (L^3T^{-1})	Raffinate Flow Rate, p. 22
Q_x (L^3T^{-1})	Extract Flow Rate, p. 22
V (L^3)	Column Volume, p. 12
f (L^3T^{-1})	TMB Fluid Flow Rate, p. 12
f_s (L^3T^{-1})	Solid Phase Volumetric Flow Rate, p. 12
k_f (T^{-1})	Mass Transfer Coefficient, p. 40
m $(-)$	Flow Rate Ratio, p. 15
q (ML^{-3})	Adsorbed Phase Mass Concentration, p. 21
q_e (ML^{-3})	Equilibrium Concentration, p. 24
q_m (ML^{-3})	Saturation Concentration, p. 24

$t\ (T)$	Time, p. 21
$v\ (LT^{-1})$	Interstitial Velocity, p. 21
$v_m\ (LT^{-1})$	Effective Velocity, p. 21
$z\ (L)$	Axial Coordinate, p. 21
$y\ (-)$	Predicted States, p. 11
$y_{sp}\ (-)$	Reference Trajectory, p. 11
$h\ (T)$	Integration Time Step, p. 29
$\Lambda(-)$	Optimization's objective function weight, p. 31
$\Theta_{CPU}\ (T)$	Computational time, p. 55
$\Theta_{sample}\ (T)$	Sampling time, p. 55
$\ell\ (L)$	Column Length, p. 21
$\gamma\ (-)$	Adsorptivity, p. 15
$\omega_1\ (-)$	Economical weight, p. 34
$\omega_2\ (-)$	Set point weight, p. 34
$\theta\ (T)$	Switch Time, p. 12
$\varepsilon\ (-)$	Overall Bed Void Fraction, p. 15
$\varepsilon_b\ (-)$	Bed Void Fraction, p. 12
$\varepsilon_p\ (-)$	Interparticle Void Fraction, p. 15

List of Abbreviations

BC	Boundary Condition, p. 21
BDF	Backwards Differentiation Formula, p. 30
CSS	Cyclic Steady State, p. 12
DAE	Differential Algebraic Equation, p. 17
FD	Finite Differences, p. 26
GPA	Global Polynomial Approximation, p. 25
GUI	Graphical User Interface, p. 41
IC	Initial Condition, p. 21
IUPAC	International Union of Pure and Applied Chemistry, p. 5
IVP	Initial Value Problems, p. 30
LDF	Linear Driving Force, p. 41
LEM	Local Equilibrium Model, p. 24
LP	Linear Programming, p. 16
MPC	Model Predictive Control, p. 11
MTZ	Mass Transfer Zone, p. 6
MoL	Method of Lines, p. 26
NMPC	Nonlinear Model Predictive Control, p. 11
ODE	Ordinary Differential Equation, p. 26
PDE	Partial Differential Equation, p. 21
PID	Proportional Integral Derivative, p. 11

PI	Proportional Integral, p. 19
PZQ	Praziquantel, p. 1
RMPC	Repetitive Model Predictive Control, p. 19
SMB	Simulated Moving Bed, p. 2
TMB	True Moving Bed, p. 7
UOP	Universal Oil Products, p. 9
WHO	World Health Organization, p. 1

Chapter 1

Introduction

"Oh, be some other name! What's in a name? That which we call a rose, by any other name would smell as sweet"

Juliet, from William Shakespeare's *"Romeo and Juliet"*

1.1 Motivation

Schistosomiasis is currently the second most occurring parasitical disease in the world, outnumbered only by malaria. World Health Organization (WHO) estimates that there are about 210 millions of people infected nowadays (WANG *et al.*, 2014) and also 600 to 800 millions of people at risk of infection due to poor sanitation practices (CIOLI *et al.*, 2014). Thus, the most risky and affected regions are Sub-Saharan Africa, Asia Southeast and Brazilian Northeast, as shown in Figure 1.1.

Praziquantel (PZQ) is the main drug on schistosomiasis treatment and many pharmaceutical trials have shown its high effectiveness (KUMAR and GRYSEELS, 1994). Although it is an inexpensive chemotherapy treatment, PZQ is produced as a racemic mixture of its enantiomers. That is a major problem, because R(–)praziquantel is the only active component in the racemate. The counterpart enantiomer, S(+)praziquantel, grants the pill a bitter taste — which make children treatment difficult — and has low-level toxicity, rising the probability of undesired side effects (WANG *et al.*, 2014).

Pure PZQ enantiomers production methods have been proposed in recent

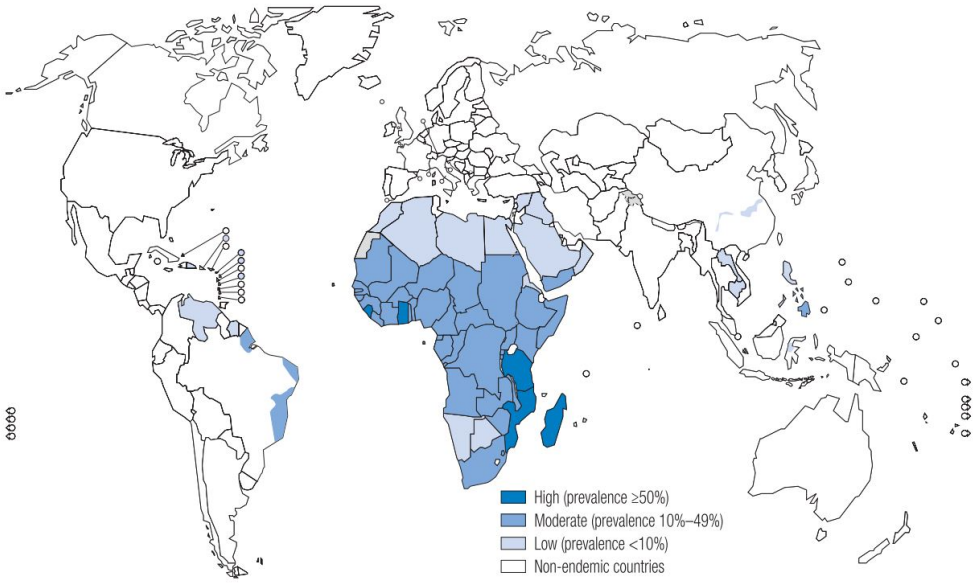

Figure 1.1: World Schistosomiasis Distribution (SAVIOLI and DAUMERIE, 2010)

.

years, for example: (i) continuous chromatography (LIM *et al.*, 1995); and (ii) enantioselective synthesis (CEDILLO-CRUZ *et al.*, 2014). Although the direct synthesis seems to be a suitable way to obtain the active molecule, there are not enough studies evaluating its industrial chain of production in order to prove the process could be profitable, since limitations as the availability of enantioselective and effective catalysts persists.

On the other hand, continuous chromatography such as Simulated Moving Bed (SMB) has been studied for many years and since mid 1990s applied to chiral separations. Several authors (CHIN and WANG, 2004; RAJENDRAN *et al.*, 2009; SCHULTE and STRUBE, 2001) have also shown that SMB is much superior to other chromatographic processes, either in continuous countercurrent, or batch operation, as it requires less solvent consumption and energy added to the system.

1.2 Objective

In this work, a study of praziquantel enantioseparation by simulated moving bed chromatography covering the process modeling, optimization and control is carried out. Some specific goals are:

(i) Build representative model of SMB unit;

(ii) Optimize the operational parameters for maximum productivity attaining purity requirements in permanent regime;

(iii) Propose a control strategy for praziquantel separation in simulated moving bed;

(iv) Develop a software for simulation and control of SMB systems.

1.3 Dissertation structure

This document is composed by five chapters followed by an appendix section. The motivation and objectives of this work are presented in Chapter 1.

In Chapter 2, a brief review of enantiomeric separation as well as an overview on chromatographic processes focusing in simulated moving bed modeling, optimization and control are presented. Some comments on model predictive control are made at the end of the chapter.

Chapter 3 covers the modeling, simulation, optimization and control strategies used in this work.

In Chapter 4, a comparison between simulation results and experimental data available in literature is presented. Moreover, the theoretical results for the optimization and control of a simulated moving bed designed for praziquantel enantioseparation is discussed.

Conclusions and suggestions for future works are presented in Chapter 5.

In the appendix section, algorithms for global polynomial approximation and a detailed explanation about the developed software package are presented. Also, a compilation of additional control problems is commented.

Chapter 2

Literature Review

What we know is not much. What we do not know is immense.

Laplace's last words
(Reported in *"Éloge historique de M. le Marquis de Laplace"* by Fourier, 1829)

2.1 Enantiomeric Separations

Chirality was first observed by Pasteur in 1848, for this reason he is considered the founder of the field of stereochemistry. Even in its beginning, chirality was recognized to have an important role in the way physiologic activities of living organism work. Although it is known for sure that enantiomers of a molecule are in fact two different substances, these can not be distinguished in achiral environments, for they have the same solubility, the same boiling and melting points and identical infrared spectrum and reaction rates with non-chiral reactants (SOLOMONS and FRYHLE, 2001).

All those similarities make chirality an intriguing phenomena and, because of that, scientific community believed it would be nearly impossible to separate enantiomers. The first researchers to propose a mechanism for enantioseparation were Gil-Av and collaborators, in 1966, under severe criticism. In a gas chromatography system, Gil-Av observed that enantiomers of a molecule interacted differently with chiral stationary phases and used that property to separate amino acid enantiomers. At that time, only a restricted spectrum of enantiomers could be separated (SCHURIG, 2001), but, nowadays, CHIRBASE DATA BANK

has a detailed and comprehensive description of over than 220,000 chiral methods extracted from journals and patents.

Even though pharmaceutical industry was aware of the potential damage an optically active drug could do to the human body — as it is a highly stereospecific environment —, that fact has been largely neglected. Just in recent history, scientific community pressured governmental agencies to restrict the use of asymmetric drugs in its racemic form. In order to fit in the constant renewing standard legislation, the pharmaceutical industry began to show interest in methods for resolution and purification of enantiomers since mid 1990s (LIM *et al.*, 1995; SCHURIG, 2001).

With respect to preparative separation of praziquantel, the only reported works in literature are from LIM *et al.* (1995) and LIM and CHING (1996). In those studies, a preliminary design of a simulated countercurrent chromatographic system is presented using methanol as mobile phase and a cellulose adsorbent. Both investigations are empirical approaches and no equilibrium data was generated. The initial operating conditions were selected based on chromatograms from batch separation and constantly optimized in an erratic way, based on concentration profiles obtained at each experimental run.

2.2 Chromatographic Processes

Chromatography is a class of separation techniques based on the principle of mass transfer. It can be classified according with the separation mechanism as adsorption, partition, ion-exchange, exclusion, hydrophobic or affinity chromatography (GOMES, 2009).

According to IUPAC's definition, adsorption *"[...] is an increase in the concentration of a dissolved substance at the interface of a condensed and a liquid or gaseous phase due to the operation of surface forces."*. In other words, adsorption is the phenomena in which molecules from a gas or liquid adhere to a solid surface. This adhesion can be classified into two groups, namely: (i) by weak intermolecular forces (physisorption); or (ii) by chemical bonding (chemisorption) between adsorbed molecule and adsorbent surface. The equilibrium relationship between the fluid and solid phases is given by a mathematical expression named *adsorption isotherm*.

Physisorption is milder than chemisorption. It has lower adsorption heat and smaller temperature range of occurrence. In contrast to physisorption,

chemisorption is irreversible, can only form single layers and the species might dissociate. Additionally, it is more selective than physisorption (ROMANIELO, 1999).

Even though adsorption is a known phenomena since the eighteen century, its first industrial applications came up in early 1900s, as the necessity for purification processes — such as the H_2S removal from natural gas — arose in oil and gas industry. Then, adsorption processes were employed as a mean of increasing the associated value of production streams. Its full economic potential was discovered in early 1950s, when it was applied on separation of mixtures into streams enriched in different valuable components. Among such separations were the recovery of aromatic hydrocarbons from oil, as well as linear paraffins from branched and cyclic isomers (RUTHVEN, 1984).

Activated carbon and silica gel were the mainly adsorbents used in early applications of chromatographic processes, but, in late 1950s, molecular sieves like zeolites became commercially popular, thus enhancing adsorption as a separation process. In mid 1990s, with the discovery of natural and synthetic chiral adsorbents such as cellulose-triacetate and poly-trisphenil-methylmethacrilate, respectively, chromatography began to be employed in enantioseparations (SCHULTE and STRUBE, 2001).

The simplest chromatographic separation system is the fixed-bed adsorption. The process comprises a packed column filled with an adsorbent material (the stationary phase) and fed with a stream (the mobile phase) in which there is either a desired component (the adsorbate) to be extracted, or an undesired one to be removed. Adsorption does not occur over all the column at the same time, instead, it only occurs in a particular region called Mass Transfer Zone (MTZ), which moves from inlet to outlet along the bed. While the adsorbent has capacity to adsorb the component, there will exist a driving force promoting the mass transfer between the phases. As this capacity decreases, the system goes toward an equilibrium state in which the driving force ceases and the stationary phase reaches its maximum amount of adsorbate. In case all the column reaches the equilibrium state, it is said to be saturated and becomes useless for separation purposes until it is cleaned (regenerated) with an adsorbate-free solvent (desorbent). As a result, fixed-bed adsorption is an intrinsically batch process. That property is a disadvantage of fixed-bed adsorption, once industrial processes are desired to operate continuously.

Cyclic batch processes were designed in order to bypass the bottlenecks brought up by fixed-bed adsorption. The idea of such processes lies on simulta-

neous operation of two or more columns. While one of the columns acts as an adsorbent bed, the remaining ones act as regenerators. At a predetermined time span, each bed role is interchanged, the adsorber starts to be regenerated, while the freshest one receives the load, thus, completing a cycle. Some techniques can be applied in order to speed up the regeneration step and consequently reduce the cycle length. Usually, this is achieved by raising the bed temperature (Thermal Swing Adsorption, TSA) or by lowering its pressure (Pressure Swing Adsorption, PSA), but other strategies are also employed (RUTHVEN, 1984). Compared to batch processes, cyclic batch has higher productivity, but also higher implantation costs. Both are equally solvent and adsorbent demanding, thus, operational costs might be an issue (THOMAS and CRITTENDEN, 1998).

Another class of chromatographic processes is the moving-bed adsorption, also known as True Moving Bed (TMB). TMB processes are designed for binary separation and comprise a vertical column – or a series of columns – fed at the bottom with the desorbent and at the top with the adsorbent. In order to minimize both solvent and adsorbent consumption, these streams are recycled. The goal of countercurrent flow is to maximize mass transfer between the phases by making all bed regions perform either adsorption or regeneration at the same time. The binary mixture to be separated is fed in somewhere at the middle of the bed and two outlet streams are gathered above (raffinate) and below (extract) the feeding point. Each one of these streams are enriched in a single component. The regions intercalated by the extract, feeding and raffinate streams are called "zones" (or "sections") and each one has a purpose in the separation (ROUSSEAU, 1987). A schematic of the TMB process is shown in Figure 2.1.

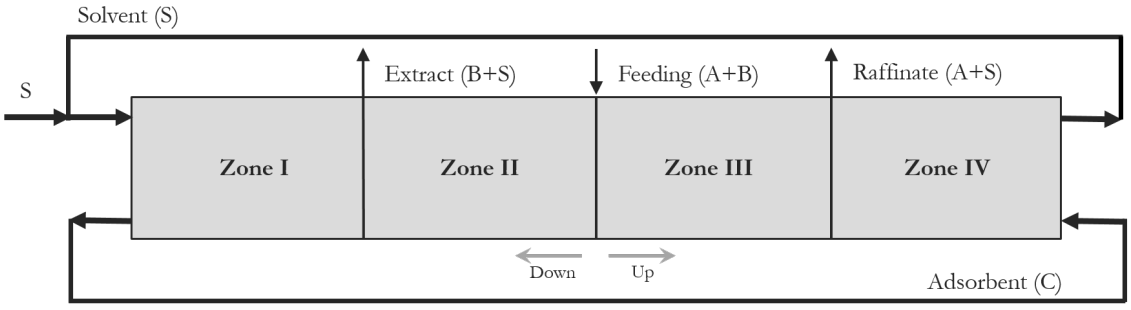

Figure 2.1: True moving bed schematic.

The role of Zone III is to remove the strongly adsorbed solute *B* (see Figure 2.1) from the feeding stream. As *B* gets adsorbed, it should go down along with the adsorbent *C*, and *A* should go up along with the solvent *S*, leaving

the process at the raffinate port. In Zone II, solute B is separated from A and partially leaves the process at extract port. Zone I is the solid regeneration region in which major quantities of solute B are still adsorbed. The contact with solvent promotes its desorption, flowing upwards and leaving the column at the extract port. In Zone IV, some solvent is recovered for recycling as A get adsorbed and flows downwards along with the adsorbent (ROUSSEAU, 1987).

In spite the fact that true moving bed process can greatly cut the operational costs due to an economic usage of solvent and adsorbent compared to batch and cyclic batch processes, it is very difficult to maintain countercurrent flow of fluid and solid from a technical point of view. That problem has been solved with the development of simulated moving bed processes.

2.3 Simulated Moving Bed Chromatography

An SMB unit is a connected series of fixed-bed columns with a recycle pump circling solvent in the arrangement. Additionally, a pump delivers fresh solvent to the system and another one delivers the mixture load. Two more pumps are diametrically placed between the solvent and feeding points, withdrawing the raffinate and extract streams. A schematic of the system is shown in Figure 2.2.

Relative movement between mobile and stationary phases is imposed by the inlet and outlet streams periodic switching in the same direction of the fluid flow. In classical SMB operating mode, all streams advance together one column per section with a constant switching time. A cycle is completed when all the injection/collection streams return to its initial configuration. In the past couple decades, other operation modes have been developed, which are well described by GOMES (2009).

The concept of the simulated moving bed was first presented in 1949 (CHIN and WANG, 2004) for aromatics and olefins separation from petroleum as a practical implementation of the TMB process. Indeed, SMB and TMB are equivalent at most operation conditions of industrial interest, and virtually identical at the limit of infinitesimal switching time and infinity number of beds per section, each one measuring an infinitesimal length. The same zones identified in TMB also occur in SMB, however they are not stationary, but move along with the inlet/outlet streams cycle (RAJENDRAN *et al.*, 2009).

The early applications of SMB was in petrochemical industry for difficult

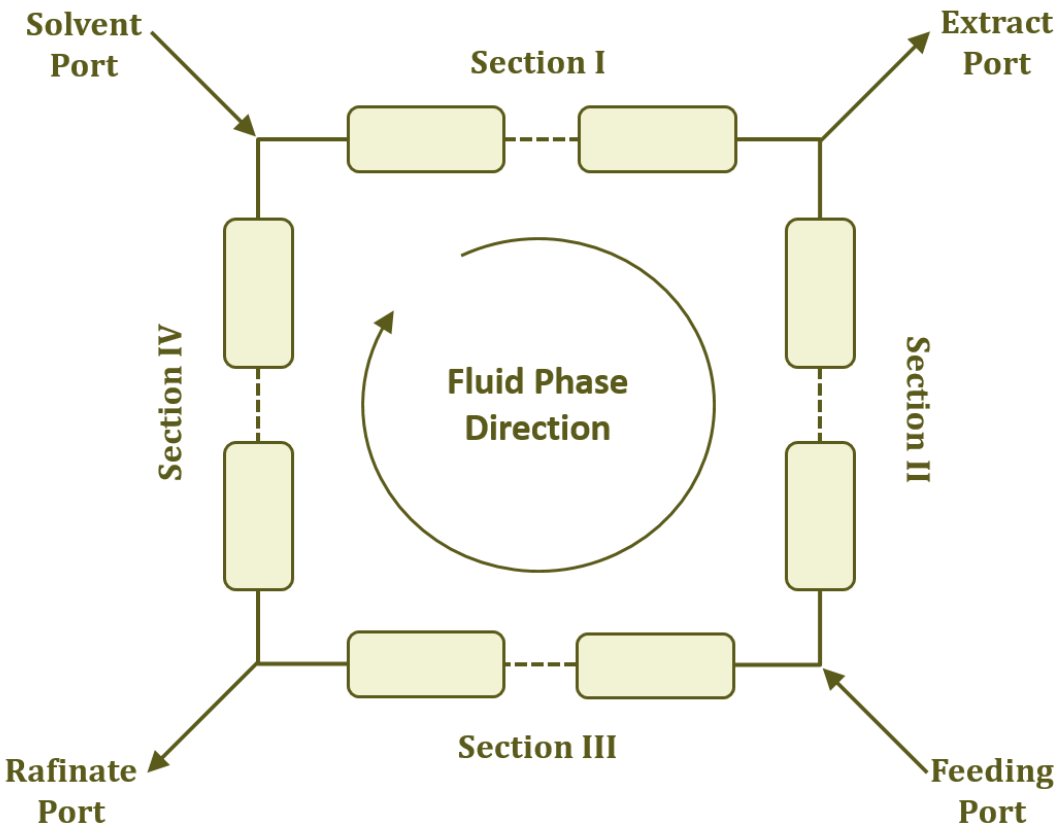

Figure 2.2: Simulated moving bed schematic.

separations where distillation processes were impractical due to high energy demands. In the 1960s, *Universal Oil Products, Inc.* (UOP) extended the concept of SMB and began to commercialize a number of new process for petrochemicals (CHIN and WANG, 2004). A few years later, SMB technology was successfully employed in sugar industry for mono and oligosacharides separation (SCHULTE and STRUBE, 2001) and, in early 1990s, SMB was used for xylenes isomers separation. At the same time, it was also used for enantioseparations (SCHULTE and STRUBE, 2001). Once chiral separations was successfully achieved, SMB technology drew attention of pharmaceutical and fine-chemicals industry. In 1997, the first large-scale SMB manufacturing plant was installed by *UCP Pharma* and, since then, several units have been developed for drug purification (RAJENDRAN *et al.*, 2009).

The major obstacles SMB technology had to surpass along with its development were related to instrumentation. Although it consists only of packed columns, pumps and valves, the latter ones have non-trivial designs. The valving system is the heart of simulated moving beds and can comprise single or multiples valves that perform the switches between the inlet and outlet streams.

A very complete discussion on valve instrumentation design and application can be found in CHIN and WANG (2004).

2.4 Model Predictive Control (MPC)

Model predictive control is an advanced control technique based on process models widely used in modern engineering. It mainly differs from standard PID control in the way current controlled actions are calculated. While PID uses a pre-computed control law, MPC's control action is result, in most of the cases, of an on-line dynamic optimization within a finite horizon, starting from the current plant states at each sampling instant (save the case of linear models without constraints, in which there is an explicit control law). Although a dynamic optimization returns a series of control actions over the finite prediction horizon (H_p), only the first one is implemented on the plant (MAYNE *et al.*, 2000).

The main applications of MPC began in petrochemical industry, but currently it is widespread in process industry in general. Among the reasons for its success is that it can handle multivariable problems naturally, works at optimal and more profitable operation points and is able to take into account constraints, which is a great advantage because many control systems have their performance limited by presence of constraints (MACIEJWOSKI, 2000).

As computing time is a fundamental issue to real-time optimization (it has to be done within a time constraint given by the sampling period, after all), the models employed in MPC tend to be as simplified as possible. Often, linear models are used to describe plant dynamics, as they will comprise a convex optimization problem. However, most chemical processes have nonlinear nature, so usually the first step in controller design is either to identify a linear model (or a set of linear models) that correlates inputs and outputs or to apply linearization techniques in order to have a local model.

Nevertheless, some control algorithms do employ nonlinear models to predict the plant future states. That class of algorithms is called Nonlinear Model Predictive Control (NMPC). As result, computational efficiency became of critical matter in NMPC strategies, as it transforms the once linear MPC into a nonconvex nonlinear problem which is doubtless more complex and harder to solve. The reason for nonlinear models to be incorporated at controllers is that they can represent the plant whatsoever the operation point that is chosen (CANNON, 2004).

Besides the model, another important element of MPC algorithms is the cost function to be minimized. The most common functions take into account the deviation between the predicted outputs at the considered horizon ($\boldsymbol{y}$) and a reference trajectory ($\boldsymbol{y_{sp}}$) and the deviation between the manipulated variables ($\boldsymbol{u}$) and their target trajectory ($\boldsymbol{u_{tg}}$). Additionally, the control effort given by the manipulated variables variation ($\Delta\boldsymbol{u}$) within the control horizon (H_c) is also considered (CAMACHO and BORDONS, 2007). This function is often given by:

$$J = \underbrace{(\boldsymbol{y} - \boldsymbol{y_{sp}})^T \boldsymbol{\mathcal{Q}} (\boldsymbol{y} - \boldsymbol{y_{sp}})}_{\text{Set point}} + \underbrace{(\boldsymbol{u} - \boldsymbol{u_{tg}})^T \boldsymbol{\mathcal{S}} (\boldsymbol{u} - \boldsymbol{u_{tg}})}_{\text{Target}} + \underbrace{\Delta\boldsymbol{u}^T \boldsymbol{\mathcal{R}} \Delta\boldsymbol{u}}_{\text{Control effort}} \tag{2.1}$$

where $\boldsymbol{\mathcal{Q}}$, $\boldsymbol{\mathcal{S}}$ and $\boldsymbol{\mathcal{R}}$ are matrices used to tune the controller by weighting set point, target and control effort, respectively (GONÇALVES, 2013).

The optimization constraints are usually valves operational limits, safe limits of temperature or pressure, physical restriction like impossibility of reverse flow *et cetera* (CAMACHO and BORDONS, 2007).

More information about control theory can be found in the referenced literature.

2.5 SMB Analysis

More than a hundred papers have been published just in the last decade regarding the SMB process. Many of them are focused on modeling, simulation, optimization or control of industrial units and a short overview on the different attempts to approach the problem will be presented here. The modeling, simulation, optimization and control strategies used in this work are discussed later on Chapter 3.

2.5.1 Modeling

According to GUIOCHON *et al.* (2006), two distinct approaches have been followed for modeling simulated moving beds, namely:

(i) The fixed-bed (or direct) approach, which represents the real SMB configuration — a series of fixed-bed columns considering the periodic switching of inlet and outlet streams; and

(ii) The true moving bed approach, which assumes the SMB to be equivalent to the TMB system. *"This model neglects the dynamics associated with the periodic switching of the columns and gives the mean concentration profiles over a switching period"*(GUIOCHON *et al.*, 2006).

Equivalency between TMB and SMB can be established through the following relationships:

$$f_s = \frac{(1-\varepsilon_b)V}{\theta} \tag{2.2}$$

$$Q_j = f_j + \frac{q_s \varepsilon_b}{1-\varepsilon_b} \tag{2.3}$$

where f_s $[L^3T^{-1}]$ is the solid flow rate; ε_b $[-]$ is the bed void fraction; V $[L^3]$ is the SMB column volume; θ $[T]$ is the switching time of SMB unit; f $[L^3T^{-1}]$ and Q $[L^3T^{-1}]$ are the fluid flow rates in TMB and equivalent SMB in a section j, respectively.

Each approach has its own particularities. The fixed-bed approach, by instance, is a much more representative model of the unit; however, it is way more complex and computer demanding than the TMB approach. Moreover, it does not reach a common steady state, but rather a Cyclic Steady State (CSS) in which the concentration profiles are still varying with time, and moving along with the fluid phase in a wave form through the bed.

The cyclic steady state is characterized once the dynamic behavior of each zone is identical within each switching period, as illustrated in Figure 2.3. As can be seen in Figures 2.3a and 2.3b, the concentration profiles for amino acid enantiomers uridine and guanosine are not the same at different time instants t_k, so the cyclic steady state is not reached. In contrast to that, it is shown in Figures 2.3c and 2.3d the full developed cyclic steady state — note that the profile are the same at different time instants t_k, only displaced in relation to the spatial coordinate.

Another way to distinguish the CSS is to fix a point in SMB length and track the evolution of a component concentration. As the time dependent behavior between two cycles are identical at the cyclic steady state, it is reached when periodicity is observed (ERDEM *et al.*, 2004). A typical time-varying concentration profile for guanosine in extract port is shown in Figure 2.4.

The conventional method for CSS determination is called *sequential approach*, which consists in solve the dynamic model cycle by cycle until the peri-

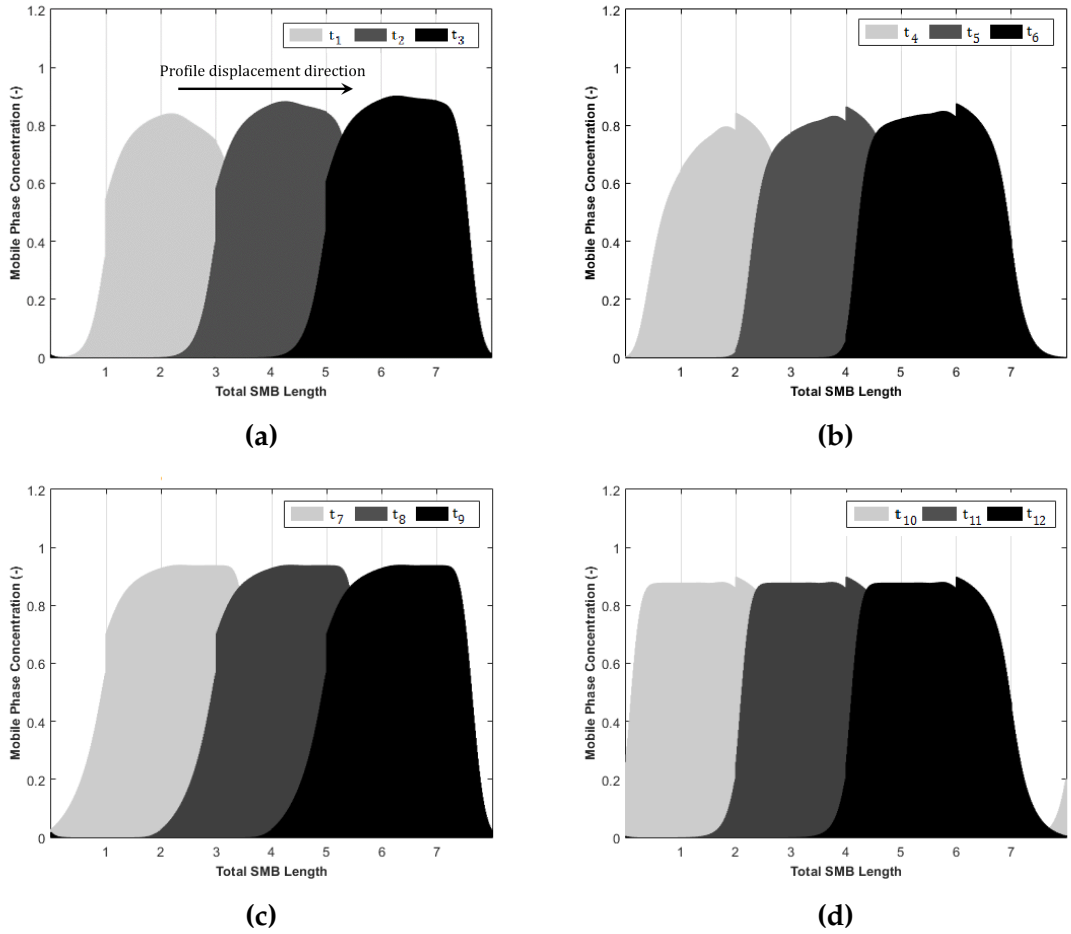

Figure 2.3: Cyclic stady state characterization: (a) Uridine and (b) Guanosine internal concentration profiles at different time instants in transient regime; (c) Uridine and (d) Guanosine internal concentration profiles at different time instants in cyclic steady state.

odicity condition is satisfied. Although it is a simple method, it is also a computationally expensive one. In order to accelerate the CSS computation, YAO *et al.* (2010) presented a method based on the "quasi-envelope" concept, in which SMB is treated as a pseudo-oscillatory process. In their method, only the initial cycles are simulated. The CSS is estimated from that data and the known oscillatory period θ, that is, the switching time.

Until early 2000's, several authors (LEÃO and RODRIGUES, 2004; SILVA *et al.*, 2004) largely explored the TMB approach since computational power was more limited than nowadays. There are also reports of direct modeling in the same period (DÜNNEBIER *et al.*, 1998; KLATT *et al.*, 2002) but for simplified cases when analytic solution is available (*e.g.*, the case of linear adsorption isotherms). As powerful CPUs have become available at a lower cost in recent years, the fixed-bed approach application has increased (ABEL *et al.*, 2005; GROSSMANN *et al.*, 2010; SUVAROV *et al.*, 2014).

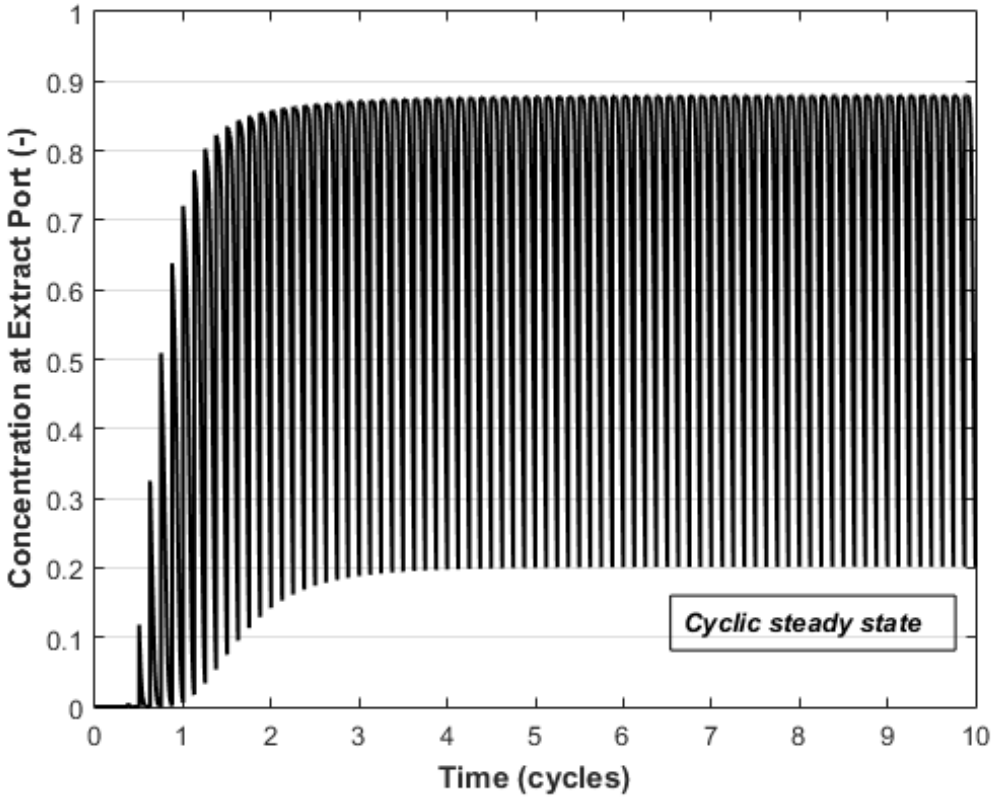

Figure 2.4: Guanoine concentration profile in extract port.

2.5.2 Optimization

For optimization and design purposes, a good starting point is the triangle theory, which is based on equilibrium theory for the TMB process. Its application allows to build a parametric operating region in which total separation is guaranteed (ERDEM *et al.*, 2004).

Defining the flow rate ratio parameters m_j $[-]$ as the the ratio between the net fluid flow rate and adsorbed phase flow rate in a section j of a TMB unit, according to the expression:

$$m_j = \frac{q_j - q_s \varepsilon_p}{q_s(1 - \varepsilon_p)} \tag{2.4}$$

where ε_p $[-]$ is the interparticle void fraction; and converting it for an equivalent SMB unit using Equations (2.2)–(2.3):

$$m_j = \frac{Q_j \theta - V\varepsilon}{V(1 - \varepsilon)} \tag{2.5}$$

where $\varepsilon\,[-]$ is the overall bed void fraction, given by:

$$\varepsilon = \varepsilon_b + \varepsilon_p(1-\varepsilon_b) \tag{2.6}$$

complete separation is attained by choosing Q_j and θ as m_j remain inside the triangles formed by the following constraints:

For linear isotherms:

$$H_B < m_1 < \infty \tag{2.7}$$
$$H_A < m_2 < H_B \tag{2.8}$$
$$H_A < m_3 < H_B \tag{2.9}$$
$$\frac{-\varepsilon_p}{1-\varepsilon_p} < m_4 < H_A \tag{2.10}$$

For Langmuir isotherms:

$$\gamma_A < m_1 < \infty \tag{2.11}$$
$$m_{2,min} < m_2 < m_3 < m_{3,max} \tag{2.12}$$
$$\frac{-\varepsilon_p}{1-\varepsilon_p} < m_4 < m_{4,max} \tag{2.13}$$

where $H[-]$ and $\gamma[-]$ are the Henry constant and the adsorptivity of the ith component. The limiting quantities $m_{2,min}$, $m_{3,max}$ and $m_{4,max}$ are defined functions of parameters m_2 and m_3. In the triangles shown in Figure 2.5, the theoretical optimum is localized at the vertex W, as that is the condition of maximum productivity in which full separation can be achieved. Further discussion about the triangle theory can be found in MAZZOTTI *et al.* (1997) and SCHIMIDT-TRAUB (2005).

Although widely employed in SMB optimization due its simplicity, triangle theory may lead to sub-optimal or even unfeasible operating points, as it accounts for the adsorption thermodynamics but neglects mass transfer resistance and dispersion effects. An alternative to that is the model-based optimization which is a more reliable technique and can exploit the full optimization potential of nonlinear processes (TOUMI *et al.*, 2007).

A classical optimization problem of SMB units is the simultaneous maximization of productivity and minimization of solvent consumption while extract

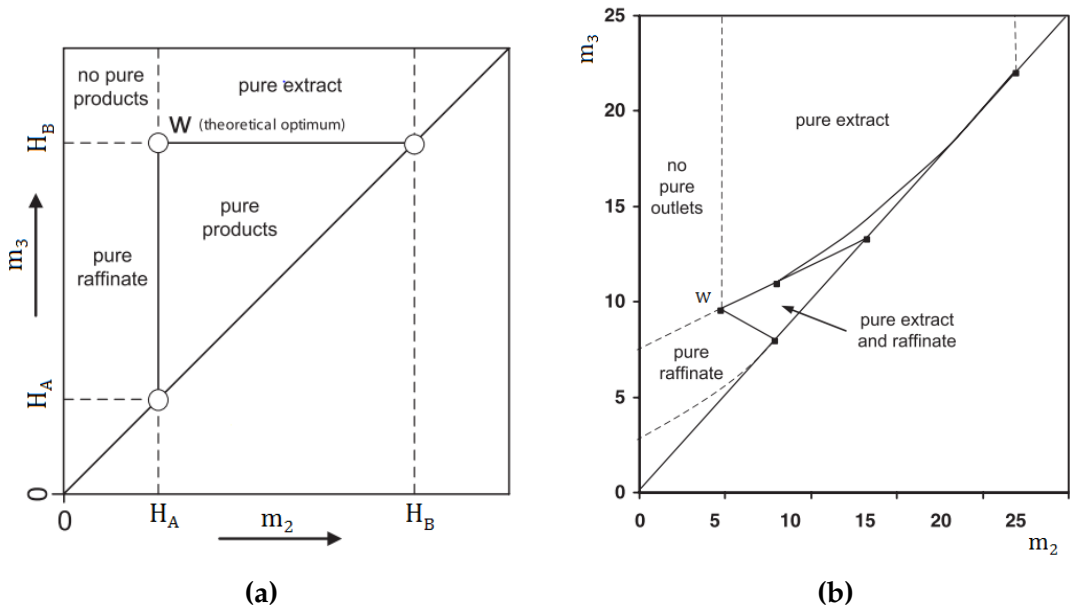

Figure 2.5: Triangular regions for: (a) Linear isotherms separations and (b) Langmuir isotherms separations (adapted form SCHIMIDT-TRAUB (2005)).

and raffinate purity requirements are attained, thus, consisting in a constrained multi-objective optimization problem. Several approaches have been reported in the literature to treat this problem. The most relevant ones are described below.

ABEL *et al.* (2004) employed a simplified time-varying model obtained from linearization of the fixed-bed model resulting in a linear cost function together with linear constraints, which consists in a Linear Programming (LP) problem. LP problems have the advantage to be a convex optimization, which means that the optimum is global. However, linear models are result of local approximations, therefore, valid for a limited region; due to that, better solutions may be lost.

TOUMI *et al.* (2007) compared two different optimization strategies based on first principles model. The main discussion is how to obtain the SMB cyclic steady state profile that leads to the minimum operational costs. In their first attempt, the CSS was reached through successive simulations in each step of optimization (the sequential approach). The optimizing variables were the operating parameters. At their second attempt, the optimization problem was formulated as a multi-stage optimal control with the cyclic steady state set as an additional equality constraint and the problem was solved with the multiple shooting method (the simultaneous approach). According to the authors, the latter strategy was more efficient and less time consuming.

AGRAWAL *et al.* (2014) applied the Simultaneous Optimization and Model

Correction (SOMC) scheme for sugar purification. In short, SOMC schemes consists in an iterative method in which: (i) a model-based optimization is conducted and (ii) the decision variables are implemented in a pilot unit; (iii) if the experimental results differs from the predicted ones, regarding a certain tolerance, this data is used to (iv) re-estimate the parameters of the model; with the updated parameters, (v) a new optimization is carried out. Optimization and correction are repeated systematically until the predicted and observed purities converge to the same value. The authors emphasize that SOMC is not a control technique to maintain the quality of the products, but is an experimental technique for bench-scale experiments in which only the CSS performance is optimized. The advantages of SOMC scheme is that simplified models can be used without losing accuracy, as the parameters are constantly updated according to the conditions the unit is operating. Also, it is a good scheme for cases in which shortcuts such as the triangle theory do not exist, such as, for example, ternary separations. The authors claim that the strategy predict product purities sufficiently accurately in the range of purity of 75% to 90%, which covers most operations conditions of practical interests for sugar separation.

LI *et al.* (2014) used two different surrogate models in order to replace the full-order detailed SMB model: (i) a coarse spatial discretization by orthogonal collocation in finite elements of the first principles model; and (ii) a reduced-order model from the Proper Orthogonal Decomposition (POD) method. In comparison to the full-order model, the surrogate models are less accurate, but cheaper to solve numerically. The POD resulting model are a local model, therefore, valid only in the neighborhood of the reference point it is derived. In order to overcome this difficulty, the authors employed the trust-region optimization framework to maximize the feeding flow rate while purity requirements are attained and compared the results of both surrogate models with the full-order model. With their strategy, they showed that the coarse and the reduce-order models can replace the complete model without losing accuracy and also reducing computational time in about 50%.

2.5.3 Control

Due to its natural characteristics (slow dynamics, several constraints for both controlled and manipulated variables, utter need to operate at optimal conditions), simulated moving bed is an ideal process for Model Predictive Control (MPC) application. That fact is reflected on the amount of publications addressing the theme in the past 15 years in comparison to other forms of control

structures.

KLOPPENBURG and GILLES (1999) presented one of the first model-based control structure for SMB processes. They used the TMB model to design a nonlinear continuous controller and a state estimator. The control technique employed was the asymptotically exact input/output linearization, selecting as controlled variables the purities of extract and raffinate streams and as manipulated variables the volumetric flow rates of these same streams. That control scheme lead to persistent offsets of controlled variables from their set points in the case of plant-model mismatch or when unknown disturbances occurred, in such cases the authors recommended the coupling of PI feedback controllers.

ABEL *et al.* (2005) applied the concept of *repetitive model predictive control* (RMPC) — which is based on the idea that possible model prediction errors and the effect of period-invariant disturbances can be compensated using the measurements of the plant outputs — in an experimental unit for separation of nucleosides. The components concentrations on extract and raffinate ports are measured with UV detectors and the remaining states are estimated with a Kalman filter. A linearized time-discrete model is employed in the controller using the flow rate ratios m_j as manipulated variables while the switching time θ remains constant; the purities were the controlled variables. Despite using a simplified model, the strategy showed to be very robust, as the controller could handle well measured and unmeasured disturbances, and also had a good performance in a plant-model mismatch problem.

SONG *et al.* (2006) presented a novel control strategy based on process identification. The main disadvantage in using identified models is that, depending on the region of operation, SMB has different dynamical behavior, therefore, a different identified model must be obtained before each optimization step. In their control scheme, they tried to control purities while maximizing productivity and minimizing solvent consumption, selecting as manipulated variables the flow rate ratios m_j. Their results showed that the strategy have a good performance for disturbance rejection and set point tracking.

GROSSMANN *et al.* (2008) introduced the *cycle to cycle* concept. The novel feature in this concept is that the formulation of the control problem allows to perform measurements, optimization and take control actions only once every cycle, using past information such as the previous average concentration profiles as feedback to the next cycles. This approach allows expensive optimization to be performed since more time between the control actions is available. A linear time-varying model based on SMB complete model was employed for state

predictions. The authors studied five scenarios considering: (i) plant-model mismatch; (ii) feed and (iii) solvent pumps malfunction; (iv) set point tracking; and (v) effect of time delay in the measurements. Also, they compared the optimal operating point reached by the controller with an offline optimization. They claim the results agree rather well, except the minimization of the desorbent consumption.

SUVAROV *et al.* (2014) extend the cycle to cycle approach and presented an adaptive model-based controller applying a simple discrete-time model of the concentration fronts movement derived from wave theory. The optimization variables were the flow rate ratios m_j and the switching time θ. Robustness is achieved by adding a feedback layer and an online parameter estimator. The controller showed good disturbance rejection, stability and robustness properties, using very little information from the adsorption characteristics of the tested separation systems.

2.6 Final Remarks

Due to its wide range of application, simulated moving bed chromatography is a very well studied process in the separation engineering field. The SMB modeling and simulation strategies are already consolidated in literature, but the optimization and control problems are still subject of numerous researches. The main reason for this is the powerful computation processing capacity available in the modern PCs; a couple decades ago it was very limited and expensive, which made difficult to apply online optimization and model predictive control strategies with full SMB models.

The main contribution of this work is the application of a non-linear model predictive control strategy to the SMB process using a first principles model, which is more powerful as it can represent the plant whatever the operation region. Additionally, an easy-to-use software to aid the modeling, simulation, optimization and control of binary separations in simulated moving beds is provided, and a complete study of praziquantel separation is presented for the first time in literature.

Chapter 3

Methodology

Bran thought about it. "Can a man still be brave if he's afraid?"
"That is the only time a man can be brave" his father told him.

Ned Stark, from George Martin's
Game of Thrones

3.1 Introduction

A software package for modeling, simulation, optimization and control of the simulated moving bed process was developed in order to assist and to facilitate its analysis. In this chapter, the mathematical models and the solution methods implemented in the software are presented in Sections 3.2.1 and 3.2.2. The strategies and algorithms used for the optimization and control problems are also discussed in Sections 3.3 and 3.4. In Section 3.5, an overview on the software's user interface and some of its features are pointed out. More detailed instructions regarding the software usage are presented in the Appendix A.

Although the separation of praziquantel is illustrated in Chapter 4 as the main case study, the software was made general so it can be applied for a broad variety of binary systems. Additionally, it was designed to be as intuitive and user friendly as possible, seeking to ease and to speed up comparison studies.

3.2 Modeling and Simulation

3.2.1 Modeling

A generalized mathematical model following the direct approach was developed for four-section simulated moving bed units as the one shown in Figure 2.2. The fixed-bed adsorption model is the base for the SMB model and is already well established in the literature (SHAFEEYAN *et al.*, 2014). The fluid-phase mass balance for the *i*th component in the *k*th column is given by:

$$\underbrace{\frac{\partial C_{i,k}}{\partial t}}_{\substack{\text{Accumulation}\\ \text{rate}}} = \underbrace{-v_{m,k}\frac{\partial C_{i,k}}{\partial z}}_{\text{Advection rate}} + \underbrace{D_{i,k}\frac{\partial^2 C_{i,k}}{\partial z^2}}_{\text{Diffusion rate}} - \underbrace{\left(\frac{1-\varepsilon_k}{\varepsilon_k}\right)\frac{\partial q_{i,k}}{\partial t}}_{\text{Mass transfer rate}} \tag{3.1}$$

with the initial and boundary conditions:

$$\text{IC:} \quad C_{i,k}(0,z) = C_{0,i,k}(z) \tag{3.2}$$

$$\text{BCs:} \quad D_{i,k}\frac{\partial C_{i,k}(t,z)}{\partial z}\bigg|_{z=0} = v_{m,k}\left[C_{i,k}(t,0) - \bar{C}^{j}_{i,k}(t)\right] \tag{3.3}$$

$$\frac{\partial C_{i,k}(t,z)}{\partial z}\bigg|_{z=\ell_k} = 0 \tag{3.4}$$

where C $[ML^{-3}]$ is the fluid-phase mass concentration; t $[T]$ is the time; v_m $[LT^{-1}]$ is the effective velocity; z $[L]$ is the axial coordinate; D $[L^2T^{-1}]$ is the effective dispersion coefficient in terms of the overall bed void fraction; q $[ML^{-3}]$ is the adsorbed-phase mass concentration; C_0 is the initial concentration profile inside the columns at $t = 0$; $\bar{C}^j(t)$ is the column inlet concentration with the superscript $j = I, II, III, IV$ counting over the sections; and ℓ $[L]$ is column length. The index $i = A, B$ identifies the components (A or B) and $k = 1, 2, \ldots, N$ count over the N columns in the system.

The effective velocity v_m is a function of the interstitial velocity (v) given by:

$$v_m = \frac{\varepsilon_b}{\varepsilon}v \tag{3.5}$$

In a simulated moving bed arrangement, the column inlet concentration $\bar{C}(t)$ depends on the section and the location of the column within the section as

follow:

Section I, 1st column:

$$\bar{C}^{I}_{i,k}(t) = \frac{Q_{IV} C^{j}_{i,k-1}(t, \ell_{k-1})}{Q_I} \tag{3.6}$$

Section III, 1st column:

$$\bar{C}^{III}_{i,k}(t) = \frac{Q_{II} C_{i,k-1}(t, \ell_{k-1}) + Q_f C_{f,i}}{Q_{III}} \tag{3.7}$$

Any other column:

$$\bar{C}^{j}_{i,k}(t) = C_{i,k-1}(t, \ell_{k-1}) \tag{3.8}$$

where C_f is the feeding stream concentration.

As the flow rates are identical for all the columns within the same section, the interstitial velocities, v_k, can be obtained from nodal balances at the connections between the sections:

For section I:

$$Q_I = Q_d + Q_{IV} \qquad \text{and} \qquad v_k = \frac{Q_I}{\varepsilon_{b,k} S_k} \tag{3.9}$$

For section II:

$$Q_{II} = Q_I - Q_r \qquad \text{and} \qquad v_k = \frac{Q_{II}}{\varepsilon_{b,k} S_k} \tag{3.10}$$

For section III:

$$Q_{III} = Q_{II} + Q_f \qquad \text{and} \qquad v_k = \frac{Q_{III}}{\varepsilon_{b,k} S_k} \tag{3.11}$$

For section IV:

$$Q_{IV} = Q_{III} - Q_x \qquad \text{and} \qquad v_k = \frac{Q_{IV}}{\varepsilon_{b,k} S_k} \tag{3.12}$$

in which $S\ [L^2]$ is the column cross sectional area; $Qd,\ Q_r,\ Q_f$ and $Q_x\ [L^3T^{-1}]$ are

the desorbent, raffinate, feeding and extract volumetric flow rates, respectively. It is pointed out that at least one of the internal flow rates must be specified in order to the linear system composed by Equations (3.9)–(3.12) have a unique solution.

According to SHAFEEYAN *et al.* (2014), the dynamical models of adsorption columns can be classified according to: (i) the solid-fluid equilibrium nature; as well as the (ii) complexity of mathematical models required to describe the mass transfer mechanisms occurring between the phases. Both factors are computed in the mass transfer term in Equation (3.1).

The Local Equilibrium Model (LEM) assumes that mass transfer resistances at the solid-fluid interface and inside the adsorbent particle are negligible, so there is an instantaneous equilibrium between the mobile and stationary phases. That is the simplest way to describe the term $(\partial q/\partial t)$ and there are several reports in literature (ERDEM *et al.*, 2004; GROSSMANN *et al.*, 2010; SUVAROV *et al.*, 2014) that successfully employ the LEM to enantiomeric separations. In this case:

$$\frac{\partial q_{i,k}}{\partial t} = \frac{\partial q_{e,i,k}}{\partial t} \tag{3.13}$$

q_e $[ML^{-3}]$ is the *adsorption isotherm*, an algebraic expression that relates the equilibrium concentration to the fluid phase concentration. The most common isotherms are the *linear*, *Langmuir* and *competitive Langmuir* isotherms, respectively expressed by:

$$q_{e,i} = H_i C_i \tag{3.14}$$

$$q_{e,i} = \frac{q_{m,i} K_i C_i}{1 + K_i C_i} \tag{3.15}$$

$$q_{e,i} = \frac{q_{m,i} K_i C_i}{1 + \sum_{i=1}^{M} K_i C_i} \tag{3.16}$$

where q_m $[ML^{-3}]$ is the saturation concentration and K $[L^{-3}M]$ is the adsorption constant. Combinations of these isotherms are also frequent:

linear + Langmuir:

$$q_{e,i} = H_i C_i + \frac{q_{m,i} K_i C_i}{1 + K_i C_i} \tag{3.17}$$

and linear + competitive Langmuir:

$$q_{e,i} = H_i C_i + \frac{q_{m,i} K_i C_i}{1 + \sum_{i=1}^{M} K_i C_i} \tag{3.18}$$

The physical and mathematical aspects of adsorption isotherms can be found in ROMANIELO (1999).

Another widespread mass transfer model is the Linear Driving Force (LDF). The main assumption in this model is that the mass transfer rate is proportional to the difference between the particle outer surface concentration (which is assumed to be in equilibrium with the fluid phase) and the average concentration within the particle. The overall mass transfer resistance is represented by a single coefficient, $k_f[T^{-1}]$, which is the effective transfer coefficient through the film around the particles; for nonlinear isotherms, it is a function of the fluid-phase concentration and the gradient $\frac{\partial q_i}{\partial C_i}$. Thus:

$$\frac{\partial q_{i,k}}{\partial t} = k_{f,i}(q_{e,i,k} - q_{i,k}) \tag{3.19}$$

In order to use the LDF model in a proper manner, the total porosity (ε) and the effective velocity (v_m) in Equation (3.1) must be replaced by the bed porosity (ε_b) and the interstitial velocity (v), respectively:

$$\underbrace{\frac{\partial C_{i,k}}{\partial t}}_{\substack{\text{Accumulation} \\ \text{rate}}} = \underbrace{-v_k \frac{\partial C_{i,k}}{\partial z}}_{\text{Advection rate}} + \underbrace{D_{ax,i,k} \frac{\partial^2 C_{i,k}}{\partial z^2}}_{\text{Diffusion rate}} - \underbrace{\left(\frac{1 - \varepsilon_{b,k}}{\varepsilon_{b,k}}\right) \frac{\partial q_{i,k}}{\partial t}}_{\text{Mass transfer rate}} \tag{3.20}$$

where $D_{ax,i,k}[L^2 T^{-1}]$ is the axial dispersion coefficient SCHIMIDT-TRAUB (2005).

More sophisticated models are available in the referenced literature (RUTHVEN, 1984; SHAFEEYAN *et al.*, 2014; THOMAS and CRITTENDEN, 1998) in which macro- and micro-pore diffusion resistances are discussed, however, those models were not used in this work.

The energy balance was not included into the model because the system is assumed to operate isothermally. This assumption is plausible, because the adsorption heat tends to be very low when physisorption is the only acting mechanism promoting mass transfer. As result, the mathematical model comprises a set of $2N$ Partial Differential Equations (PDE) when considering the local equilibrium model or $4N$ PDEs when considering linear driving force instead.

3.2.2 Spatial Discretization

In order to solve the PDEs system, the Method of Lines (MoL) was employed. The basic idea in this method is to approximate the spatial derivatives by an algebraic expression given by a discretization method and numerically integrate the resulting Ordinary Differential Equation (ODE) or Differential-Algebraic Equation (DAE) system with respect to the time (the remaining independent variable). Although the Finite Differences Method (FDM) is the most common way to discretize the spatial domain, finite volumes, finite elements or collocation methods, among others, can also be applied. First-, second- and fourth-order finite differences methods and the Global Polynomial Approximation (GPA) method were implemented in the developed software and are discussed below.

Finite Differences Method

In FDM, the first derivative can be approximated by a finite differences formula as follows:

$$\frac{\partial C_{i,k}(t,z)}{\partial z} \approx \frac{C_{i,k}(t)|_{\eta} - C_{i,k}(t)|_{\eta-1}}{\Delta z} \tag{3.21}$$

where the index $\eta = 1, 2, 3, \ldots, n$ designates the position z_η; thereby, the once continuous domain is transformed into a discrete one with n internal elements spaced by a length Δz with $1 \leq \eta \leq n$ and $\eta \in \mathbb{Z}$. Thus, a single PDE becomes a system of n ODEs. Equation (3.21) is a first-order approximation and is called *upwind differentiating scheme* because only backwards information is used in the approximation.

A second-order finite differences formula can also be used to approximate the first derivative:

$$\frac{\partial C_{i,k}(t,z)}{\partial z} \approx \frac{C_{i,k}(t)|_{\eta+1} - C_{i,k}(t)|_{\eta-1}}{2\Delta z} \tag{3.22}$$

which is called *central differentiating scheme* because the information is centered in discretization point η. However, for advective predominant systems it may cause unrealistic oscillations due to numerical errors propagation. For that kind of systems, the upwind scheme is more suited. High resolution non-oscillatory methods are available for first order derivatives discretization in hyperbolic PDEs, but they are out of the scope of this work. Further comments on the topic can be found elsewhere (MALISKA, 2004; WESSELING, 2001).

For systems in which the dispersion term is relevant, the second derivative is more accurately approximated by central finite differences formulas:

$$\frac{\partial^2 C_{i,k}(t,z)}{\partial z^2} \approx \frac{C_{i,k}(t)|_{\eta+1} - 2C_{i,k}(t)|_{\eta} + C_{i,k}(t)|_{\eta-1}}{(\Delta z)^2} \tag{3.23}$$

hence, Equation (3.1) is approximated by the set of equations:

$$\begin{aligned}\frac{dC_{i,k}|_{\eta}}{dt} = &- v_k \frac{C_{i,k}|_{\eta} - C_{i,k}|_{\eta-1}}{\Delta z} + \\ &+ D_{i,k} \frac{C_{i,k}|_{\eta+1} - 2C_{i,k}|_{\eta} + C_{i,k}|_{\eta-1}}{(\Delta z)^2} - \left(\frac{1-\varepsilon_k}{\varepsilon_k}\right) \frac{dq_{i,k}|_{\eta}}{dt}\end{aligned} \tag{3.24}$$

The boundary conditions in Equations (3.3) and (3.4), after a proper discretization, are given by:

$$\text{BC1:} \quad C_{i,k}|_{\eta=0} = \frac{\bar{C}_{i,k}(t) + \dfrac{D_{i,k}}{v_k \Delta z} C_{i,k}|_{\eta=1}}{1 + \dfrac{D_{i,k}}{v_k \Delta z}} \tag{3.25}$$

$$\text{BC2:} \quad C_{i,k}|_{\eta=n+1} = C_{i,k}|_{\eta=n} \tag{3.26}$$

Then, Equation (3.24) can be solved along with Equations (3.25) and (3.26) with standard ODE integration algorithms.

Fourth-order (upwind and central) finite differences approximations were also used to discretize the equations. These high-order formulas can be found in MAIA (2015).

Besides simplicity, another advantage of finite differences method is that the resulting ODE system is *sparse*, meaning that its jacobian matrix is composed mostly by null elements. If proper algorithms are used to handle sparse systems, both time and storing capacity can be drastically reduced as processing and memory will not be wasted on the zeroes.

Global polynomial approximation

Another discretization method applied for the z-coordinate in Equation (3.1) is the *polynomial approximation*. This method consists in approximate the

spatial profiles by a polynomial of order $n+1$ in the form:

$$C_{i,k}(t,z) \approx \sum_{\xi=0}^{n+1} \psi_\xi(z) C_{i,k}(t,z_\xi) \tag{3.27}$$

where

$$\psi_\xi(z) = \prod_{\substack{\eta=0 \\ \eta\neq\xi}}^{n+1} \left(\frac{z - z_\eta}{z_\xi - z_\eta} \right) \tag{3.28}$$

is the Lagrange's interpolating polynomial with the property:

$$\psi_\xi(z_\eta) = \delta_{\eta,\xi} = \begin{cases} 1, & \xi = \eta \\ 0, & \xi \neq \eta \end{cases} \tag{3.29}$$

where z_ξ are the roots of the Legendre's orthogonal polynomial of order n in the interval $z = [0,1]$. In order to increase the numerical performance, the dependent and independent variables of the model (C, t, z and q) should be normalized by a proper change of variables. By substituting Equation (3.27) in (3.1):

$$\begin{aligned} \sum_{\xi=0}^{n+1} \psi_\xi(z_\eta) \frac{dC_{i,k}(t,z_\xi)}{dt} = & -v_k \sum_{\xi=0}^{n+1} \left. \frac{d\psi_\xi(z)}{dz} \right|_{z_\eta} C_{i,k}(t,z_\xi) \\ & + D_{i,k} \sum_{\xi=0}^{n+1} \left. \frac{d^2\psi_\xi(z)}{dz^2} \right|_{z_\eta} C_{i,k}(t,z_\xi) - \left(\frac{1-\varepsilon_k}{\varepsilon_k} \right) \frac{dq_{i,k}(t,z_\eta)}{dt} \end{aligned} \tag{3.30}$$

and by defining:

$$A_{\eta,\xi} = \left. \frac{d\psi_\xi(z)}{dz} \right|_{z_\eta} \tag{3.31}$$

$$B_{\eta,\xi} = \left. \frac{d^2\psi_\xi(z)}{dz^2} \right|_{z_\eta} \tag{3.32}$$

(the procedure for calculating the matrices **A** and **B** is presented in the Appendix B) Equation (3.30) becomes:

$$\frac{dC_{i,k}(t)|_\eta}{dt} = \sum_{\xi=0}^{n+1}[(D_{i,k}B_{\eta,\xi} - v_k A_{\eta,\xi})C_{i,k}(t)|_\xi] - \left(\frac{1-\varepsilon_k}{\varepsilon_k}\right)\frac{dq_{i,k}(t)|_\eta}{dt} \tag{3.33}$$

Like in FD discretization, $C_{i,k}|_{\eta=0}$ and $C_{i,k}|_{\eta=n+1}$ are given by the boundary conditions in Equations (3.3) and (3.4) after they have been properly discretized:

BC1:

$$C_{i,k}|_0 = \frac{A_{0,n+1}\sum_{\xi=1}^{n} A_{n+1,\xi}C_{i,k}|_\xi - A_{n+1,n+1}\left(\frac{v_k\bar{C}_{i,k}(t)}{D_{i,k}} + \sum_{\xi=1}^{n} A_{0,\xi}C_{i,k}|_\xi\right)}{\left(A_{0,0} - \frac{v_k}{D_{i,k}}\right)A_{n+1,n+1} - A_{0,n+1}A_{n+1,0}} \tag{3.34}$$

BC2:

$$C_{i,k}|_{n+1} = \frac{A_{n+1,0}\left(\frac{v_k\bar{C}_{i,k}(t)}{D_{i,k}} + \sum_{\xi=1}^{n} A_{0,\xi}C_{i,k}|_\xi\right) - \left(A_{0,0} - \frac{v_k}{D_{i,k}}\right)\sum_{\xi=1}^{n} A_{n+1,\xi}C_{i,k}|_\xi}{\left(A_{0,0} - \frac{v_k}{D_{i,k}}\right)A_{n+1,n+1} - A_{0,n+1}A_{n+1,0}} \tag{3.35}$$

Equation (3.33) forms an ODE system and can also be solved along with Equations (3.34) and (3.35) with regular ODE system integrators.

In contrast to finite differences, global polynomial approximation leads to much smaller discretized systems, as it is a higher order method. However, the resulting system is *dense* (*i.e.*, its jacobian matrix is predominantly nonzero).

3.2.3 Initial Value Problems (IVP)

An initial value problem is an ODE (or a set of ODEs) in which the dependent variables are known at the starting point of integration, as expressed

by:

$$\begin{cases} \dfrac{dy}{dt} = f(t, y) \\ y(t_0) = y_0 \end{cases} \tag{3.36}$$

Numerical methods for IVP solving are grouped into two major categories, namely: (i) single step methods; and (ii) multiple step methods.

By integrating Equation (3.36) in the interval $[t_{k-1},\ t_k]$ for all $1 \leq k \leq n$ and $k \in \mathbb{Z}$:

$$\int_{t_k-1}^{t_k} \frac{dy}{dt}\, dt = y(t_k) - y(t_{k-1}) = \int_{t_{k-1}}^{t_k} f[t, y(t)]\, dt \tag{3.37}$$

therefore

$$y(t_k) = y(t_{k-1}) + \int_{t_{k-1}}^{t_k} f[t, y(t)]\, dt \tag{3.38}$$

The main idea behind the single step methods is approximate the integral in the right-hand side by a quadrature formula, for example a rectangular quadrature formula:

$$\int_{t_{k-1}}^{t_k} f[t, y(t)]\, dt \approx h \cdot f(t_{k-1}, y_{k-1}) \tag{3.39}$$

or

$$\int_{t_{k-1}}^{t_k} f[t, y(t)]\, dt \approx h \cdot f(t_k, y_k) \tag{3.40}$$

with $h = t_k - t_{k-1}$. Then, Equation (3.36) can be rewritten as:

$$y_k \approx y_{k-1} + h \cdot f(t_{k-1}, y_{k-1}) \tag{3.41}$$

or

$$y_k \approx y_{k-1} + h \cdot f(t_k, y_k) \tag{3.42}$$

so the state value at an instant k is successively approximated explicitly by Equation (3.41) or implicitly by Equation (3.42), from the starting point t_0 until a determined final point t_n, thus, composing a time series for the state variable with

$n+1$ elements. These equations are know as *Euler formulas* and can be generalized along with all the others single step methods known as *Runge-Kutta methods* in the form:

$$g_i = h \cdot f\left[t_{k-1} + hc_i\ ,\ y_{k-1} + \sum_{j=1}^{\nu} a_{i,j} g_j\right], \qquad \text{for } i = 1,\ 2, \ldots,\ \nu \tag{3.43}$$

$$y_k = y_{k-1} + \sum_{j=1}^{\nu} \omega_j g_j \tag{3.44}$$

where the coefficients c_i, w_i, and $a_{i,j}$ are selected according to the method order (in general, higher order means more accuracy); and ν is the number of stages (g).

In multiple step methods, the integrand $f[t,\ y(t)]$ in the right-hand side integral of Equation (3.36) can be approximated by a polynomial of degree $(m-1)$ through interpolation, considering the m previous known points y_{k-1}, y_{k-2}, $\ldots$, y_{k-m}. Then, the integral is evaluated and y_k can be estimated. Examples of multiple step methods are the Adams–Bashforth, Adams-Molton and Backwards Differentiation Formula (BDF), with the first one being explicit and the latter two implicit. All of these methods can be generalized in the form:

$$y_k = \sum_{i=1}^{m_1} a_{k,i} \cdot y_{k-i} + h_k \sum_{i=0}^{m_2} b_{k,i} \cdot f(t_{k-i}, y_{k-i}) \tag{3.45}$$

in which the coefficients $a_{k,i}$ and $b_{k,i}$ are tabulated; and the time step, h, is variable along with the integration.

It is worth mentioning that implicit methods, multiple or single step, require the solution of a nonlinear algebraic system at each integration step (usually the method of Newton is applied) which is a disadvantage as the costs to build the jacobian matrix often surpasses the costs of solving the original problem (ASCHER and PETZOLD, 1998).

On the other hand, for stiff problems[1], an explicit method requires impractically small time steps h (which greatly rises the number of steps) in order to keep the error bounded, as it is conditionally stable. For such kind of situations, an implicit method is more appropriated; due to its better stability, fewer steps are needed and extra computation is compensated (ASCHER and PETZOLD,

[1]Stiffness can be characterized in many ways, nevertheless it is related to multiple time scales. When, within the same problem, different phenomena with widely varying time scales are considered, or when two or more systems with very different dynamics are coupled, the problem is stiff (ASCHER and PETZOLD, 1998).

1998).

Efficiency of implicit methods for large sparse systems can be highly improved using sparse algebra to handle jacobian computation. In Chapter 4, a comparison between dense and sparse algorithms is presented.

3.2.4 Simulation strategy

The adopted simulation strategy is described below:

(i) In order to identify each column, they are numbered, *a priori*, from the first column of section I until the last one of section IV — the Nth column. Although the sections move along with the SMB operation, the columns remain fixed in space;

(ii) The equations are firstly solved from an arbitrary initial condition in the time interval $[0, b\theta]$, in which b is a switching counter and set to the unity ($b = 1$) at this step;

(iii) All the streams are switched to the next columns according to the flow direction;

(iv) The equations are solved again, but now from the previous state, in the time interval $[b\theta, (b+1)\theta]$;

(v) The switching counter is updated $b \leftarrow b + 1$;

(vi) Steps (iii) through (v) are repeated until cyclic steady state is reached.

This method was chosen because it is more accurate in terms of physical representability than the TMB approach. Also, it is more intuitive because conversion rules for the operating parameters (θ, Q_j) are not necessary. The only drawback is the resulting high-dimension partial differential equation system[2] to be solved but it can be handled by applying efficient numerical techniques.

3.3 Optimization Strategies

The full economic potential of simulated moving bed can be attained by optimizing the internal flow rates, Q, in the SMB sections. As discussed earlier,

[2]In the direct approach, there are $4(N-1)$ more PDEs than the TMB approach, when linear driving force is considered, or $2(N-1)$ PDEs, with the local equilibrium model.

there are many ways to formulate the optimization problem; in this work, the maximization of productivity was carried out considering an economic objective function expressed as follows:

$$F = Q_x \langle C_{x,B} \rangle \Lambda_x + Q_r \langle C_{r,A} \rangle \Lambda_r - Q_d \Lambda_d - \phi_x - \phi_r \tag{3.46}$$

where $\langle C_{x,B} \rangle$ and $\langle C_{r,A} \rangle$ are the average concentrations in the extract and raffinate at the cyclic steady state; Λ_x, Λ_r and Λ_d are weighting factors; and the terms ϕ_x and ϕ_r are penalties for off-specification purities in extract and raffinate given by:

$$\phi_p = \lambda_p \max\left(0, P_{p,min} - \langle P_p \rangle\right) \tag{3.47}$$

where $\langle P_p \rangle$ is the average purity ; $P_{p,min}$ is the minimum acceptable purity; λ_p is a weighting factor; and the index $p = r, x$ identifies the ports. Actually, these penalties have the role to replace nonlinear constraints for the purities, such as:

$$\langle P_p \rangle \geq P_{p,min} \tag{3.48}$$

The average quantities are calculated by integrating the concentrations in time as given by:

$$\langle C_{p,i} \rangle = \frac{1}{t_f} \int_0^{t_f} C_{p,i}(t) dt \tag{3.49}$$

$$\langle P_r \rangle = \frac{1}{t_f} \int_0^{t_f} \frac{C_{r,A}(t)}{C_{r,A}(t) + C_{x,B}(t)} dt \tag{3.50}$$

$$\langle P_x \rangle = \frac{1}{t_f} \int_0^{t_f} \frac{C_{x,B}(t)}{C_{r,A}(t) + C_{x,B}(t)} dt \tag{3.51}$$

in which t_f is the final integration time.

Unlike most of the works used as reference[3], the objective function F is maximized in regard to Q rather than m. Also, the feasible region is not defined by the triangle theory, but by the following set of physical constraints given by Equations (3.9)–(3.12):

$$Q_I \geq Q_{IV} \tag{3.52}$$

[3] ABEL *et al.* (2004); AGRAWAL *et al.* (2014); GROSSMANN *et al.* (2008); LI *et al.* (2014); SONG *et al.* (2006), among others.

$$Q_I \geq Q_{II} \tag{3.53}$$

$$Q_{III} \geq Q_{IV} \tag{3.54}$$

$$Q_{III} \geq Q_{II} \tag{3.55}$$

as all the external flow rates (Q_d, Q_x, Q_f, Q_r) must be greater than zero; also, the maximum flow rate the pumps provides:

$$0 \leq Q_j \leq Q_{max} \tag{3.56}$$

The optimization was conducted with MatLab's optimization toolbox. The adequate routine for constrained problems is the *fmincon* function. In order to use it properly, the maximization problem must be converted into a minimization one in the way:

$$\max_{Q_j} F = \min_{Q_j} -F \tag{3.57}$$

and the linear inequality constraints given by Equations (3.52)–(3.55) must be put in the matrix notation $\mathbf{Ax} \leq \mathbf{b}$, with:

$$\mathbf{A} = \begin{bmatrix} -1 & 0 & 0 & 1 \\ -1 & 1 & 0 & 0 \\ 0 & 0 & -1 & 1 \\ 0 & 1 & -1 & 0 \end{bmatrix} \qquad \mathbf{x} = \begin{bmatrix} Q_I \\ Q_{II} \\ Q_{III} \\ Q_{IV} \end{bmatrix} \qquad \mathbf{b} = \begin{bmatrix} 0 \\ 0 \\ 0 \\ 0 \end{bmatrix}$$

Equation (3.56) is represented by two vectors containing the lower ($\mathbf{lb}$) and upper ($\mathbf{ub}$) bounds for the optimization variables:

$$\mathbf{lb}^T = [0\ 0\ 0\ 0]$$

$$\mathbf{ub}^T = [Q_{I,max}\ Q_{II,max}\ Q_{III,max}\ Q_{IV,max}]$$

There are four optimization algorithms available in the *fmincon* function, namely: (i) interior-point; (ii) active set; (iii) sequential quadratic programming (SQP); and (iv) trust region reflective.

The most explored algorithm in this work was the interior point. The general idea in this algorithm is to solve a sequence of approximated problems. For

example, given the original optimization problem:

$$\begin{aligned}
&\min_{x} f(x) \\
&\text{subject to: } h_i(x) = 0,\ i = 1, 2, \ldots, m \\
&\qquad\qquad g_j(x) \leq 0,\ j = 1, 2, \ldots, p \\
&\qquad\qquad x \in X \subseteq \mathbb{R}^n
\end{aligned}$$

For each $\mu \geq 0$ there is an approximated problem of the form:

$$\begin{aligned}
&\min_{x,s} f_\mu(x) = min_{x,s} f(x) - \mu \sum_{j}^{p} \ln s_j \\
&\text{subject to: } h_i(x) = 0,\ i = 1, 2, \ldots, m \\
&\qquad\qquad g_j(x) + s_j = 0,\ j = 1, 2, \ldots, p \\
&\qquad\qquad x \in X \subseteq \mathbb{R}^n
\end{aligned}$$

in which s_j are the slack variables, restricted to be positive to keep the logarithmic barrier function bounded. The role of a barrier function in a objective function is to penalize violation of constraints. At the limit when $\mu \to 0$, the minimum of f_μ coincides to the minimum of f. The main advantage of this method is that the sequence of equality constrained approximated problems is easier to solve than the original inequality constrained problem (MATHWORKS, 2014).

3.4 Control Strategy

A nonlinear model predictive control was implemented in order to attain the purity specification at both (extract and raffinate) ports in the event of measured or unmeasured disturbances. The control strategy is presented in Figure 3.1 and described below.

The controller's objective function is given by:

$$J = \underbrace{\left(Q_x \langle C_{x,B} \rangle + Q_r \langle C_{r,A} \rangle - Q_d\right) \omega_1}_{\text{Economical Term}} - \underbrace{\left[(P_{x,min} - \langle P_x \rangle)^2 + (P_{r,min} - \langle P_r \rangle)^2 \right] \omega_2}_{\text{Set point}} \tag{3.58}$$

in which ω_1 and ω_2 are weighting factors. This objective function is not a usual

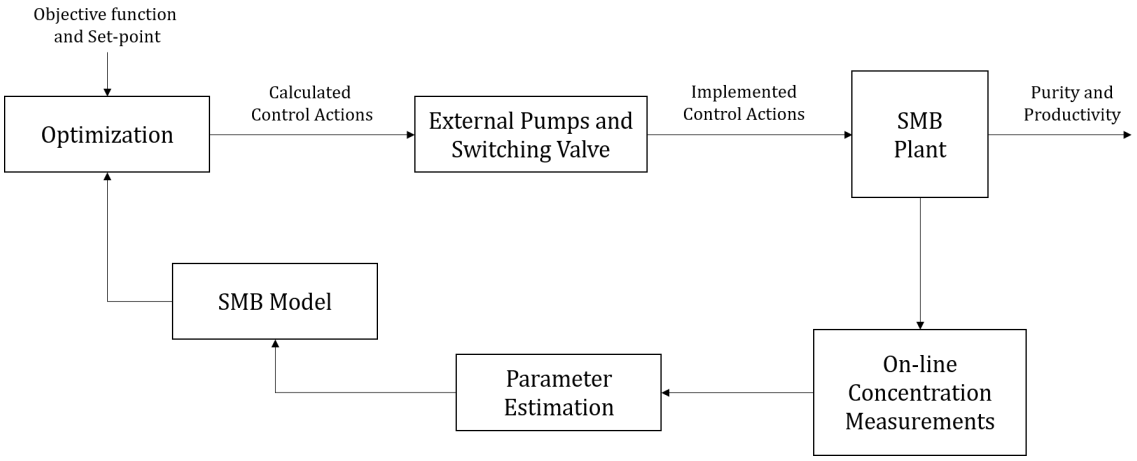

Figure 3.1: Adopted control structure for the simulated moving bed process

cost function involving just a tracking error for model predictive control. Instead of a multi-layer hierarchical architecture in which optimization and control are carried out at different sampling periods, both steps were merged together and the productivity was added in Equation (3.58) as an economical term, similar to the strategy presented by MORO and ODLOAK (1995) in which this term is a linear combination of the manipulated and controlled variables. Also, instead of evaluating the average concentrations and purities at cyclic steady-state, which would be the goal of a real-time optimization layer, they are evaluated at the end of the prediction horizon, H_p.

The same structure of the plant model was used in the controller, but uncertainties in parameters were added. In the controller's algorithm, the equations are integrated starting from the current states of the plant — which is assumed to be available from the on-line measurements step — until the end of the prediction horizon, in order to calculate the average quantities in Equation (3.58).

Five cases of instrument malfunction were considered:

(i) Solvent pump malfunction;

(ii) Extract pump malfunction;

(iii) Feeding pump malfunction;

(iv) Raffinate pump malfunction;

(v) Switching valve malfunction.

In case any of the four pumps fails, the controller optimizes the flow rates delivered by the other three and also the switching time. In case of switching

valve malfunction the four flow rates are optimized. Therefore, the controller works with four manipulated variables and two controlled variables whatever the control problem is.

The optimization step at the NMPC follows almost the same strategy presented in Section 3.3. The main difference is that one of the inequality constraints in Equations (3.52)–(3.55) is substituted for an equality constraint depending on what pump has failed:

Solvent pump malfunction (Instead of Equation (3.52))

$$Q_I - Q_{IV} = Q_d^* \tag{3.59}$$

Extract pump malfunction (Instead of Equation (3.53))

$$Q_I - Q_{II} = Q_x^* \tag{3.60}$$

Feeding pump malfunction (Instead of Equation (3.54))

$$Q_{III} - Q_{IV} = Q_r^* \tag{3.61}$$

Raffinate pump malfunction (Instead of Equation (3.55))

$$Q_{III} - Q_{II} = Q_f^* \tag{3.62}$$

where Q_d^*, Q_x^*, Q_r^* and Q_f^* are the flow rates delivered by the defective pumps. As result, the calculated control actions are the optimized internal flow rates. In order to implement them in the external pumps, Equations (3.9)–(3.12) must be used as a conversion rule.

The parameter estimation step shown in Figure 3.1 is necessary in order to deal with unmeasured disturbances — such as temperature oscillations, for example, that affect the adsorption equilibrium — and modeling errors as well. The measured concentrations are fed to the estimator at every sampling point, which is considered equal to the switching period, and the estimation is carried out. Hence, the optimizer always deals with updated plant information.

The function *lsqnonlin* of MatLab's optimization toolbox is used for parameter estimation, which solves nonlinear least squares problems. Among the available algorithms, the *Levenberg-Marquardt* was chosen.

Moreover, the online measurements are supposed to be made at a sampling time smaller than the time interval between the control actions and averaged within that same time interval. According to ABEL *et al.* (2005), polarimeters and UV detectors can be coupled in order to perform such fast assessment.

3.5 Developed Software

In order to compare the efficacy and performance of different models, as well as numerical efficiency, a software was developed in MATLAB® v7.6. Its Graphical User Interface (GUI) is presented in Figure 3.2. The equations presented in Section 3.2.1 are all available to model an SMB unit with the software. The parameters related to the binary mixture (feed concentrations, mass transfer coefficient *etc.*) can be provided in the *Less Retained* and *More Retained Component Parameters* panels. Information about the columns (geometry, void fraction, number of columns in the SMB arrangement *etc.*) can be provided in the *Column Parameters* panel. The internal flow rates are specified in their respective panel; in case the optimization option is activated those are the values for the optimum initial guess.

In the *Model Details* panel, the isotherm can be selected as well as the mass transfer model; it is also possible to select the boundary condition type and *turn on* or *off* the axial dispersion term in Equation (3.1). In the *Solver Control* panel the details of simulation are set (*e.g.* switching time, number of cycles) as well as the numerical methods (discretization method, integration algorithm *etc.*). With *Simulation Control* panel the simulation progress can be monitored and the *Output Control* panel is responsible to generate the results.

A control module was also developed and is presented in Figure 3.3. A virtual plant, which can be build with the modeling app, must be provided to the control app. In the *Model Uncertainties* panel, one can choose to use the same virtual plant model to be the controller's model (a perfect model); or to use a model with different parameters (plant-model mismatch). In the latter case, the controller's model can be build in the *Controller Model* panel. With the *Solver Details* tab, the user can set the weights $(\omega_1,\ \omega_2)$ and the stopping criteria for the NMPC's optimization step.

In the *Controller Settings* the set point values for the extract and raffinate purities and the prediction horizon can be set. Also, the failure of pumps and valves can be selected.

The system evolution (controlled and manipulated variables, productivity, internal flow rates, computation time *etc.*) can be monitored in real-time with the charts in the panel at the right side of the GUI.

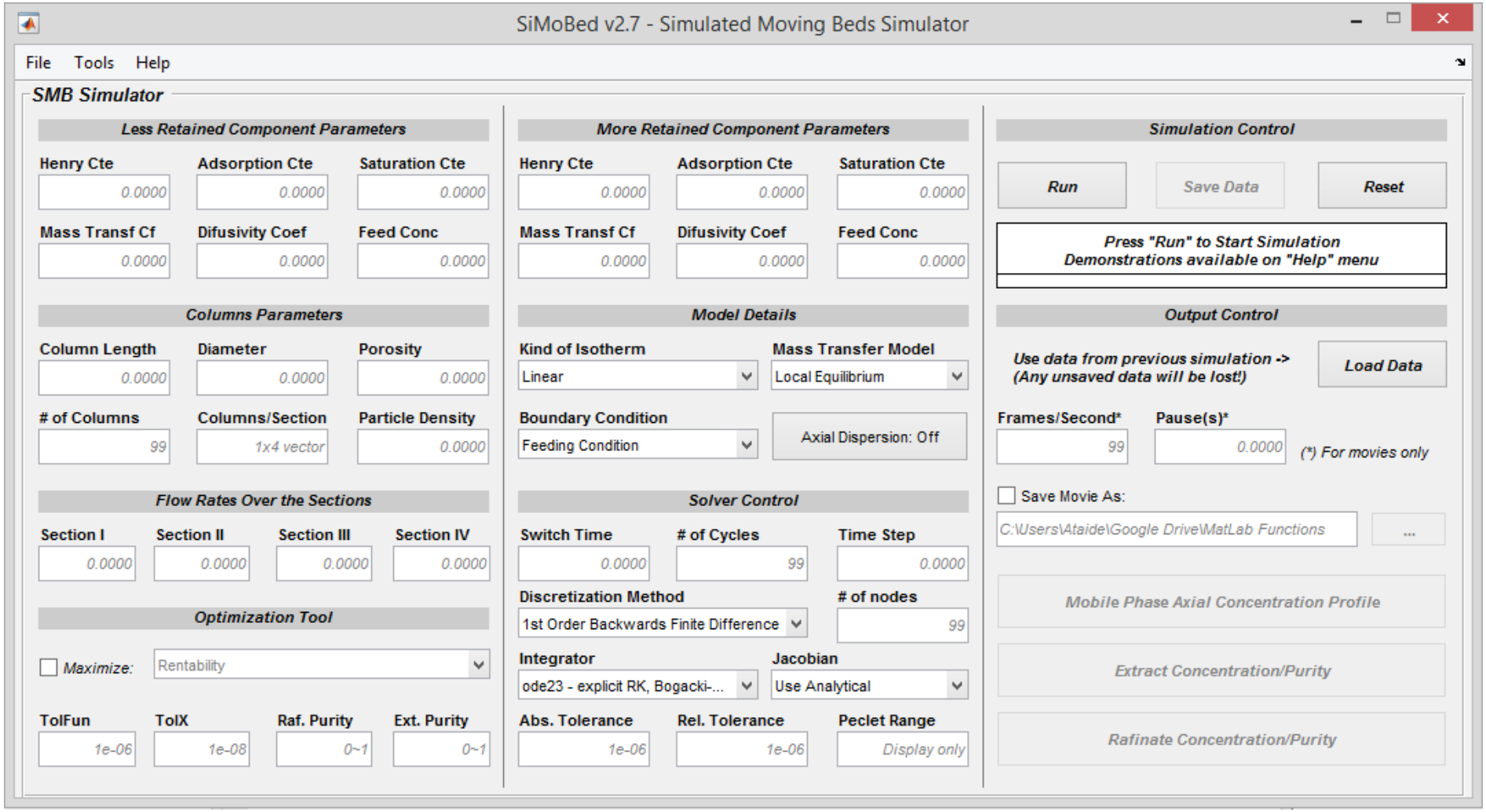

Figure 3.2: Developed software for modeling, simulation and optimization of SMB systems.

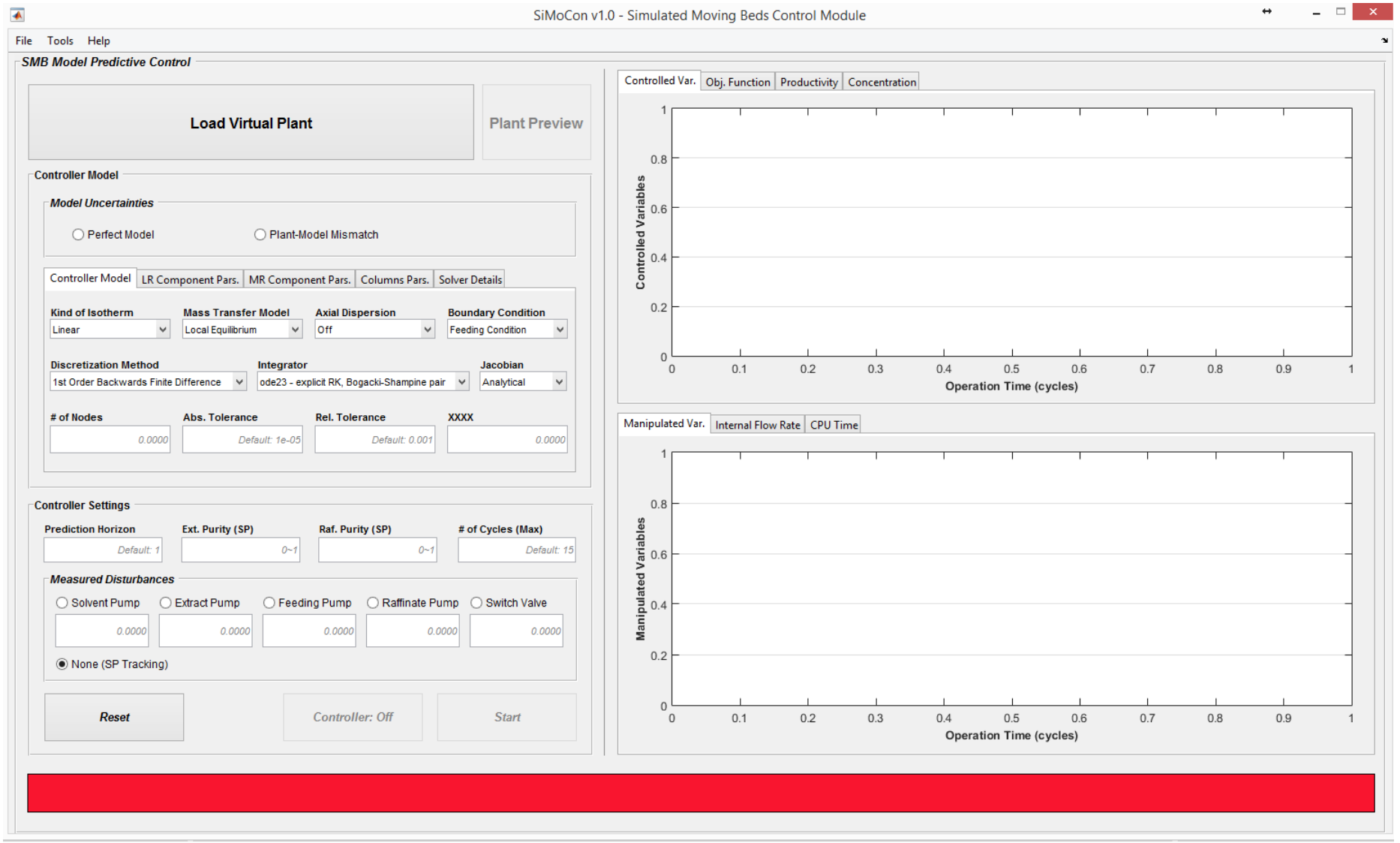

Figure 3.3: Developed software for control of SMB systems.

Chapter 4

Results and Discussion

Science is much better at finding things that exist than at ruling out things that don't.

Marcelo Gleiser

4.1 Simulation and Model Validation

In order to validate the modeling and simulation strategies, a comparative study between theoretical results obtained in this work and experimental data available in literature was carried out.

Preliminarily, the work of ABEL *et al.* (2005) was used as reference, in which the separation of bio-molecules uridine (A) and guanosine (B) was attained in a simulated moving bed system composed by eight columns of same length and diameter in a 2-2-2-2 configuration, that is, two columns in each section. The adsorption equilibrium is represented by the linear isotherm and the parameters provided by the authors are disposed in Table 4.1.

Five experimental runs under different operating conditions were reproduced in the developed simulation software, and the average purities at extract and raffinate ports in permanent regime were compared. In order to investigate the representability of the mass transfer models, the LDF model and the LEM were compared. The four methods for the spatial coordinate discretization, described in Section 3.2.2, were also investigated in order to compare the computational effort required to solve the equations.

Not surprisingly, the results for both mass transfer models (regardless the

Table 4.1: SMB parameters for the uridine (A)/guanosine (B) separation. Adapted from ABEL *et al.* (2005).

Column Parameters	Value	Equilibrium and Mass Transfer Parameters	Value	Operating Parameters	Value
$\ell(cm)$	10	H_B	2.299	$C_{f,B}(g/L)$	0.05
$d(cm)$	1	H_A	1.335	$C_{f,A}(g/L)$	0.05
ε	0.375	$k_{f,B}(min^{-1})$	19128	$\theta(min)$	2
$D_B(cm^2/min)$	1.02	$k_{f,A}(min^{-1})$	15204	$Q_I(cm^3/min)$	8.769
$D_A(cm^2/min)$	0.84			$Q_{IV}(cm^3/min)$	3.841

solution method) were the same. This is due to the high value of the coefficients $k_{f,A}$ and $k_{f,B}$; that means that the film around the particle does not offer resistance to mass transfer, therefore, the equilibrium between the phases is achieved very fast, or even instantaneously, which is the assumption of the local equilibrium model. These results are gathered in Table 4.2

Table 4.2: Comparison between LEM and LDF models for the uridine/guanosine separation.

Model	LEM (Raffinate/Extract Purities)	LDF (Raffinate/Extract Purities)
1st Order Finite Differences	99.91%/99.70%	99.90%/99.70%
2nd Order Finite Differences	100.0%/99.96%	100.0%/99.95%
Global Polynomial Approximation	100.0%/100.0%	100.0%/100.0%

Initially, the spatial domain was discretized by first order finite differences in a coarse mesh with 15 elements. Thereafter, a mesh test was conducted by doubling the number of grid points ($n = 30$, 60, 120 and 240). A mesh was considered refined when the maximum difference between the CSS concentrations obtained with two subsequent meshes was lesser than one percent, that is:

$$\max\left(\left|\frac{C_{i,k}^{\langle n_j\rangle}(t_\infty,z)-C_{i,k}^{\langle n_{j-1}\rangle}(t_\infty,z)}{C_{i,k}^{\langle n_j\rangle}(t_\infty,z)}\right|\right)\leq 0.01$$

As the two last meshes have attained the criterion, the chosen one was that with 120 elements. The same procedure was employed to the other finite

Table 4.3: Comparison between theoretical and experimental purities in CSS. Experimental data and operating parameters extracted from ABEL *et al.* (2005).

Run	Q_{II}	Q_{III}	P_r (exp)	P_r	P_x (exp)	P_x	$Error_r$ (%)	$Error_x$ (%)
1	5.670	6.876	99.6	100	99.8	100	0.40	0.20
2	5.719	6.926	99.1	100	99.7	100	0.90	0.30
3	5.817	7.024	95.8	97.6	99.8	100	1.80	0.20
4	5.964	7.171	89.7	89.3	99.7	100	−0.47	0.30
5	4.983	6.754	99.6	100	99.8	100	0.40	0.20

differences discretization methods, and the obtained results were: 120 elements for second order and 60 elements for forth order finite differences. For the global polynomial approximation, the first mesh had 6 points and the subsequent ones were increased by adding two elements until the above criterion was matched with 20 points.

An explicit second order Runge-Kutta and an implicit 5th order BDF integration algorithms (*ode23* and *ode15s* in MatLab, respectively) were selected to solve the system of ordinary differential equations, adopting 10^{-5} and 10^{-3} for the absolute and relative accuracies, respectively. To reach permanent regime, 20 cycles were necessary.

The errors between experimental and theoretical values are presented in Table 4.3. To obtain these results, the parameters in Table 4.1 were used; as the columns are assumed to be identical, the void fraction and dispersion coefficients are identical as well. Also, the LEM and a first order discretization with 120 elements were selected. With a maximum relative deviation of 1.8%, the results agree rather well with the experimental data.

In Table 4.4, the computational effort — measured in spent CPU time — for each discretization method is presented. The software was running inside MatLab on a PC equipped with intel core i7-3770K 3.50GHz processor and 8GB of RAM.

The 16 PDEs discretized by finite differences in a mesh with 120 elements result in an ODE system with 1,920 equations. Implicit algorithms suffer to solve a system of such dimension because of two factors: (i) the numerical costs to build the jacobian matrix; and (ii) the numerical costs to invert it, in order to use it at the Newton step of the algorithm. As consequence, the computation time drastically increases. However, part of the time spent in those calculations is wasted, because the majority of the jacobian elements of a system discretized by FD is null, *i.e.*, the system is sparse.

Table 4.4: Computational effort for different discretization methods. Twenty cycles simulated. DM stands for Dense-Matrix and SM for Sparse-Matrix.

Discretization Method	Mesh Points	Explicit Algorithm CPU Time (s)	Implicit Algorithm	
			CPU Time (s) (DM Algebra)	CPU Time (s) (SM Algebra)
1st Order Finite Differences	120	60.1	510.6	20.8
2nd Order Finite Differences	120	31.2	568.2	24.4
4th Order Finite Differences	60	17.5	161.2	19.4
Global Polynomial Approximation	20	13.8	36.1	not applied

The jacobian was built by the perturbation of each equation in the system in relation to every state variable ($C_{i,k}|_\eta$); the inversion was carried out by using methods such as the gaussian elimination or LU decomposition. For either procedures, time can be saved by not operating on the matrix zeroes. That can be done by passing to the integrator the jacobian sparsity pattern, in order to use sparse-matrix algebra algorithms. The sparsity pattern is a matrix filled up by "1s" in the positions where the jacobian is nonzero and by "0s" otherwise. The sparsity patterns for the aforementioned system are shown in Figures 4.1 and 4.2. For first order FD discretization, only 3,824 of the 3,686,400 elements are nonzero which corresponds to 0.1037% of the matrix. Similarly, for 2nd order only 0.1555% of the matrix are nonzero and for 4th order the percentage is 0.2579%. Half of the 102,400 elements of jacobian matrix resulting from global polynomial approximation discretization are nonzero, in this case, the sparse-matrix algebra employment was not effective, indeed, it was so ineffective that integration could not finish in a timely manner.

Although global polynomial approximation discretization is a less costly method, it is not suitable for predominantly advective systems where the profiles are flat. In order to obtain good results, 20 grid points were necessary and this is an excessive number. The ratio between the advective and dispersive effects is given by the Peclet number:

$$Pe = \frac{v\ell}{D} \tag{4.1}$$

which varies, for the system in study, between 50 and 100. For Peclet above 200,

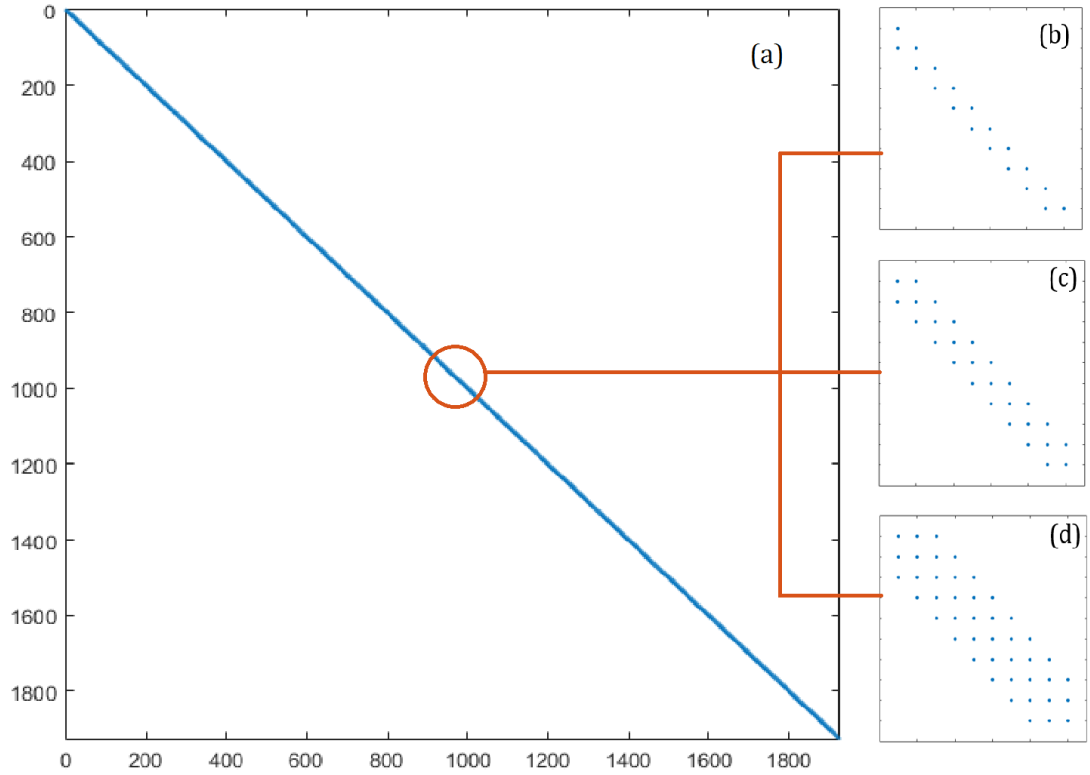

Figure 4.1: (a) Full system sparsity pattern for finite differences discretization; (b) magnification for 1st; (c) 2nd; and (d) 4th order finite difference discretization.

the number of grid points needed to obtain a converged mesh is very high; in such cases the polynomial approximation becomes less attractive than a finite differences method in terms of computational efficiency.

A simulated moving bed unit currently under construction at the *Laboratório de Cromatografia e Adsorção* (LABCADS) of *Universidade Federal do Rio de Janeiro* (UFRJ) for the separation of praziquantel was used as the physical model for this work. The system comprises 8 packed columns in a 2-2-2-2 configuration. The stationary phase is a cellulose based chiral adsorbent and the solvent is pure ethanol. All the parameters for columns, equilibrium and mass transfer were kindly provided by LABCADS (2015) and disposed in Table 4.5. The adsorption equilibrium for both enantiomers are represented by the competitive Langmuir isotherm and the axial dispersion effects could be justifiably neglected, as the Peclet number for the system is of the order 10^3. Even so, a comparison with and without the dispersion term in Equation (3.1) is present in Figure 4.3. The horizontal axis in Figure 4.3a is the dimensionless SMB length, measured in columns; and the vertical axis is the dimensionless fluid phase concentration, relative to the feeding concentration. In Figures 4.3b and 4.3c the

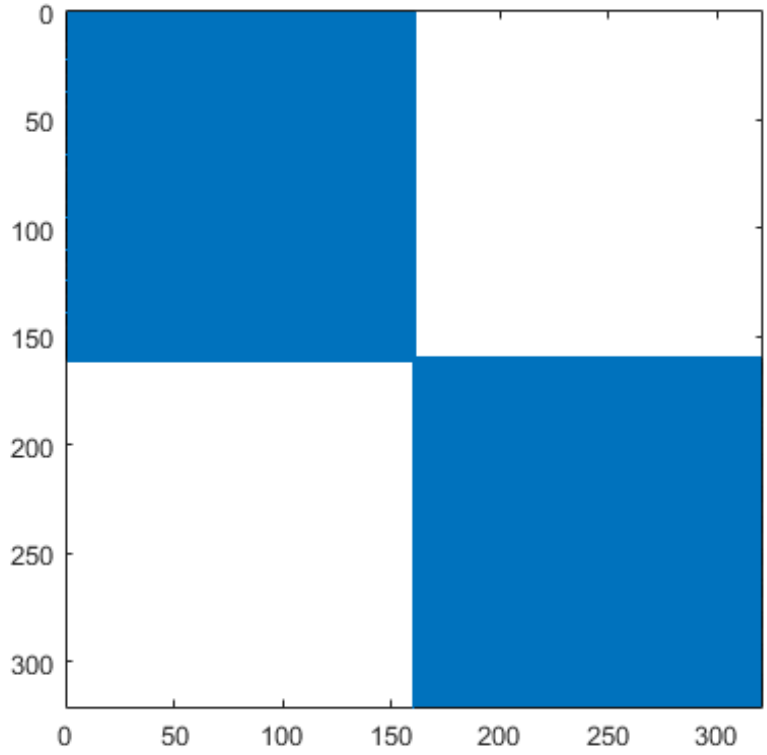

Figure 4.2: Full system sparsity pattern for global polynomial approximation discretization.

horizontal axis is the dimensionless time, measured in cycles; and the vertical axis is the dimensionless average concentration within the switching period, also relative to the feeding concentration. As it is seen, the internal profiles are very similar, as well as the outlet concentrations.

Likewise the guanosine/uridine separation, LDF and LEM were compared for praziquantel separation. The SMB concentration profiles in cyclic steady state and the extract and raffinate average concentrations for both mass transfer models are presented in Figure 4.4. Although the mass transfer effective coefficients for PZQ are two orders of magnitude lower than the previous system, the results show that inter-phase mass transfer resistances are not significant.

Unfortunately, there are no experimental data available in literature for praziquantel separation under the described conditions in order to verify the model representability. However, due to the similarity of the results obtained, the LEM was chosen for the analyses because it is less expensive in terms of computation. As the adsorption equilibrium of the praziquantel system is described by the competitive Langmuir isotherm, the jacobian sparsity pattern has less null elements, as can be seen in Figure 4.5, but in a mesh with 120 grid

Table 4.5: SMB parameters for the praziquantel separation. The index A denotes the less retained enantiomer and B the more retained one. Column, equilibrium and mass transfer parameters were provided by LABCADS (2015).

Column Parameters	Value	Equilibrium and Mass Transfer Parameters	Value	Operating Parameters	Value
$\ell(cm)$	25	$q_{m,A}(g/L)$	145	$C_{f,A}(g/L)$	1
$d(cm)$	0.46	$q_{m,B}(g/L)$	1693.3	$C_{f,B}(g/L)$	1
ε	0.82	$K_A(L/g)$	0.056	$\theta(min)$	2
$D_A(cm^2/min)$	1.1686	$K_B(L/g)$	0.0089	$Q_I(cm^3/min)$	7.467
$D_B(cm^2/min)$	1.2653	$k_{f,A}(min^{-1})$	168.94	$Q_{II}(cm^3/min)$	4.571
		$k_{f,B}(min^{-1})$	124.16	$Q_{III}(cm^3/min)$	6.912
				$Q_{IV}(cm^3/min)$	4.477

points, only 0.2076% of the jacobian matrix is nonzero.

4.2 Optimization

The flow rates in Table 4.5 are result of an infinity horizon optimization. As discussed before, the triangle theory is a good starting point for optimization and also for new separation systems design, in which previous information are scarce or even unavailable. For simplicity, the triangle for the linear isotherm was used as a starting point for the optimization problem; the Henry constants were approximated by the adsorptivities, which, for praziquantel enantiomers, are: $\gamma_A = q_{m,A}K_A = 8.12$ and $\gamma_B = q_{m,B}K_B = 15.07$.

The vertex W in Figure 2.5a are given by setting $m_{II} = \gamma_A$ and $m_{III} = \gamma_B$; additionally, there is the requirement that $m_I = m_{III}$ and $m_{IV} = m_{II}$ in order to optimize the regeneration of mobile and stationary phases. The internal flow rates are determined by isolating Q_j in Equation (2.5) as follows:

$$Q_j = \frac{(1-\varepsilon)Vm_j + V\varepsilon}{\theta} \tag{4.2}$$

which gives $Q_I = Q_{III} = 7.34\ cm^3/min$ and $Q_{II} = Q_{IV} = 4.74\ cm^3/min$. That set of flow rates with the switching time of 2 minutes lead to purities of 92.84% and 86.46% for extract and raffinate streams, respectively.

Then, the optimization was carried out as described in Section 3.3 within a horizon of 20 cycles, in order to obtain the average concentrations, $\langle C_{p,i} \rangle$, and

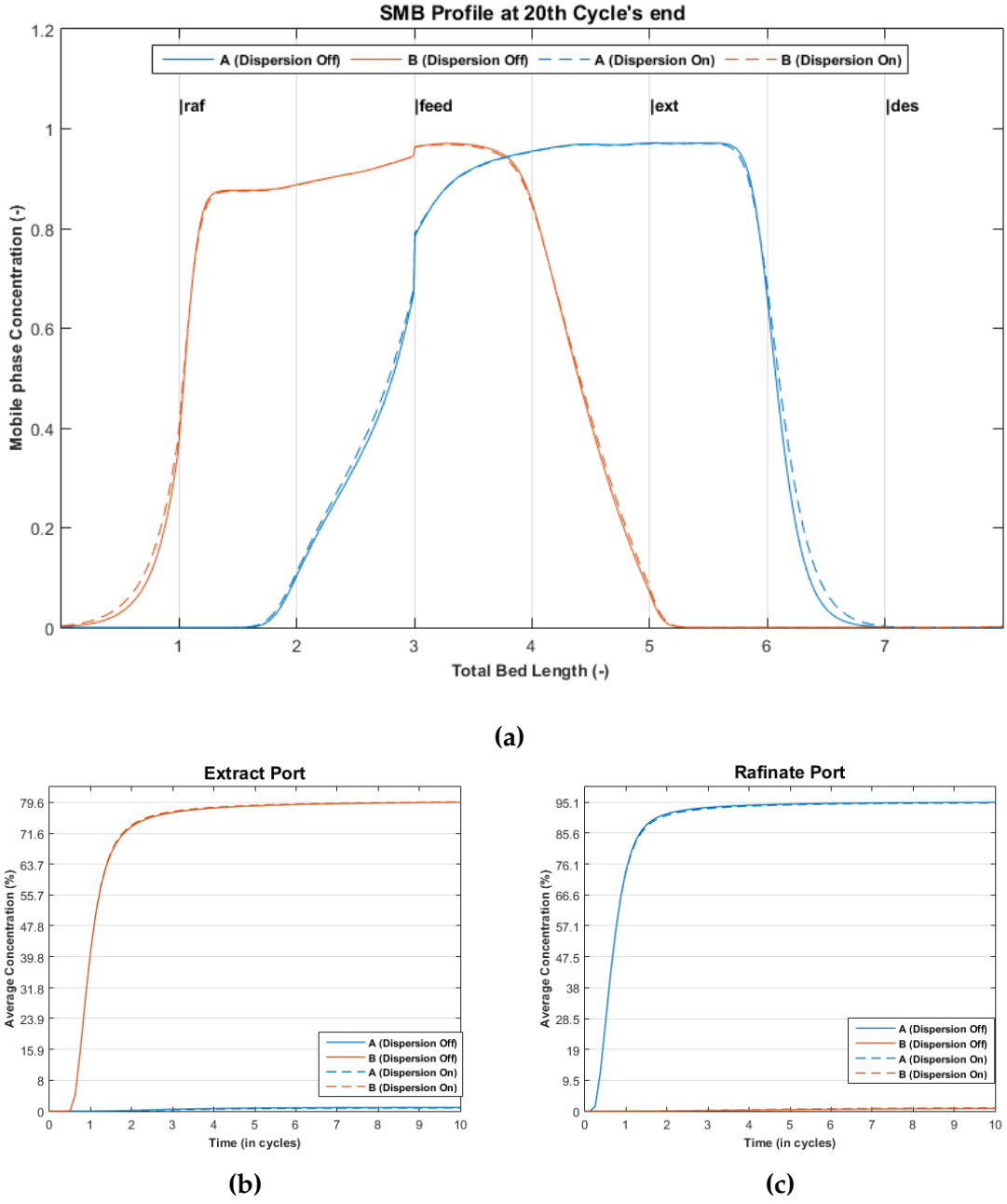

Figure 4.3: Axial dispersion effects comparison for praziquantel (a) SMB internal profiles; (b) extract port; and (c) raffinate port.

purities, $\langle P_p \rangle$, at the permanent regime. Also, the purity constraint — inserted into the objective function as penalties — were established in 99%; note that, because the functional form of the penalty, only purities below this level are penalized. The main advantage of stating the optimization problem in this way is that, if there are no nonlinear constraints, computational effort will not be wasted on the calculation of their gradient vectors (required for derivative-based methods).

The optimum operating condition is right over the purity constraints —

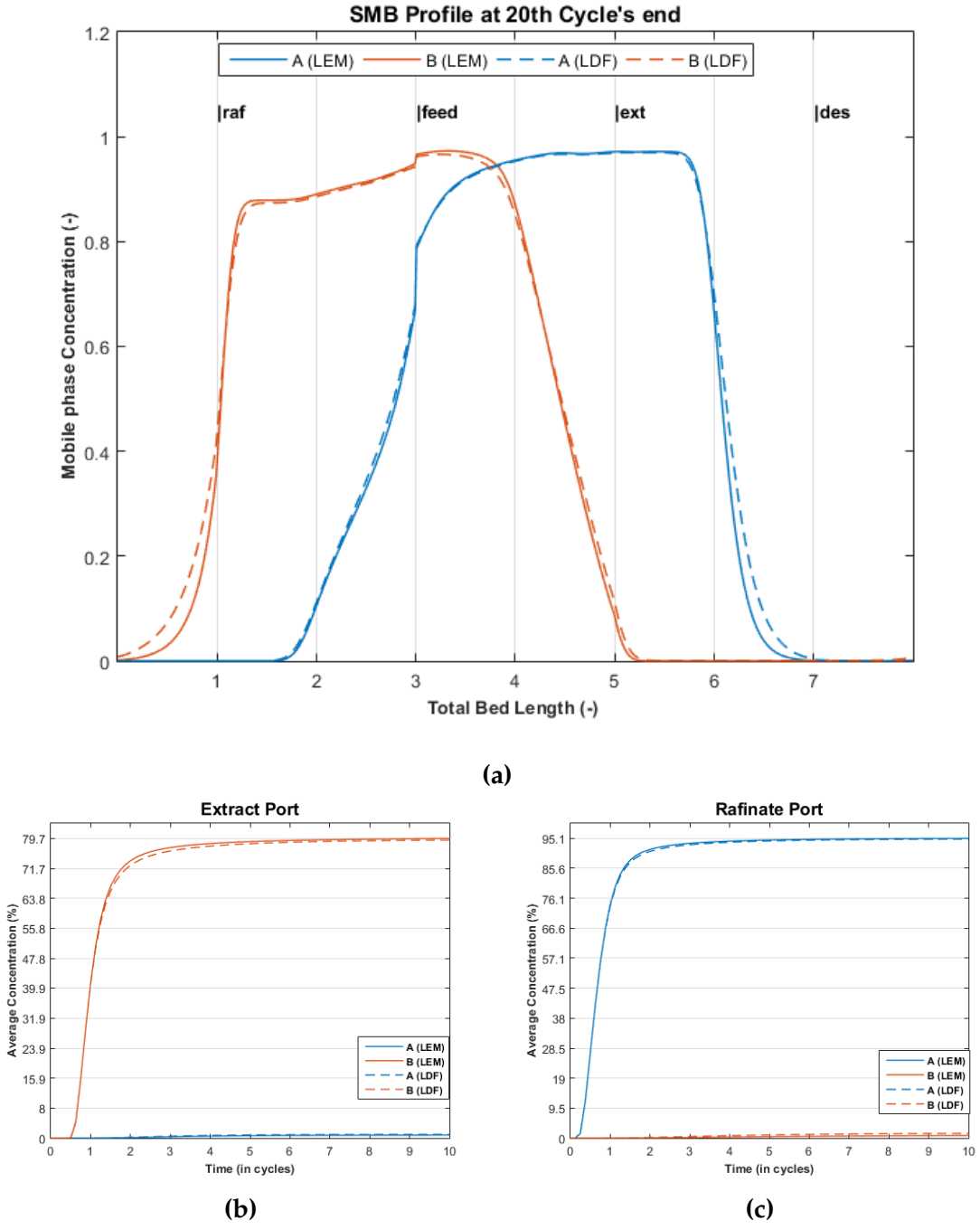

Figure 4.4: Local equlibrium and linear driving force models comparison for praziquantel (a) SMB internal profiles; (b) extract port; and (c) raffinate port.

99.01% and 99% for extract and raffinate, respectively. This is reasonable because it is expected a higher productivity when operating in a more relaxed purity condition.

This optimization strategy is very time consuming, taking about 80 minutes to finish. Three factors that contribute to this can be pointed out. First, the high cost to evaluate the objective function — this is a consequence of the sequential

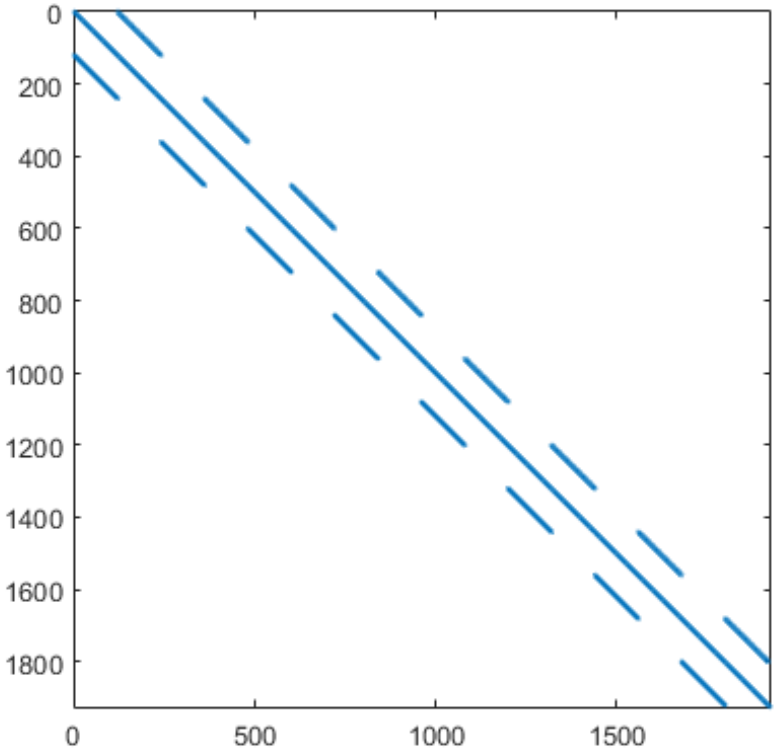

Figure 4.5: Jacobian sparsity pattern for praziquantel separation. Local equilibrium model, competitive Langmuir isotherm, no dispersion effects and 1st order finite differences discretization with 120 elements.

approach used in order to obtain the CSS average concentrations and purities. Second, the excessive number of function evaluations (around 250) in order to calculate the gradient vector, as the interior-point algorithm is a derivative-based method. Third, the great number of iterations (around 50), probably because of the shape of the objective function, which has "valley" regions — slowing down the search for the optimum — as can be seen in the two-dimension sectional cuts in Figure 4.6.

4.3 Control

A number of different control problems are presented and discussed in this section in order to evaluate the performance of the control scheme proposed in Section 3.4. It was considered, in every scenario, that the plant was operating at the optimum condition, which was determined with the off-line optimization aforementioned, and then disturbed in someway. The initial state of the plant used for all the control problems is presented in Table 4.6. The

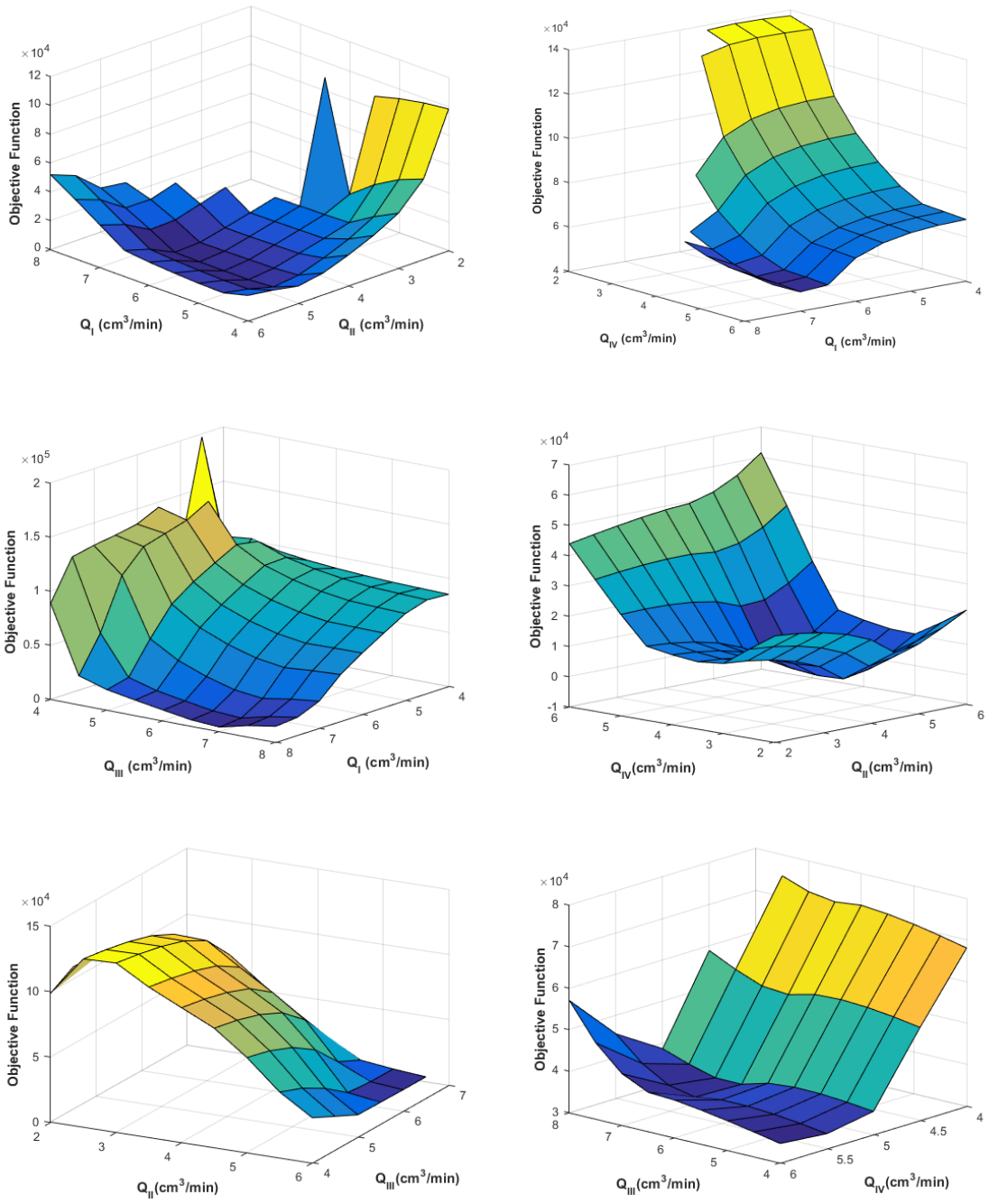

Figure 4.6: Sectional cuts of the 4D objective function given by Equation (3.46).

range of the flow rates delivered by the pumps were considered to be between 0.001 and 20 mL/min, which is the range of the HPLC pumps used in LABCADS simulated moving bed unit. The switching period lower and upper bounds were set to 1 and 10 minutes.

The case studies were grouped into two classes. The first class regards to instrumentation malfunction and set point tracking problems, the most common ones in a simulated moving bed plant; here, it was considered that the model

Table 4.6: Plant initial state for the addressed control problems.

Operating parameter	Value
Q_d	2.993 mL/min
Q_x	2.899 mL/min
Q_f	2.341 mL/min
Q_r	2.436 mL/min
θ	2 min
$\langle P_x \rangle$, $\langle P_r \rangle$	99%
$C_{f,A}$, $C_{f,B}$	1 g/L

represents the plant without error, *i.e.*, the model is perfect; also, it is worth mentioning that every time one of the pumps fail, at least one of the others must follow the disturbance in order to guarantee that the global mass balance is not violated — operationally that can be done by the employment of a Fault Detection and Diagnostics (FDD) algorithms (CORREIA DA SILVA *et al.*, 2009). The second class of problems deals with the occurrence of unmeasured disturbances and plant-model mismatch. The separation of praziquantel enantiomers was used as an illustrative example once more.

4.3.1 Solvent Pump Malfunction

Several tests were carried out considering the case in which the solvent pump had malfunctioned. At first, in Figure 4.7 the uncontrolled system response for a decay of 20% in the delivered solvent flow rate is presented — the extract pump follows the perturbation in order to avoid violation of the global mass balance. This kind of response is useful in order to gather information of the process dynamics which may come in handy for controller tuning.

The disturbance was applied at $t = 1$ cycle, as well as all other henceforth disturbances. As result, both controlled variables were displaced from the set point; the extract purity has less sensitivity to solvent flow rate fluctuations than the raffinate purity, which is evident by the levels reached when the system settled down after eleven cycles; these levels were around 98.85% and 88.10%, respectively. Also, it is possible to observe a time delay of one cycle in the raffinate purity response.

In Figures 4.8 to 4.12, the controlled system response to the same decay of 20% in the solvent pump flow rate is shown along with the manipulated variables trajectory, internal flow rates, productivity and the remaining time between the end of an optimization and the start of the next sampling. The

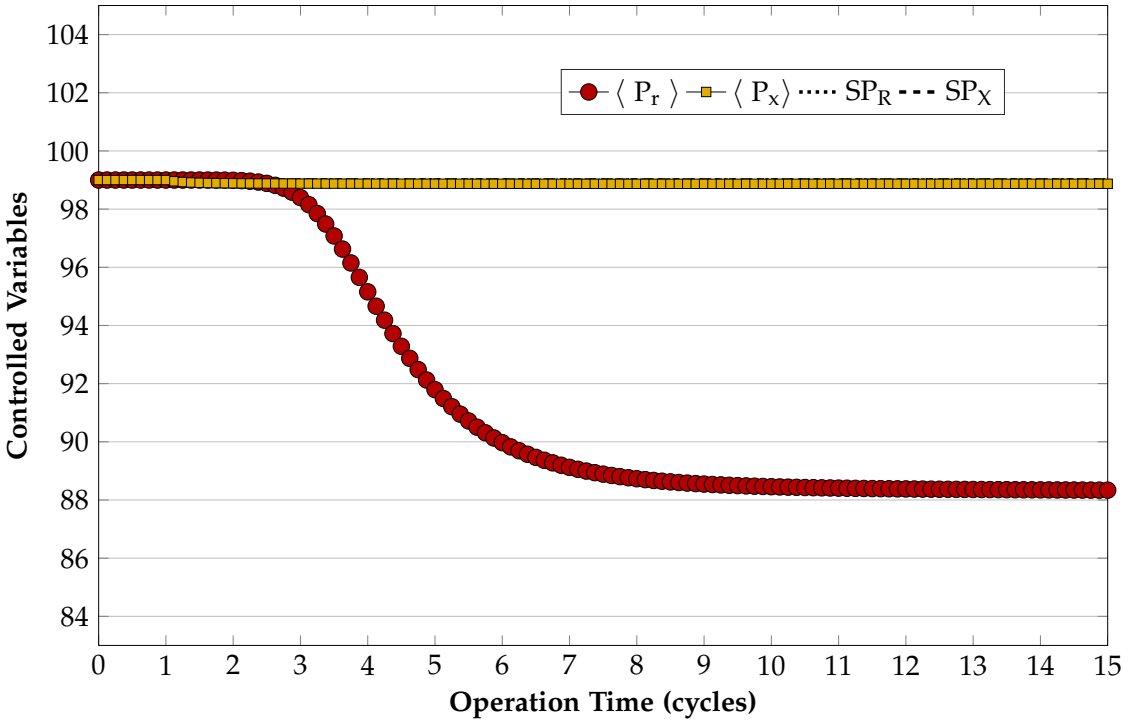

Figure 4.7: Uncontrolled system response for a perturbation of -20% in the solvent pump at $t = 1$ cycle. Set point fixed in 99%. Red circles represent raffinate purity and yellow squares represent extract purity.

prediction horizon should be such that the controller anticipates constraint violations early enough to allow corrective action. With that in mind, the value of H_p was set to one cycle — which is equivalent to eight sampling periods — and held constant while varying the cost function weights, ω_1 and ω_2, in order to tune the controller. A smaller prediction horizon, nonetheless, should not work properly because of the time delay seen by the uncontrolled behavior already discussed. The selected values, by trial-and-error, for the weights were $\omega_1 = 10$ and $\omega_2 = 1 \times 10^5$.

By the analysis of Figure 4.8, it is seen that the controller does not let the product streams get out of specification for a long time and tries to push the system in the opposite direction of the perturbation. It can also recover from the disturbance in five cycles — which is fast response — and with small control effort, as can be seen by the trajectories in Figure 4.9 where the maximum difference between two consecutive actions does not exceed 10%. At first, the extract pump accompanies the solvent pump decrease (which is fixed at $Q_d^* = 2.4\ mL/min$ over the entire time) and later available to be manipulated.

The loss of productivity seen in Figure 4.11 could not be avoided by the controller, even though the extract concentration had increased with the solvent decay in the system. That happens because the decrease in extract and raffinate

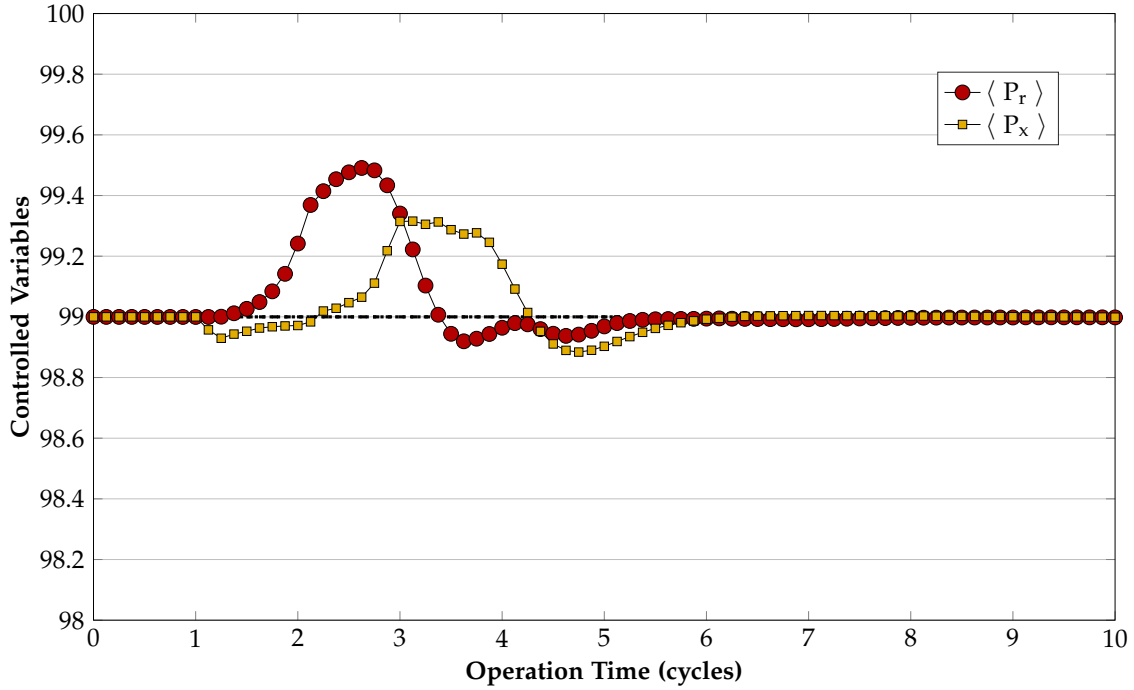

Figure 4.8: Controlled system response for -20% in solvent pump — purities in percentage.

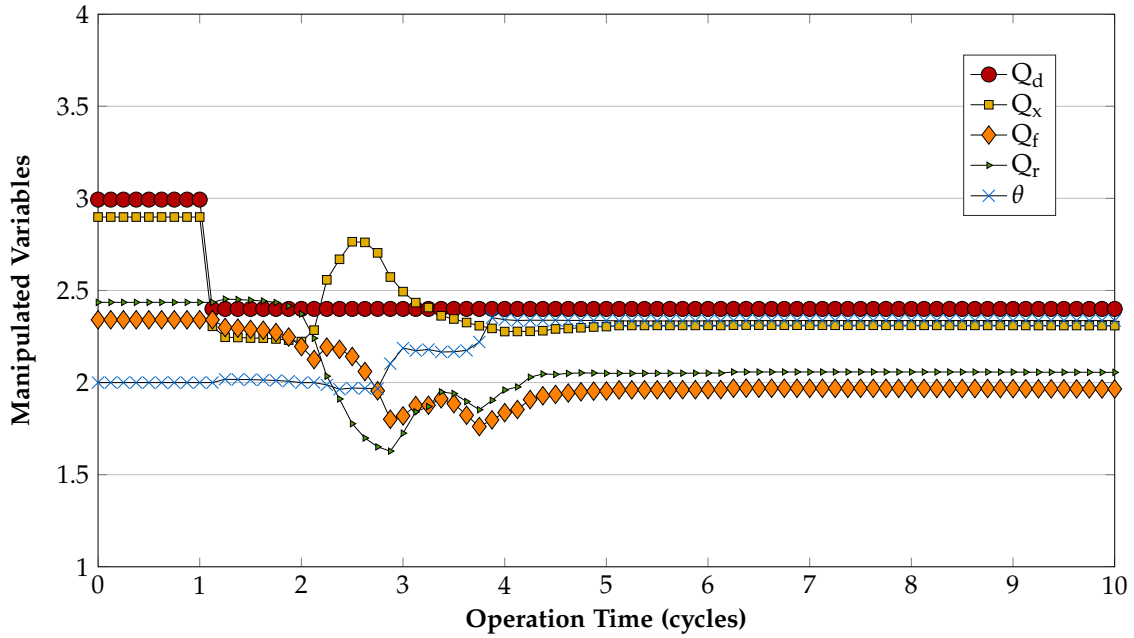

Figure 4.9: Controlled system response for -20% in solvent pump — external flow rates in mL/min and switching period in min.

flow rates are higher in magnitude, overcoming the concentration influence in the productivity. The same loss was observed by setting $\omega_1 = 0$, *i.e.*, when the economical term is not taken into account in Equation (3.58). However, $\omega_1 \neq 0$ granted the controller more stability.

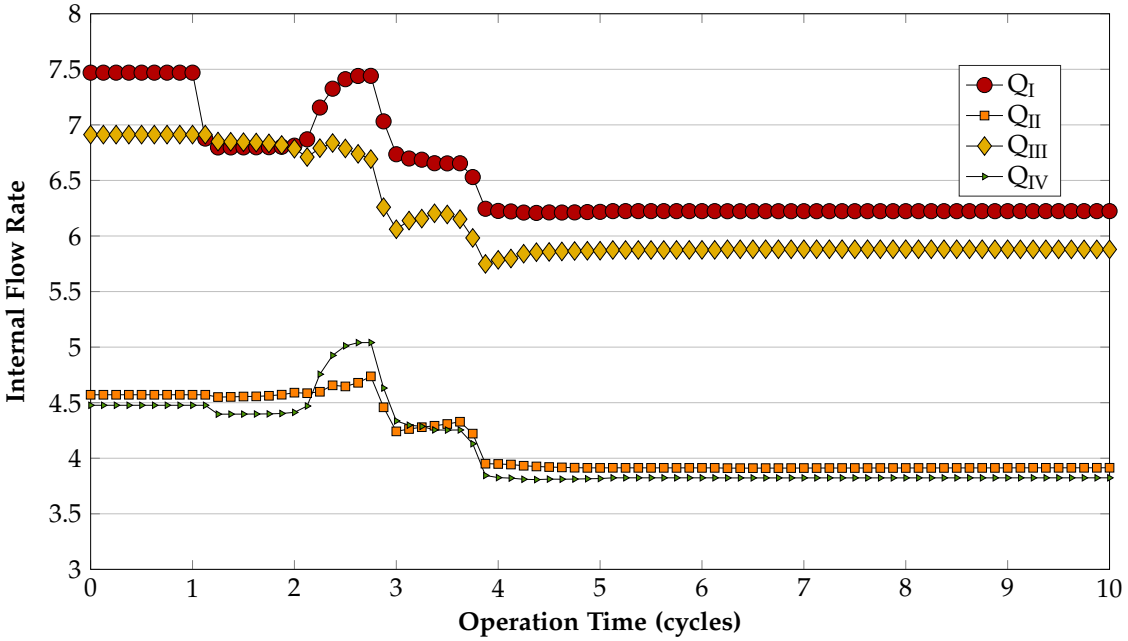

Figure 4.10: Controlled system response for -20% in solvent pump — internal flow rates in mL/min.

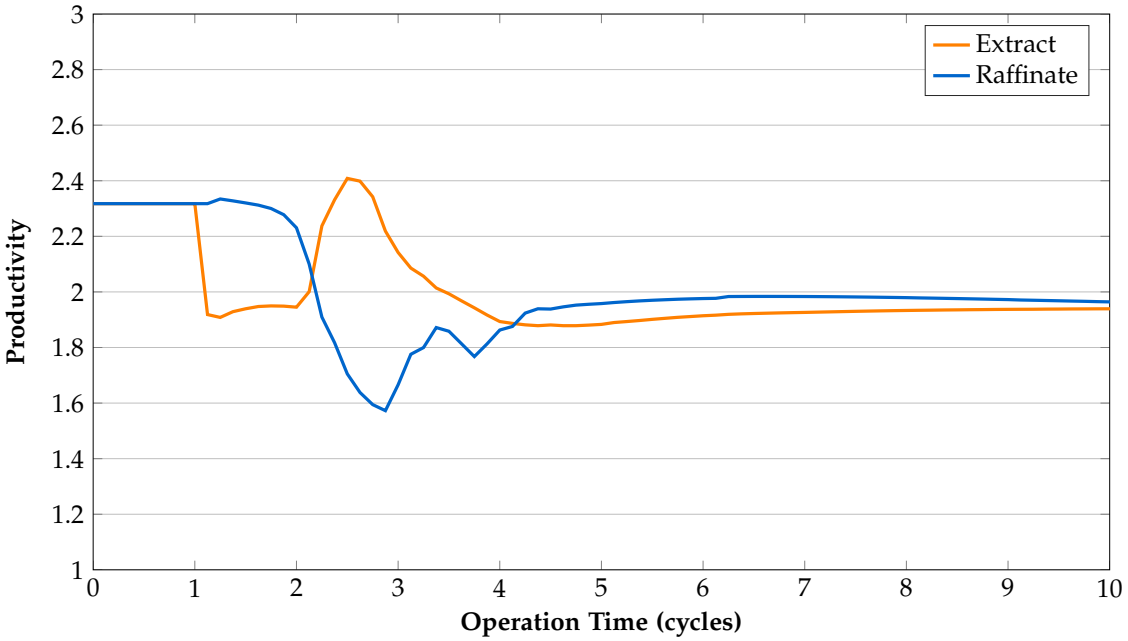

Figure 4.11: Controlled system response for -20% in solvent pump — productivity in g/min.

The idle time presented in Figure 4.12 is the difference between the spent computational time Θ_{CPU} and the sampling time Θ_{sample}, which is equal to the switching time θ; if it is negative, it means that there is still time available to implement the control action (the more negative, the better); in contrast, if it is positive, it means that computation exceeded the sampling time. It is seen in the chart that the shortest time window to apply the calculated control actions

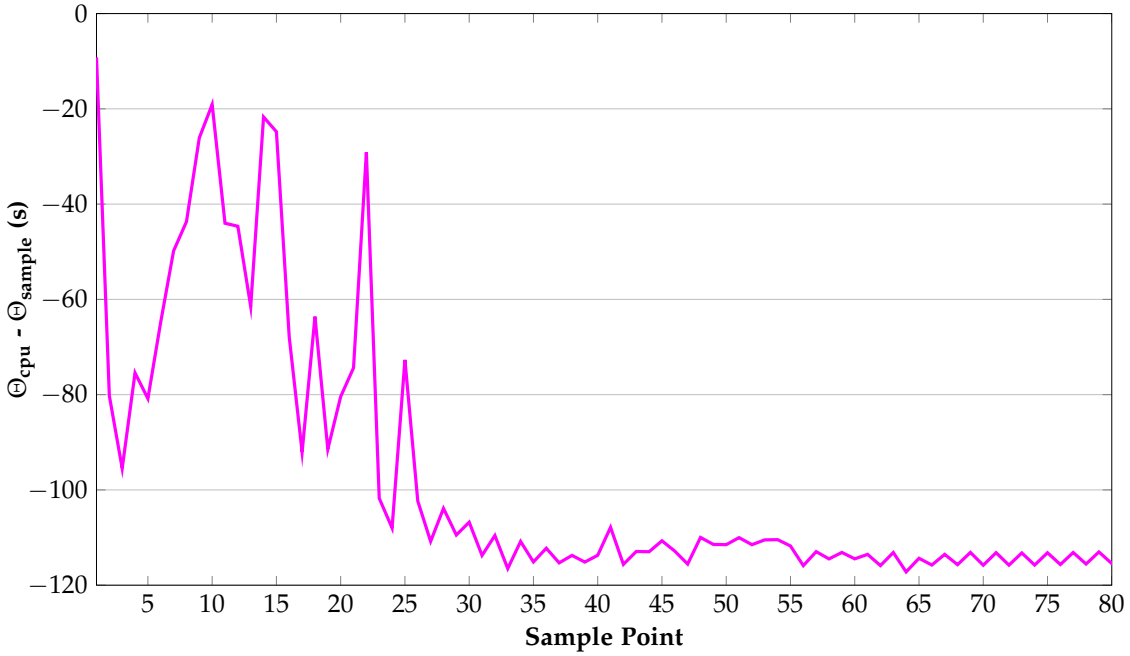

Figure 4.12: Controlled system response for −20% in solvent pump — remaining time between end of optimization and start of the next time sampling.

is the first sampling point. This is reasonable because the first optimization has the worst initial guess.

Computational time could be saved at this step by finding a set of flow rates plus the switching period that are close to the optimum and, at the same time, satisfy the equality constraint given by Equation (3.59) in order to provide them to the optimizer, in the same way that the triangle theory was used to obtain a good initial guess for the off-line optimization. Finding this set of flow rates turned out to be a difficult task. The initial guess for any other sampling point is always the last control action taken, which is known to satisfy the constraint.

In order to test the controller's efficacy, perturbation of −50% was applied at the solvent pump, which is a more challenging malfunction scenario. The results are similar to the previous case study and are compiled in Figure 4.13. It is worth to point out the faster response for the case without control, which shows the non-linearity of the SMB process mentioned in Section 2.5.3. If it was a linear process, we would expect that only the new CSS purity level differed, not its time constant as was the case.

Moreover, the controller could not handle the abrupt change in the solvent flow rate with a prediction horizon of one cycle; for this reason, H_p was set to two cycles. Even though a greater value of H_p increases the computational costs to evaluate the objective function in the controller, the time span for implement

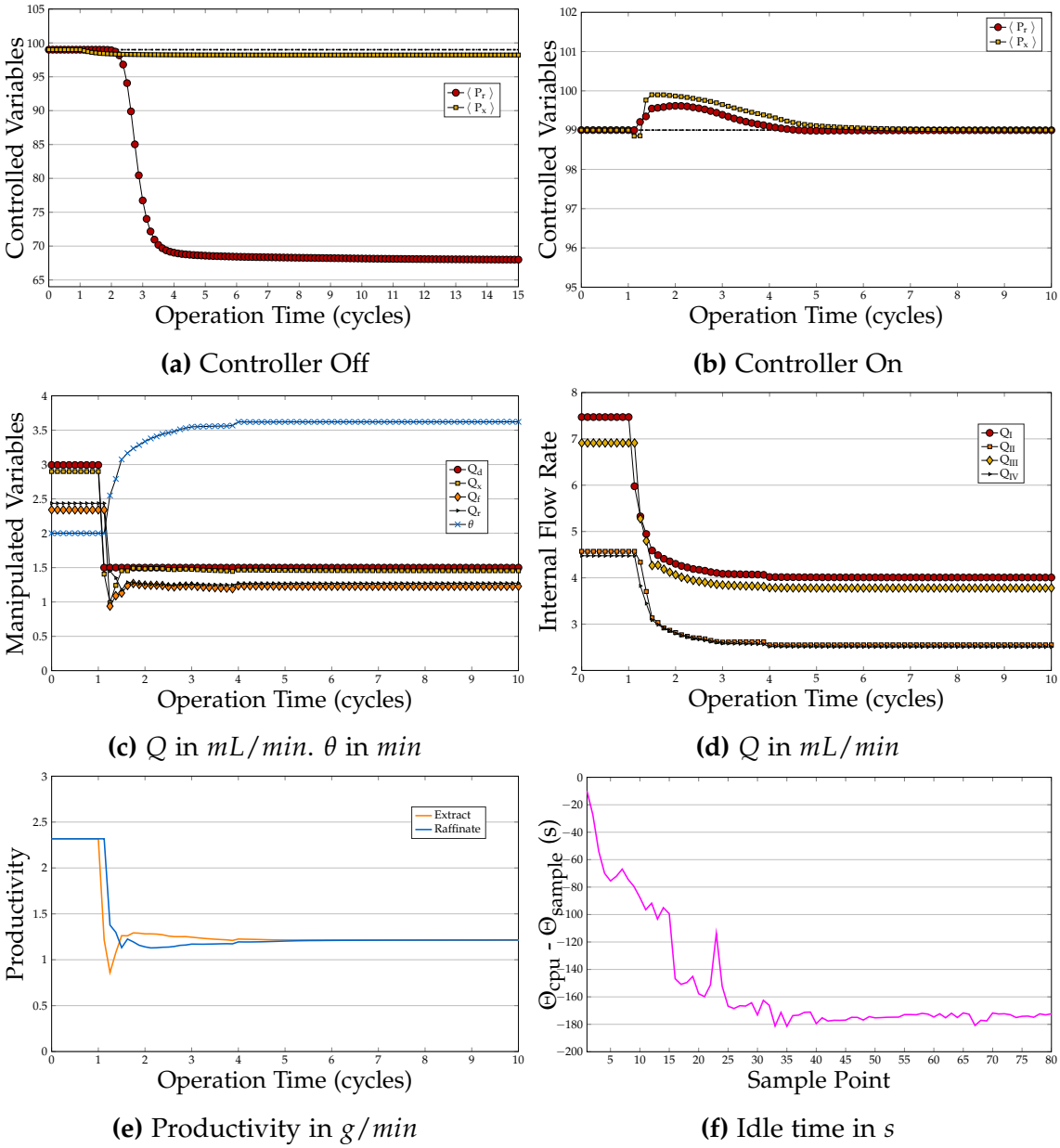

(a) Controller Off

(b) Controller On

(c) Q in mL/min. θ in min

(d) Q in mL/min

(e) Productivity in g/min

(f) Idle time in s

Figure 4.13: Compilation of the results for a decrease of 50% in the solvent pump flow rate.

the action was not compromised because the switching period (that also is the sampling time) increased as well.

Positive disturbances were also applied to the solvent pump, but they had no effect on the controlled variables or productivity, which is reasonable because the excess of solvent are removed in the extract port; moreover, it causes just a dilution of the components in the section I, without affecting their relative proportion, as its velocities remain unchanged.

4.3.2 Feeding Pump Malfunction

Feeding pump malfunction scenarios were investigated in the same manner of the previous case study. In Figure 4.14, the uncontrolled system response for a perturbation of -20% is presented. The decrease in feeding pump flow rate is followed by a decrease in raffinate pump flow rate as well, in order to not violate the global mass balance. As can be seen, the response for this perturbation is very distinguished from the solvent pump malfunction uncontrolled responses. The first difference to notice is that the raffinate purity gain is positive. Also, the time delay now occurs in the extract purity, which is reasonable because the fluctuations on the feeding flow rate are reflected instantaneously in the section III flow rate, likewise the solvent flow rate instantaneously affects section I flow rate.

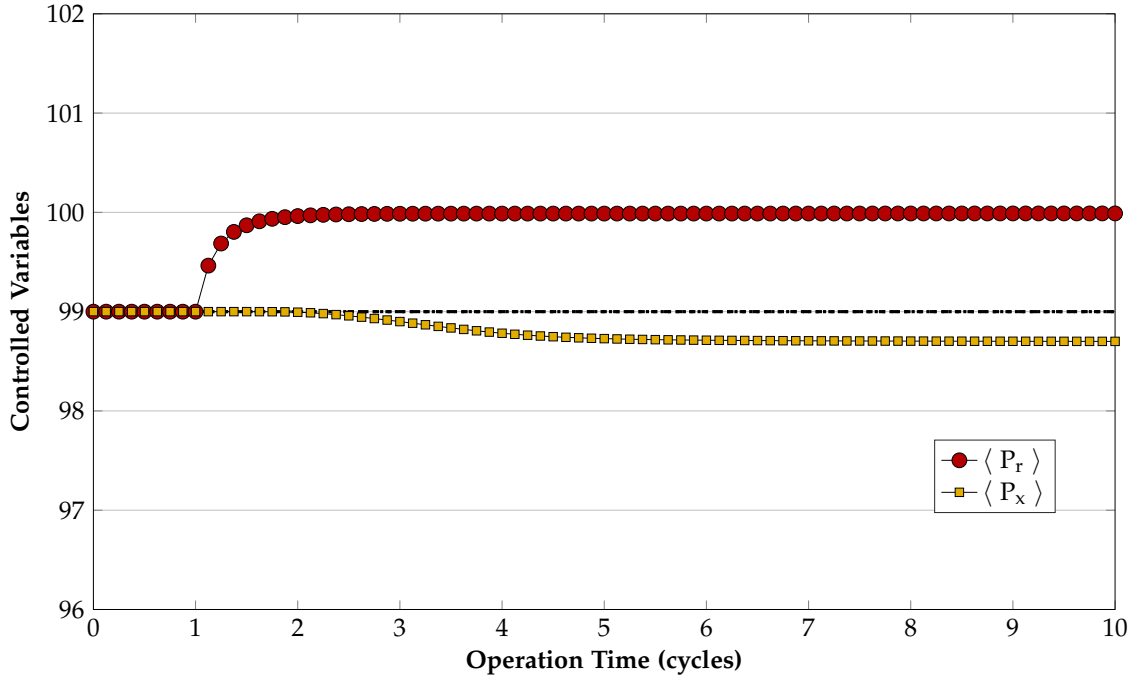

Figure 4.14: Uncontrolled system response for a perturbation of -20% in the feeding pump flow rate.

The controller was able to bring the purities back to the set point but at the cost of hard control actions. In order to reduce the stress over the pumps, a new set of tuning parameters was sought starting from the latter one and fixed in: $H_p = 2$ cycles, $\omega_1 = 100$ and $\omega_2 = 1 \times 10^5$, which lead to a stable controlled response with small control effort and feasible computation time. As mentioned before, the raffinate pump flow rate follows the decrease in the feeding pump flow rate at the first sampling point but later is freed to be manipulated.

Productivity losses could not be prevented, because of the decrease in the

extract and raffinate outlet concentrations. These results are summarized in Figure 4.15.

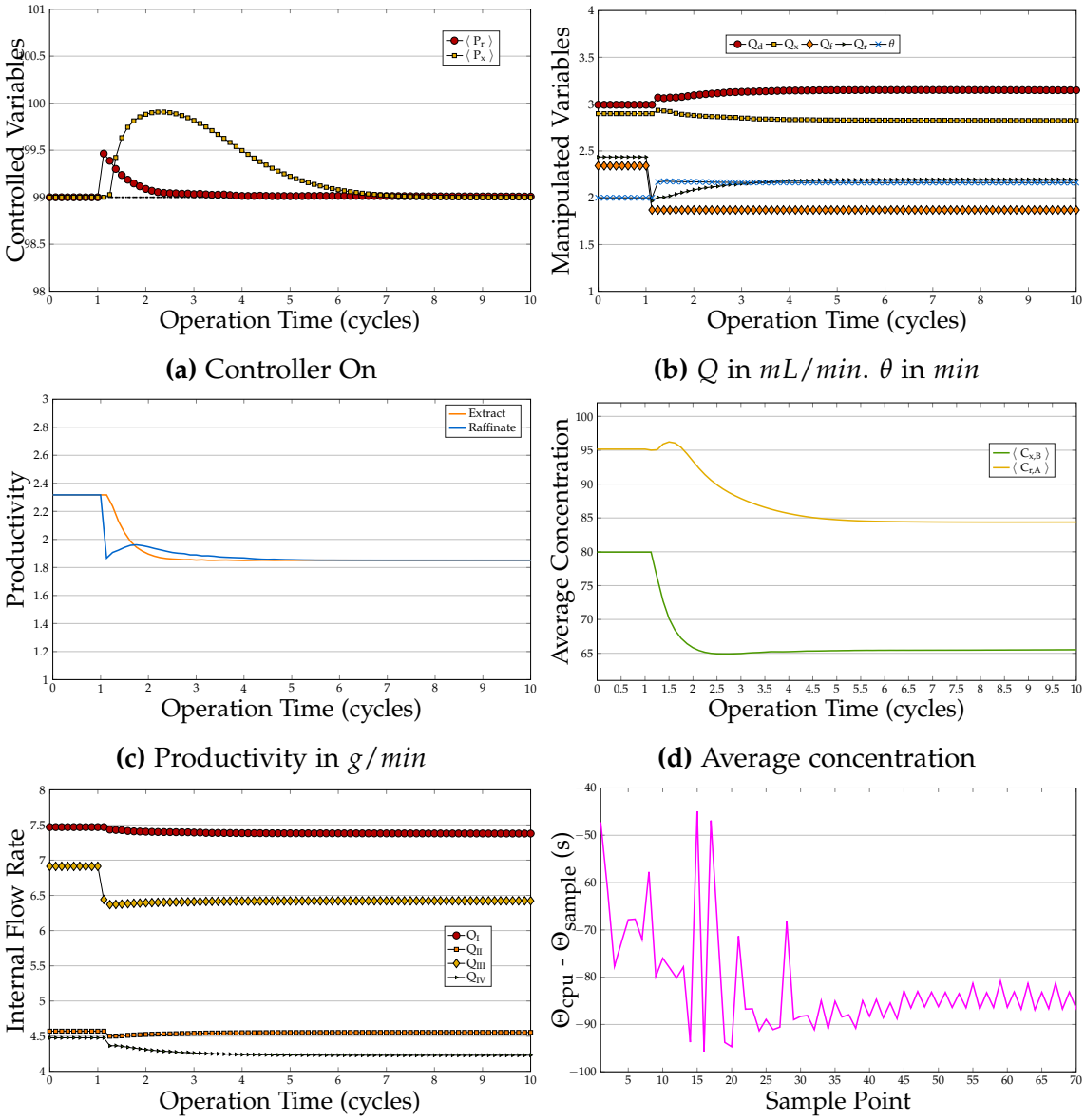

(a) Controller On

(b) Q in mL/min. θ in min

(c) Productivity in g/min

(d) Average concentration

(e) Q in mL/min

(f) Idle time in s

Figure 4.15: Compilation of the results for a decrease of 20% in the feeding pump flow rate.

Unlike the solvent pump malfunction scenario, positive perturbations in the feeding pump do affect the system. The results for a disturbance of $+20\%$ are presented in Figure 4.16. As expected, the direction of the gain in the raffinate purity changed, but the same did not happen to the extract purity; in fact, a positive perturbation did not affect it at all, which is one more evidence of the non-linearity of the SMB process.

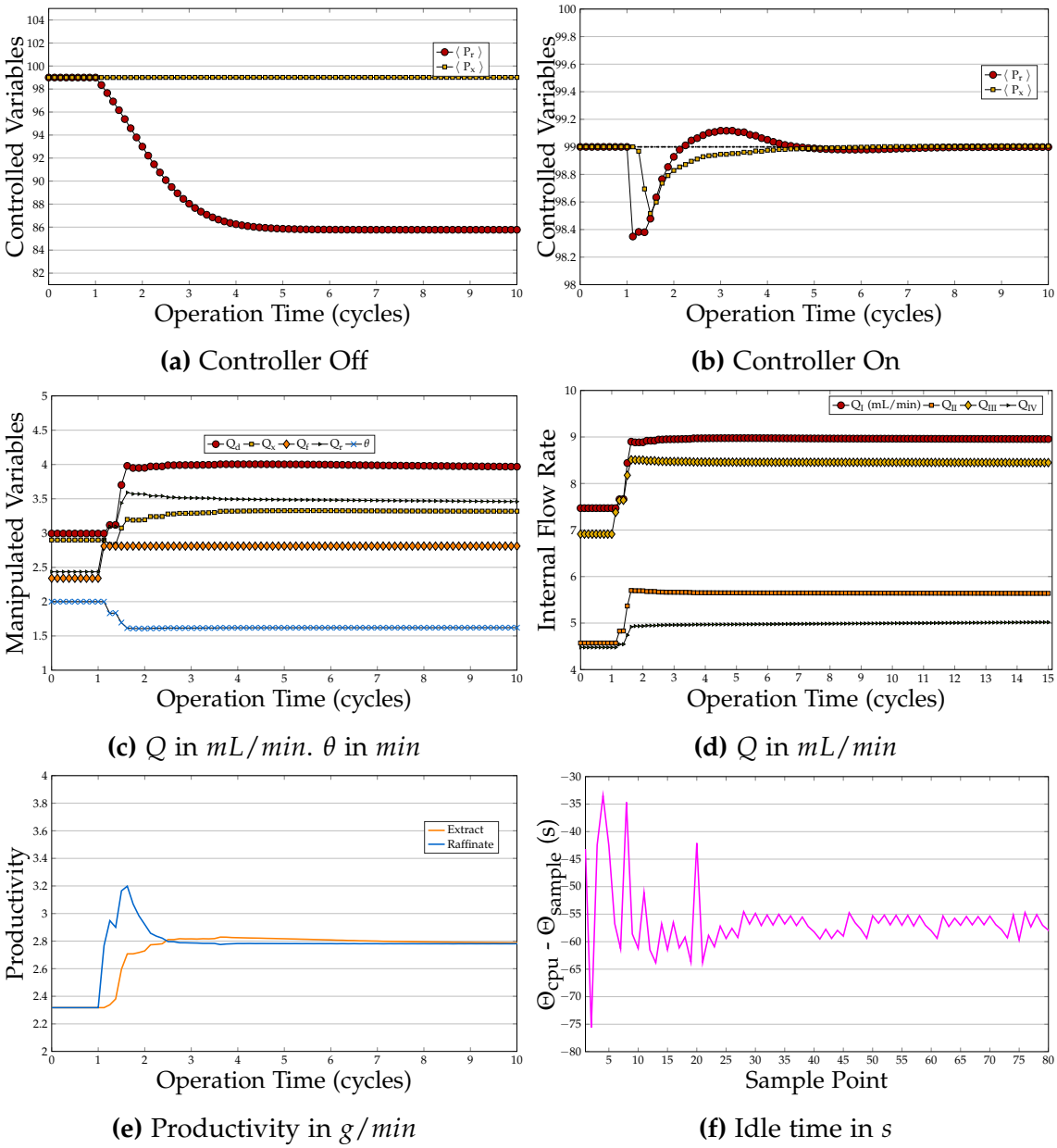

(a) Controller Off

(b) Controller On

(c) Q in mL/min. θ in min

(d) Q in mL/min

(e) Productivity in g/min

(f) Idle time in s

Figure 4.16: Compilation of the results for a increase of 20% in the feeding pump flow rate.

4.3.3 Switching Valve Malfunction

Finishing the malfunctioning scenarios, the switching valve failure is discussed. In such kind of problems, it is supposed that, for some reason, the switching period is disturbed. Positive and negative disturbances were applied to the valve but, as the results were similar, only the reduction in θ are going to be presented.

The uncontrolled and controlled responses for a decrease in 25% of the switching period are assembled in Figure 4.17. As can be seen in Figure 4.17a,

the system has an underdamped and inverse response, which is a hard task for conventional PID controllers to deal with. However, the model predictive control handled it efficiently. The values used for the tuning parameters were the same of the first case study presented in Section 4.3.1 which lead to a fast and stable response (see Figure 4.17b); after one severe control action, the manipulated variables follow a very smooth trajectory, as shown in Figure 4.17c.

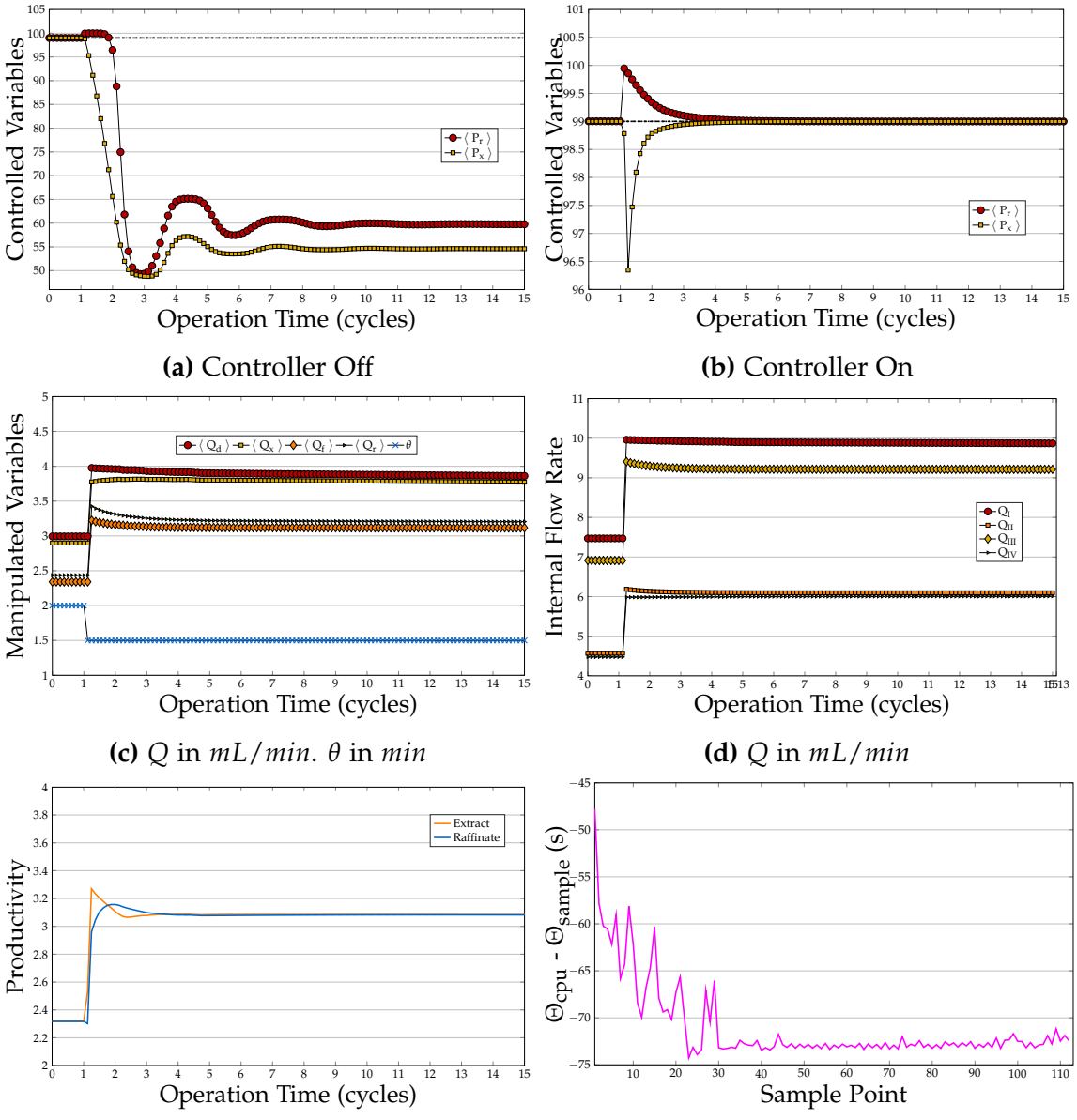

(a) Controller Off

(b) Controller On

(c) Q in mL/min. θ in min

(d) Q in mL/min

(e) Productivity in g/min

(f) Idle time in s

Figure 4.17: Compilation of the results for a decrease of 25% in the switching period.

The increase in the productivity is an expected outcome, as the flow rates and the switching time have an inverse relation, as evidenced by Equation (4.2).

4.3.4 Set Point Tracking

Change in set point is a very common control problem regardless of the process in study. The change in purity requirements along the operation is an example of this kind of problem. The current scenario addresses the situation in which the purity requirement was changed from 99% to 92% at $t = 1$ cycle. In Figure 4.18, the controlled response along with all other the results are brought together. The tuning parameters were: $H_p = 1$ cycle, $\omega_1 = 10$ and $\omega_2 = 1 \times 10^5$. It is worth remembering that, in set point changing, as in all other control scenarios in which instrumentation malfunction is not concerned, the switching time remains fixed and is not used as a manipulated variable.

4.3.5 Unmeasured Disturbances and Plant-model Mismatch

In industrial applications, the models used in controllers do not fully represent the process it is supposed to control. There are two main reasons for this: first, measurements are not free from errors, there will always be uncertainties associated to the measuring instruments which lead to uncertainties in the parameters of a model, so, the plant and model mismatch; second, it is nearly impractical to make online measurements in every variable that could possible interfere with the system response, therefore, the controller is almost always "blind" to certain disturbances, the unmeasured ones. That said, unmeasured disturbances and plant-model mismatch problems can be treated in the same way. Two cases will be presented in which the controller model differs from the plant.

In the first case study, it is considered a decrease in 10% in the adsorption isotherm parameters $q_{m,i}$ and K_i for both the enantiomers. These decrease could be result of estimation errors (uncertainties) or even temperature fluctuation (unmeasured disturbance). As usual, the uncontrolled system response is presented first. The system show an inverse response, an oscillatory module and a settle down time of six cycles. The purities in CSS are equals to 82.12% and 69.80% to extract and raffinate, respectively. In Figures 4.19b and 4.19c, the controlled system response with and without the parameter estimation step are compared. The differences between them are very clear. Without the parameter estimation, the controller tries to bring the purities back to the set point, but without any kind of information about the plant-model discrepancies, persistent offsets could not be overcome.

In contrast to that, the controlled response employing the parameter es-

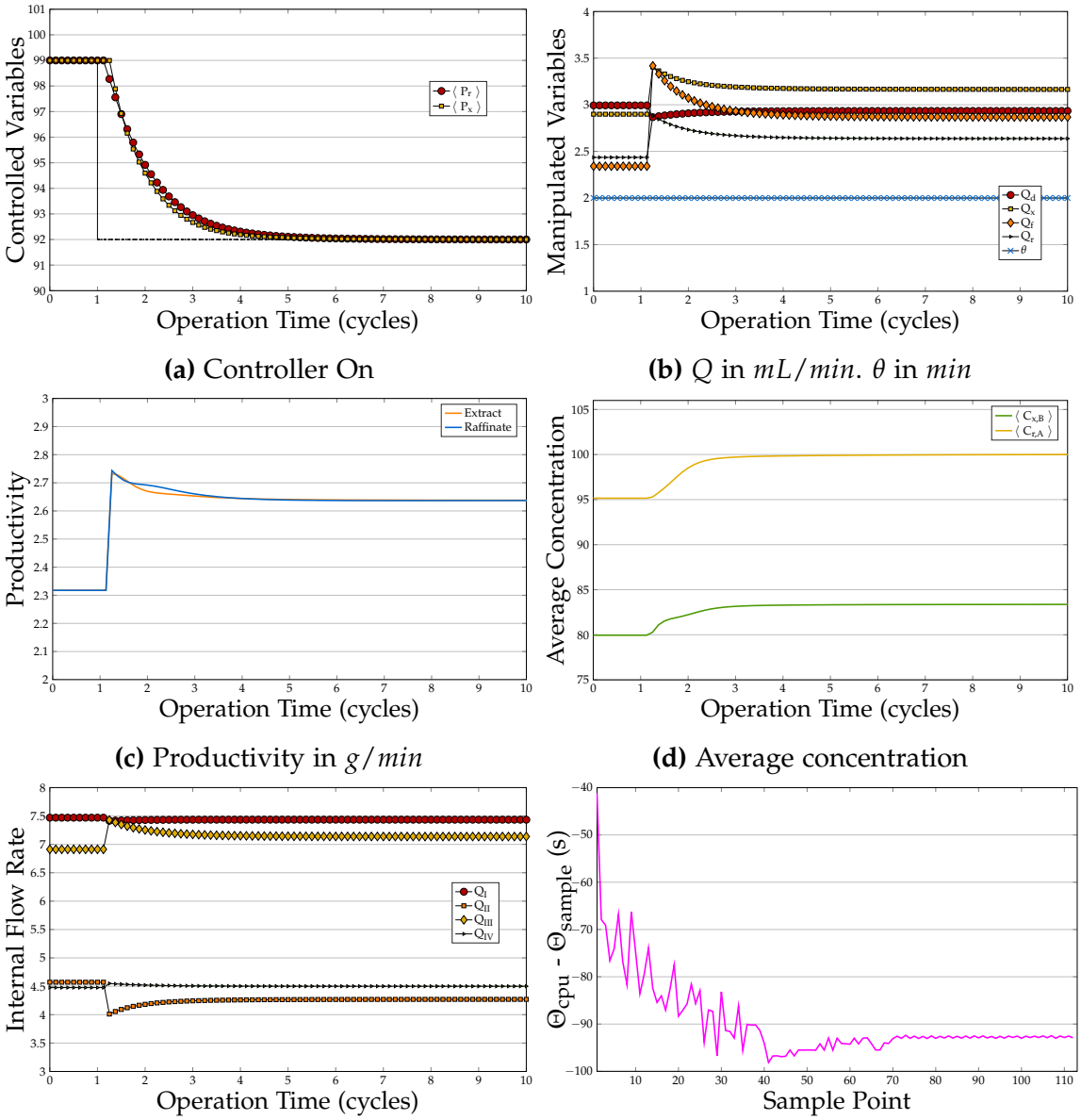

(a) Controller On

(b) Q in mL/min. θ in min

(c) Productivity in g/min

(d) Average concentration

(e) Q in mL/min

(f) Idle time in s

Figure 4.18: Compilation of the results for a set point change in purity from 99% to 92% in both outlet streams.

timation can easily fulfill the purity requirements. This strategy grants to the controller an adaptive aspect without loss of generality. Additionally, it had no negative impact on control or computational effort at all, as can be seen by the manipulated variables trajectory and idle time along with the productivity profile in Figure 4.20.

The second case study regarding the plant-model mismatch/unmeasured disturbances concerns to the change in the feeding concentration $C_{f,i}$, which is also a very common control problem in a variety of processes. Here, it is considered that a perturbation of $+100\%$ in both feeding concentrations occurred.

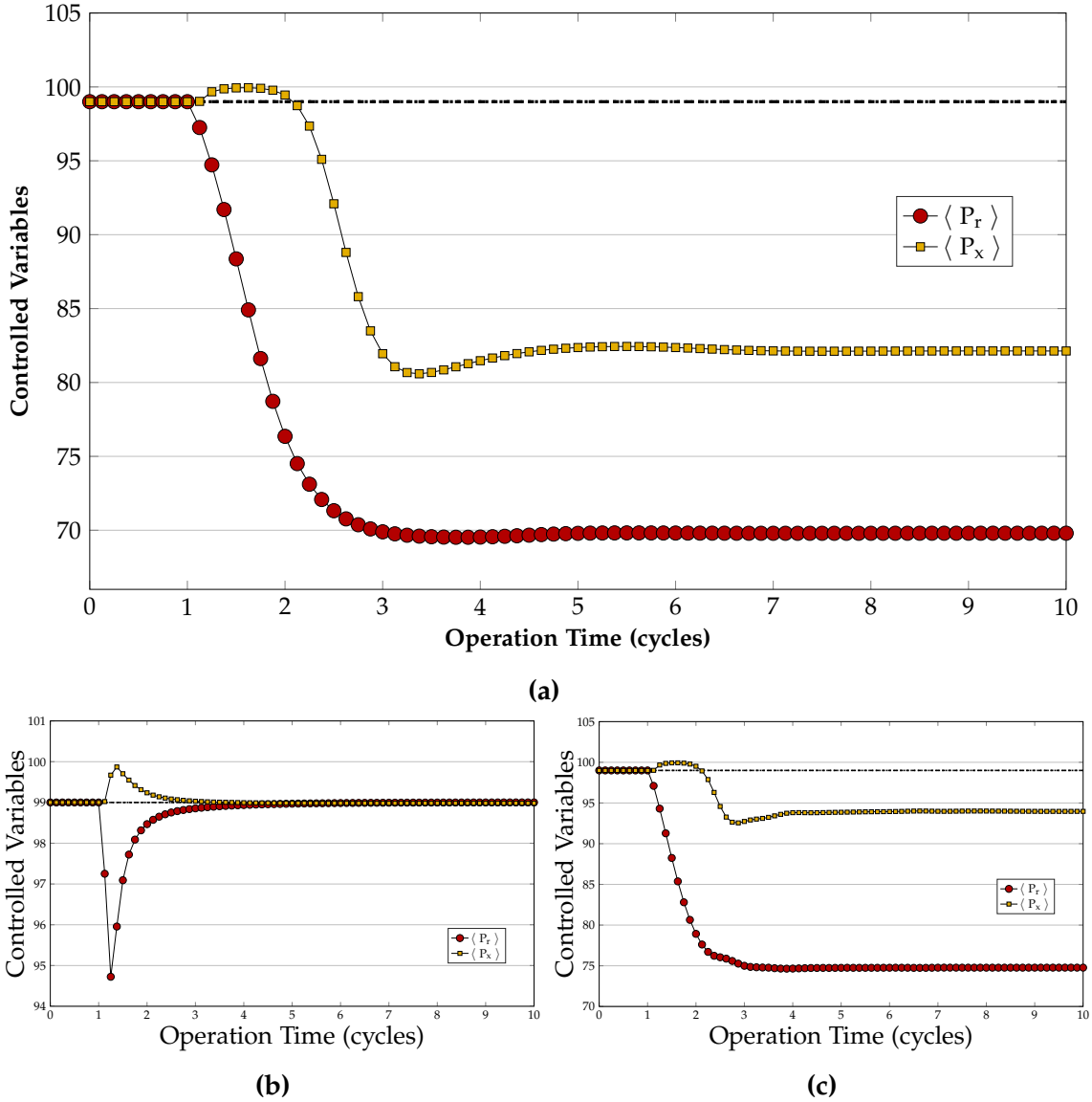

Figure 4.19: (a) Uncontrolled system response to a perturbation of -10% in the adsorption isotherm parameters $q_{m,i}$ and K_i. Comparison between the controlled system responses (b) with and (c) without the parameter estimation step for the same perturbation.

As these variables are supposed unmeasured, the controller is blind to them. Likewise the latter case, the uncontrolled system response is presented first and the controlled ones with and without carrying out the parameter estimation are compared in Figure 4.21.

The SMB response to concentrations disturbances is similar to the latter case. However, their slow dynamics is worth noting. After the step perturbation, a new permanent regime is attained after 15 cycles, three times more than the majority of the previously studied cases. Although the controlled response without the parameter estimation also have offsets, they are much smaller. On the

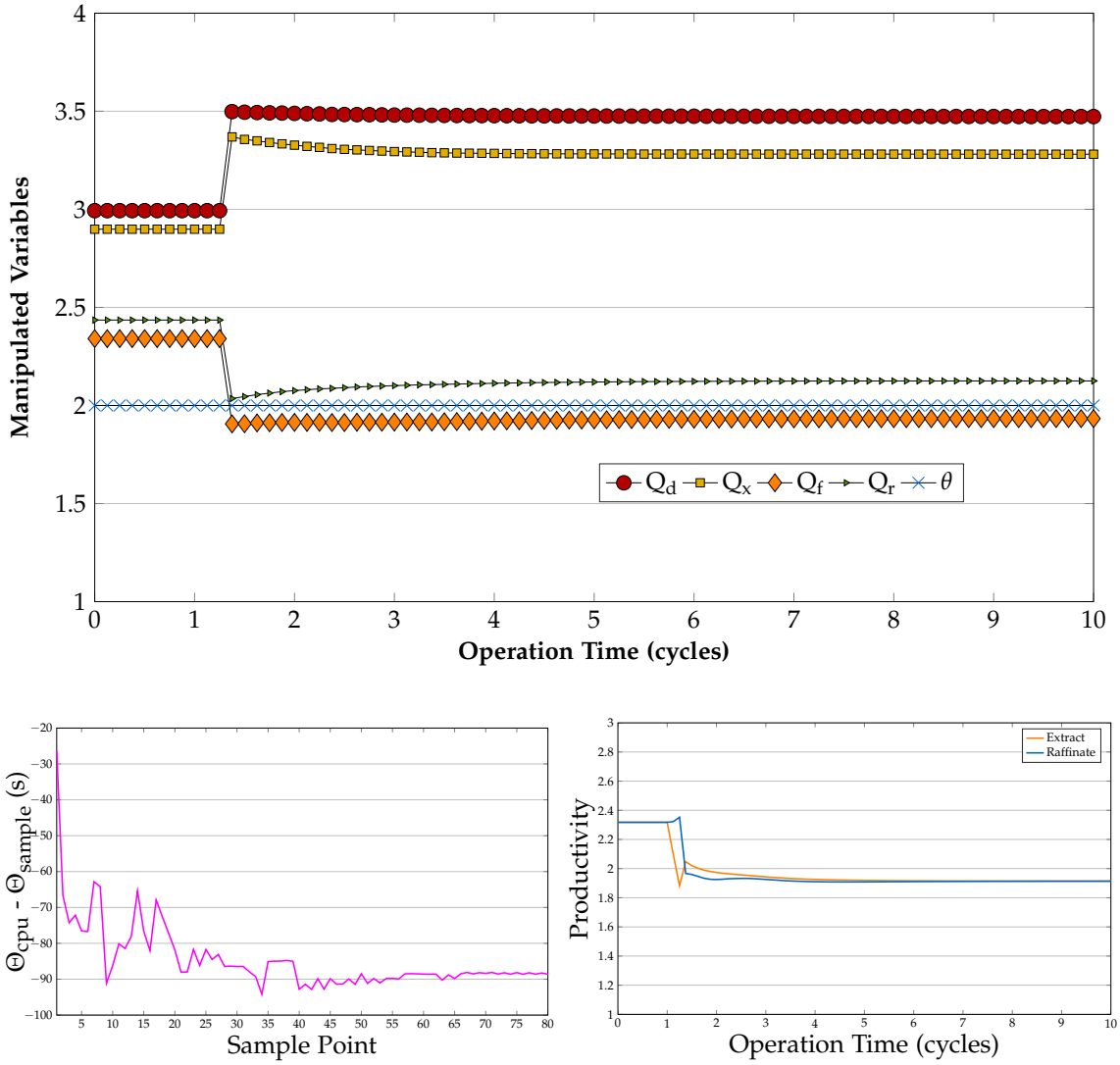

Figure 4.20: Manipulated variables trajectory, idle time and productivity for a perturbation of -10% in the adsorption isotherm parameters $q_{m,i}$ and K_i.

other hand, the controlled response with the parameter estimation can achieve the purity goals satisfactorily, as can be seen by the smooth control actions and low computation effort in Figure 4.22.

Both cases presented in this section showed that the parameter estimation step is a crucial element in the developed control scheme. The adaptability grants the controller robustness, without adding meaningful costs.

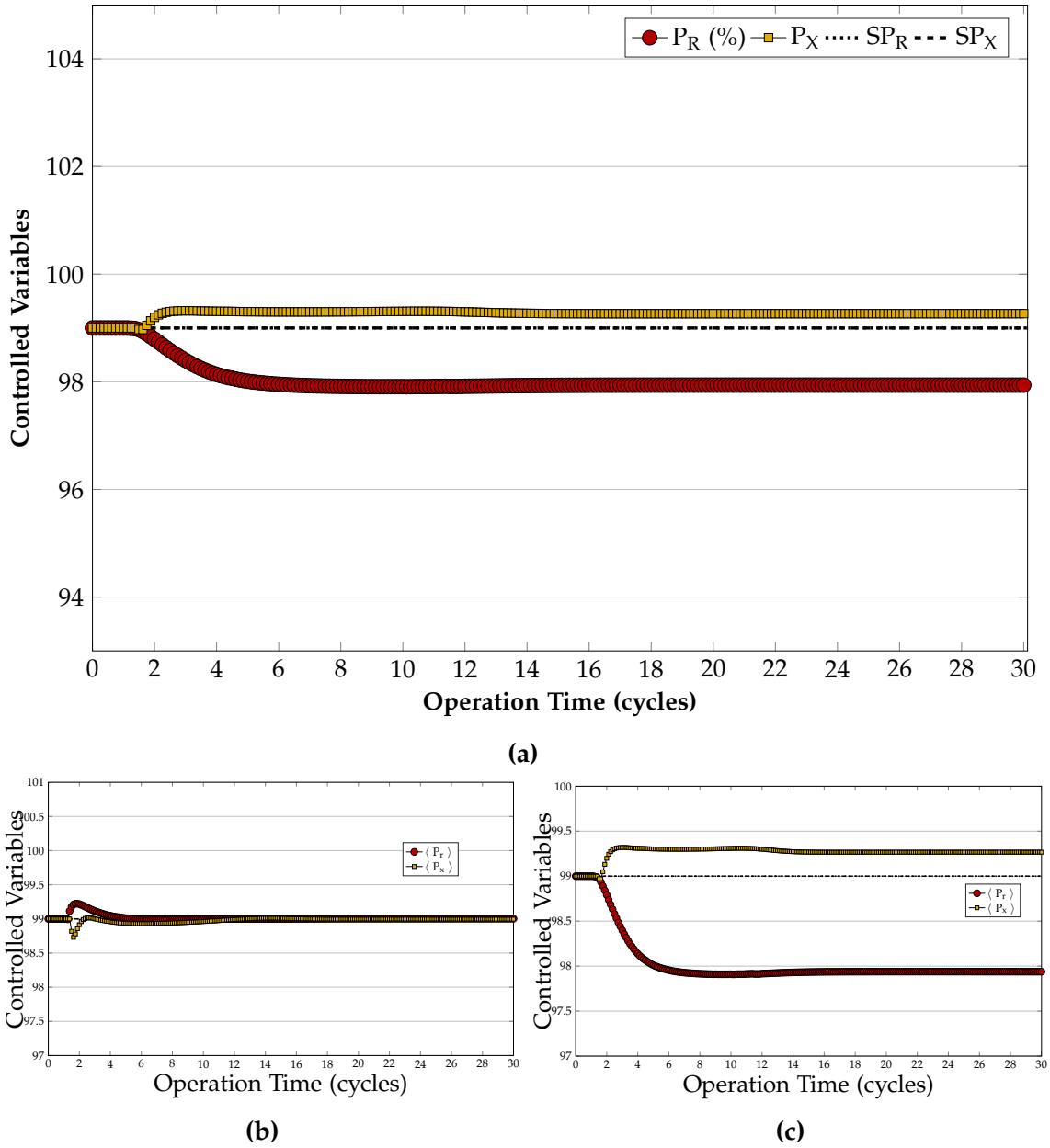

Figure 4.21: (a) Uncontrolled system response to a perturbation of +100% in the feeding concentrations $C_{f,i}$. Comparison between the controlled system responses (b) with and (c) without the parameter estimation step for the same perturbation.

4.4 Final Considerations

Extract and raffinate pump malfunction problems were also investigated, but the outcomes were very similar to that of solvent and feeding pump failure scenarios. For this reason, they were left out of the discussion. Compilation of the results for both control problems is showed in Appendix C.

One last thing that should be brought to light regards the online measure-

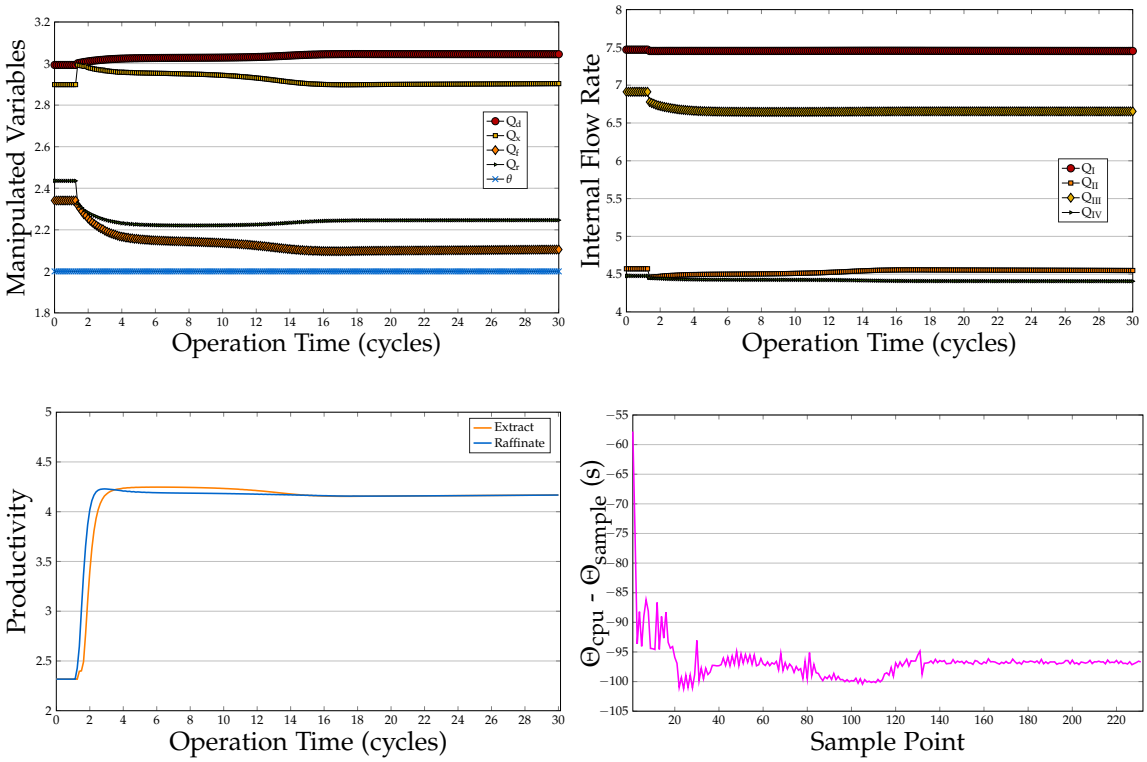

Figure 4.22: Manipulated variables and internal flow rates trajectories, productivity and idle time for a perturbation of +100% in the feeding concentrations C_f.

ment step. Although it was considered in this work that every state of the plant is measured, often this is not true, especially for distributed system. Usually, a state estimator is added to the control structure in order to build the internal concentration profiles from actual measurements, such as the outlet extract and raffinate concentrations that are easily obtained with proper instrumentation. However, that should not have an appreciable impact on the controller's performance.

Chapter 5

Conclusion

Something ends, something begins.

Geralt of Rivia, from Andrzej Sapkowski's *"The Witcher"*

A comprehensive study of the simulated moving bed chromatography process was addressed in this work using the separation of the enantiomers of praziquantel as an illustrative example for the modeling, simulation, optimization and control strategies presented. Although that was the main studied case, the developed software package was made as general as possible.

In regard to the process modeling and simulation, the direct approach was followed due to its better representability. In order to deal with its higher complexity, efficient numerical techniques like sparse-matrix algebra algorithms coupled to finite differences discretization were used to benefit from the sparsity features of such systems. Moreover, by the comparison of the two mass transfer models used, it was shown that the simplified local equilibrium model is sufficient to describe the mass transfer mechanism involved in the studied cases. Nevertheless, it would be interesting to evaluate the advantages and disadvantages of mass transfer models with higher levels of description, such as the inter and intraparticle models, that could be necessary to represent other separation systems.

The main concern about the usage of that model in a control framework was about the computational effort. However, the obtained results made it clear that the model complexity did not compromised the applicability of the control scheme. In fact, that is the reason for its excellent performance — in every simulated scenario, the controller was able to maintain the controlled variables

at the desired levels, with a fast response and smooth actuation, even in the cases in which modeling errors were inserted. Although, in order to approximate the simulated control scenarios even more to real ones, state estimators should be employed in future works.

The final thoughts go to the optimization strategy that, despite leading to good results, suffered from the high costs to obtain the cyclic steady state conditions. The computational efficiency could be increased by several ways, namely: (i) usage of derivative-free optimization algorithms, as the numerical gradient vector is very time-demanding; (ii) usage of analytical derivatives; (iii) usage of reduced-order models that conserve the accuracy but reduce the processing time; or (iv) the employment of faster techniques to obtain the cyclic steady state, as the ones reviewed in Section 3.3.

Bibliography

ABEL, S., ERDEM, G., MAZZOTTI, M., et al., 2004, "Optimizing control of simulated moving beds–linear isotherm." *Journal of chromatography. A*, v. 1033, n. 2, pp. 229–239. ISSN: 00219673.

ABEL, S., ERDEM, G., AMANULLAH, M., et al., 2005, "Optimizing control of simulated moving beds–experimental implementation." *Journal of chromatography. A*, v. 1092, n. 1, pp. 2–16. ISSN: 0021-9673.

AGRAWAL, G., SREEDHAR, B., KAWAJIRI, Y., 2014, "Systematic optimization and experimental validation of ternary simulated moving bed chromatography systems", *Journal of Chromatography A*, v. 1356, pp. 82 – 95. ISSN: 0021-9673. Availability: <http://dx.doi.org/10.1016/j.chroma.2014.06.028>.

ASCHER, U. M., PETZOLD, L. R., 1998, *Computer Methods for Ordinary Dierential Equations and Dierential-Algebraic Equations*. 1 ed. Philadelphia, SIAM.

CAMACHO, E. F., BORDONS, C., 2007, *Model predictive control*. 2 ed. London, UK, Springer.

CANNON, M., 2004, "Efficient nonlinear model predictive control algorithms", *Annual Reviews in Control*, v. 28, n. 2, pp. 229 – 237. ISSN: 1367-5788. Availability: <http://dx.doi.org/10.1016/j.arcontrol.2004.05.001>.

CEDILLO-CRUZ, A., AGUILAR, M. I., FLORES-ALAMO, M., et al., 2014, "A straightforward and efficient synthesis of praziquantel enantiomers and their 4'-hydroxy derivatives", *Tetrahedron Asymmetry*, v. 25, n. 2, pp. 133–140. ISSN: 09574166. Availability: <http://dx.doi.org/10.1016/j.tetasy.2013.11.004>.

CHIN, C. Y., WANG, N. L., 2004, "Simulated Moving Bed Equipment Designs", *Separation & Purification Reviews*, v. 33, n. 2, pp. 77–155. ISSN:

1542-2119. Availability: <http://www.tandfonline.com/doi/abs/10.1081/SPM-200042081>.

CHIRBASE DATA BANK. http://chirbase.u-3mrs.fr/. Accessed: 2015-07-11.

CIOLI, D., PICA-MATTOCCIA, L., BASSO, A., et al., 2014, "Schistosomiasis control: Praziquantel forever?" *Molecular and Biochemical Parasitology*, v. 195, n. 1, pp. 23–29. ISSN: 18729428. Availability: <http://dx.doi.org/10.1016/j.molbiopara.2014.06.002>.

CORREIA DA SILVA, G. S., SOUZA JR., M. B., LIMA, E. L., et al., 2009, "Application of a model-based fault detection and diagnosis system to a hydrotreating reactor", *Chemical engineering transactions*, v. 17, pp. 1329 – 1334.

DÜNNEBIER, G., WEIRICH, I., KLATT, K.-U., 1998, "Computationally efficient dynamic modelling and simulation of simulated moving bed chromatographic processes with linear isotherms", *Chemical Engineering Science*, v. 53, n. 14, pp. 2537 – 2546. ISSN: 0009-2509. Availability: <http://dx.doi.org/10.1016/S0009-2509(98)00076-1>.

ERDEM, G., ABEL, S., MORARI, M., et al., 2004, "Automatic Control of Simulated Moving Beds", *Industrial & Engineering Chemistry Research*, v. 43, n. 14, pp. 405–421. ISSN: 0888-5885.

GOMES, P. S., 2009, *Advances in simulated moving bed: new operating modes; new design methodologies; and product (FlexSMB-LSRE) development*. Tese de D.Sc., FEUP, Cidade do Porto, Portugal.

GONÇALVES, G. A. A., 2013, *Estratégias não lineares para o monitoramento e controle preditivo de colunas de destilação utilizando modelos de ordem reduzida*. Master's dissertation, COPPE/UFRJ, Rio de Janeiro, RJ.

GROSSMANN, C., AMANULLAH, M., ERDEM, G., et al., 2008, "'Cycle to cycle' optimizing control of simulated moving beds", *AIChE Journal*, v. 54, n. 1, pp. 194–208. ISSN: 1547-5905. Availability: <http://dx.doi.org/10.1002/aic.11346>.

GROSSMANN, C., LANGEL, C., MAZZOTTI, M., et al., 2010, "Multi-rate optimizing control of simulated moving beds", *Journal of Process Control*, v. 20, n. 4, pp. 490–505. ISSN: 09591524. Availability: <http://dx.doi.org/10.1016/j.jprocont.2009.12.001>.

GUIOCHON, G., FELLINGER, A., SHIRAZI, S. G., et al., 2006, *Fundamentals of preparative and nonlinear chromatography*. 1 ed. Boston, MA, US, Academic Press.

KLATT, K. U., HANISCH, F., DÜNNEBIER, G., 2002, "Model-based control of a simulated moving bed chromatographic process for the separation of fructose and glucose", *Journal of Process Control*, v. 12, n. 2, pp. 203–219. ISSN: 09591524.

KLOPPENBURG, E., GILLES, E., 1999, "Automatic control of the simulated moving bed process for {C8} aromatics separation using asymptotically exact input/output-linearization", *Journal of Process Control*, v. 9, n. 1, pp. 41 – 50. ISSN: 0959-1524. Availability: <http://dx.doi.org/10.1016/S0959-1524(98)00026-2>.

KUMAR, V., GRYSEELS, B., 1994, "Use of praziquantel against schistosomiasis: A review of current status", *International Journal of Antimicrobial Agents*, v. 4, n. 4, pp. 313–321. ISSN: 09248579. Availability: <http://dx.doi.org/10.1016/0924-8579(94)90032-9>.

LABCADS, 2015. "Laboratório de Cromatografia e Adsorção". Escola de Química, Universidade Federal do Rio de Janeiro. Internal Communication.

LEÃO, C. P., RODRIGUES, A. E., 2004, "Transient and steady-state models for simulated moving bed processes: Numerical solutions", *Computers and Chemical Engineering*, v. 28, n. 9, pp. 1725–1741. ISSN: 00981354.

LI, S., FENG, L., BENNER, P., et al., 2014, "Using surrogate models for efficient optimization of simulated moving bed chromatography", *Computers & Chemical Engineering*, v. 67, pp. 121 – 132. ISSN: 0098-1354. Availability: <http://dx.doi.org/10.1016/j.compchemeng.2014.03.024>.

LIM, B.-G., CHING, C.-B., 1996, "Preliminary design of a simulated countercurrent chromatographic system for the separation of praziquantel enantiomers", *Journal of Chromatography A*, v. 734, n. 2, pp. 247 – 258. ISSN: 0021-9673. Availability: <http://dx.doi.org/10.1016/0021-9673(95)01308-3>.

LIM, B.-G., CHING, C.-B., TAN, R. B., et al., 1995, "Recovery of (-)-praziquantel from racemic mixtures by continuous chromatography and crystallisation", v. 50, n. 14, pp. 2289–2298.

MACIEJWOSKI, J. M., 2000, *Predictive control with constrains*. 1 ed. Cambridge, UK, Prentice Hall.

MAIA, J. G. S. S., 2015, *Modelagem e simulação do processo de desidratação de etanol a eteno*. Master's dissertation, COPPE/UFRJ, Rio de Janeiro, RJ.

MALISKA, C. L., 2004, *Transferência de Calor e Mecânica dos Fluidos Computacional*. 2 ed. São Paulo, LTC.

MATHWORKS, 2014. "MatLab's optimization toolbox manuals". ver. R2014b.

MAYNE, D., RAWLINGS, J., RAO, C., et al., 2000, "Constrained model predictive control: Stability and optimality", *Automatica*, v. 36, n. 6, pp. 789 – 814. ISSN: 0005-1098. Availability: <http://dx.doi.org/10.1016/S0005-1098(99)00214-9>.

MAZZOTTI, M., STORTI, G., MORBIDELLI, M., 1997, "Optimal operation of simulated moving bed units for nonlinear chromatographic separations", *Journal of Chromatography A*, v. 769, n. 1, pp. 3 – 24. ISSN: 0021-9673. Availability: <http://dx.doi.org/10.1016/S0021-9673(97)00048-4>.

MORO, L. F. L., ODLOAK, D., 1995, "Constrained multivariable control of fluid catalytic cracking converters", *Journal of Process Control*, v. 5, n. 1, pp. 29 – 39. ISSN: 0959-1524. Availability: <http://dx.doi.org/10.1016/0959-1524(95)95943-8>.

RAJENDRAN, A., PAREDES, G., MAZZOTTI, M., 2009, "Simulated moving bed chromatography for the separation of enantiomers", *Journal of Chromatography A*, v. 1216, n. 4, pp. 709 – 738. ISSN: 0021-9673. Availability: <http://dx.doi.org/10.1016/j.chroma.2008.10.075>.

ROMANIELO, L. L., 1999, *Modelagem matemática e termodinâmica da adsorção gasosa multicomponente*. Doctorade's thesis, UNICAMP, Campinas, SP, Brasil.

ROUSSEAU, R. W., 1987, *Handbook of separation process technology*. 1 ed. New York, US, John Wiley & Sons.

RUTHVEN, D. M., 1984, *Principles of adsorption and adsorption processes*. 1 ed. New York, US, John Wiley & Sons.

SAVIOLI, L., DAUMERIE, D., 2010, *Working to overcome the global impact of neglected tropical diseases*. WHO NLM WC-680. Availability: <http://whqlibdoc.who.int/publications/2010/9789241564090_eng.pdf>.

SCHIMIDT-TRAUB, H., 2005, *Praparative chromatography of fine chemicals and pharmaceutical agents*. 1 ed. Dortmund, Germany, Wiley-VCH.

SCHULTE, M., STRUBE, J., 2001, "Preparative enantioseparation by simulated moving bed chromatography", *Journal of Chromatography A*, v. 906, n. 1–2, pp. 399 – 416. ISSN: 0021-9673. Availability: <http://dx.doi.org/10.1016/S0021-9673(00)00956-0>. Chiral Separations.

SCHURIG, V., 2001, "Separation of enantiomers by gas chromatography", *Journal of Chromatography A*, v. 906, n. 1–2, pp. 275 – 299. ISSN: 0021-9673. Availability: <http://dx.doi.org/10.1016/S0021-9673(00)00505-7>.

SHAFEEYAN, M. S., DAUD, W. M. A. W., SHAMIRI, A., 2014, "A review of mathematical modeling of fixed-bed columns for carbon dioxide adsorption", *Chemical Engineering Research and Design*, v. 92, n. 5, pp. 961 – 988. ISSN: 0263-8762. Availability: <http://dx.doi.org/10.1016/j.cherd.2013.08.018>.

SILVA, V. M. T., MINCEVA, M., RODRIGUES, A. E., 2004, "Novel Analytical Solution for a Simulated Moving Bed in the Presence of Mass-Transfer Resistance", *Industrial & Engineering Chemistry Research*, v. 43, n. 16, pp. 4494–4502. ISSN: 0888-5885. Availability: <http://pubs.acs.org/doi/abs/10.1021/ie030610i>.

SOLOMONS, G., FRYHLE, C., 2001, *Química Orgânica, Volume 1*. 7 ed. Rio de Janeiro, RJ, Brasil, LTC.

SONG, I. H., LEE, S. B., RHEE, H. K., et al., 2006, "Optimization-based predictive control of a simulated moving bed process using an identified model", *Chemical Engineering Science*, v. 61, n. 18, pp. 6165–6179. ISSN: 00092509.

SUVAROV, P., KIENLE, A., NOBRE, C., et al., 2014, "Cycle to cycle adaptive control of simulated moving bed chromatographic separation processes", *Journal of Process Control*, v. 24, n. 2, pp. 357 – 367. ISSN: 0959-1524. Availability: <http://dx.doi.org/10.1016/j.jprocont.2013.11.001>.

THOMAS, W. J., CRITTENDEN, B., 1998, *Adsorption technology and design*. 1 ed. Oxford, UK, Elsevier Science & Technology.

TOUMI, A., ENGELL, S., DIEHL, M., et al., 2007, "Efficient optimization of simulated moving bed processes", *Chemical Engineering and Processing: Process Intensification*, v. 46, n. 11, pp. 1067 – 1084. ISSN: 0255-2701. Availability: <http://dx.doi.org/10.1016/j.cep.2006.06.026>.

WANG, H., FANG, Z. Z., ZHENG, Y., et al., 2014, "Metabolic profiling of praziquantel enantiomers", *Biochemical Pharmacology*, v. 90, n. 2, pp. 166–178. ISSN: 18732968. Availability: <http://dx.doi.org/10.1016/j.bcp.2014.05.001>.

WESSELING, P., 2001, *Principles of Computational Fluid Dynamics*. 1 ed. Berlin, Springer.

YAO, H.-M., TADÉ, M. O., TIAN, Y.-C., 2010, "Accelerated computation of cyclic steady state for simulated-moving-bed processes", *Chemical Engineering Science*, v. 65, n. 5, pp. 1694 – 1704. ISSN: 0009-2509. Availability: <http://dx.doi.org/10.1016/j.ces.2009.11.012>.

Appendices

Appendix A

Software Package Tutorial

Here, a detailed overview of the developed software package is presented. Two different GUIs were created: (i) the first app of the package was named *SiMoBed* and addresses the modeling, simulation and optimization of a four-section simulated moving bed process for binary separations (see Figure 3.2); and (ii) the second app was named *SiMoCon*, which was designed for the process control (see Figure 3.3).

A.1 SiMoBed Application

At the top of the SiMoBed's GUI there is a menu bar with the following features: *File*, in which the user can save or load results or quit the application; in the *Tools* option, the user can open the control module SiMoCon; and in the *Help* option, two preset demonstration cases are available, one with the uridine/guanosine separation and other with the praziquantel enantiomers separation. By choosing any of those demos, the app are instantaneously configured. A praziquantel study case is presented as a tutorial below.

The parameters related to the components can be set in the *Component Parameters* panels as shown in Figure A.1. The less retained component is that of lower Henry constant (if using the linear isotherm), or lower adsorptivity (if using Langmuir isotherm). The equilibrium parameters (H_i, K_i and $q_{m,i}$) are set in the fields *Henry Cte*, *Adsorption Cte* and *Saturation Cte*, respectively; and the others ($k_{f,i}$, D_i and $C_{f,i}$), in the fields *Mass Transf Cf*, *Dispersion Coef* and *Feed Conc*. The not relevant parameters do not need to be altered — they remain with the default value of *0.0000*, as the Henry constants in the present case. The user are not required to use a specific unit system, although, he/she must be cautious

in order to avoid dimensional inconsistencies.

In all those fields the user must specify a single value; also, the entry must be a valid numerical character, otherwise, an error message will appear informing the user the nature of the error (see Figure A.2). The "comma" (,) and the "dot" (.) signs can both be used as decimal separators.

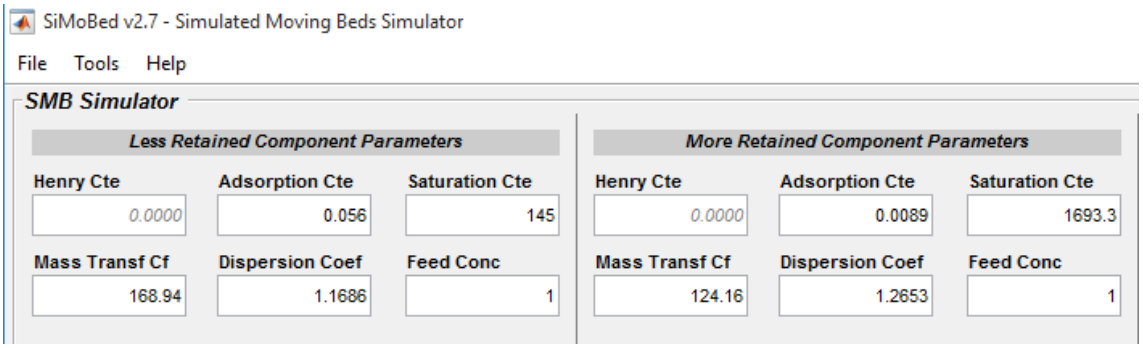

Figure A.1: Component parameters panels for the SiMoBed application.

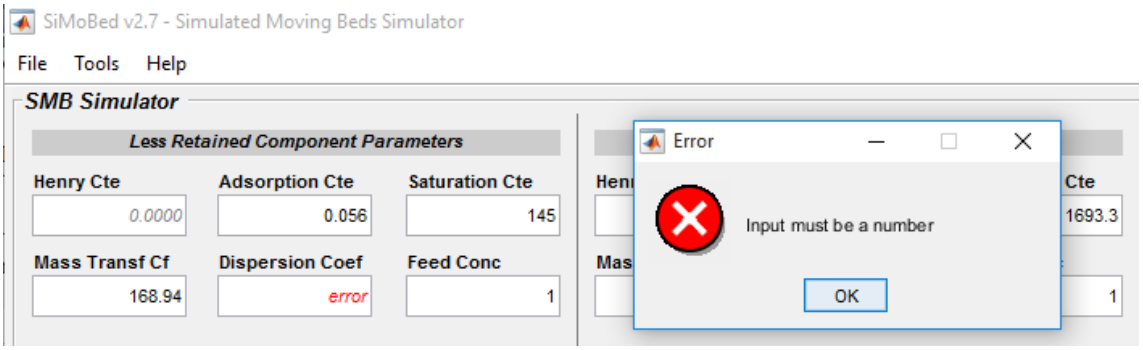

Figure A.2: Example of a syntax error: the message error *Input must be a number* is caused by setting a non numerical character in the *Dispersion Coef* field.

The column parameters (ℓ, d, ε, and N) must be set in their respective fields (*Column Length, Diameter, Porosity* and *# of Columns*). The SMB configuration is set in the field *Columns/Section* and must be a 4-by-1 or an 1-by-4 vector (in MatLab notation). The field *Particle Density* is the specific mass of the stationary phase, but it is only required as a correction factor when the Henry constants or the adsorptivities are given in a mass basis, *i.e.*, they have dimension of $[M^{-1}L^3]$, otherwise, it must have the default value of 1. The internal flow rates can be set in their respective panel. Thoses settings are shown in Figure A.3

The optimization can be carried out by marking the checkbox *Maximze* at the *Optimization Tool* panel. In this case, the user can choose one out of three different goals, namely: (i) the profitability; (ii) the productivity; or (iii) the productivity + the solvent economy. The fields *TolFun* and *TolX* are the stopping criteria for the MatLab optimization toolbox algorithms. The fields *Raf. Purity*

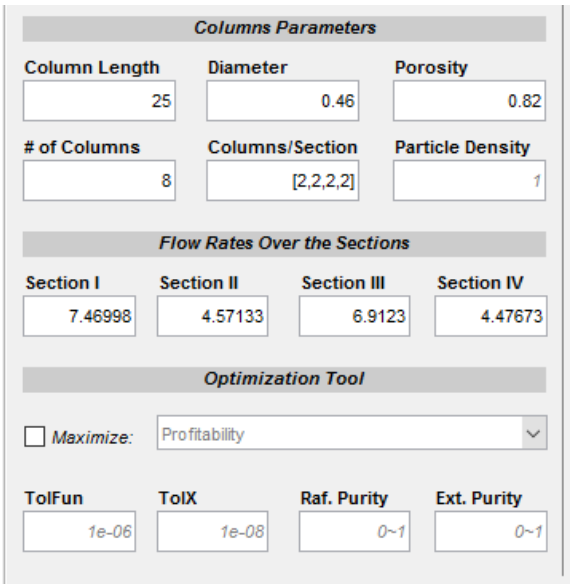

Figure A.3: Column parameters, internal flow rates and optimization tool panels.

and *Ext. Purity* are the desired purity levels in the range 0 to 1.

In the panel *Model Details* shown in Figure A.4 the user can select the characteristic isotherm of the system, as well as the mass transfer model and choose to activate or deactivate the dispersion term in the mass balance. The *Boundary Condition* field can be ignored and will be removed in a future release.

In the *Solver Control* panel, also shown in Figure A.4, the user can specify the *Discretization Method* and the mesh (*# of nodes* field). The *Switch Time* θ and the simulated number of cycles can also be set and the *Integrator* chosen — nine different algorithms are available. The jacobian matrix can be calculated numerically by the integrator, or evaluated analytically (in some cases). The integration tolerances can be selected in the fields *Abs. Tolerance* and *Rel. Tolerance*.

The simulation is started by clicking on the *Run* button in the *Simulation Control* panel. Its progress is show in the light bar at the bottom of the panel and it can be interrupted at any time by clicking on the *Stop* button (see Figure A.5). With the integration finished, the results can be saved for later analysis by clicking on the *Save Data* button. It is worth to point out that before simulation starts, the software runs a diagnostics in order to detect some input errors, for example, missing parameters; if any problem is identified, a message error is returned to the user after the *Run* button is pressed (see Figure A.6). The application comes back to its default setting by pressing the button *Reset*.

The results can be visualized in the *Output Control* panel. The user can choose to analyze the results of a current simulation, or he/she can load previous

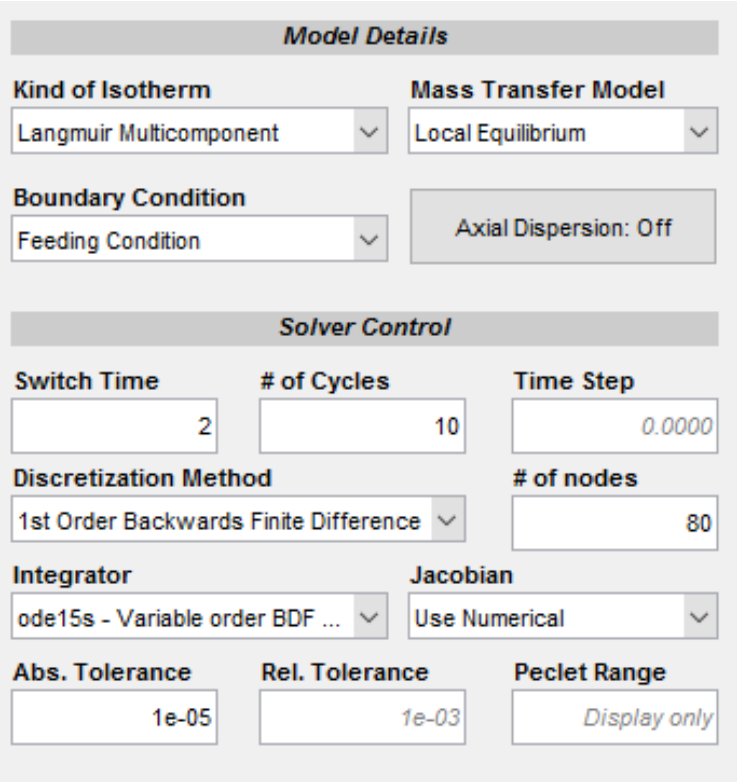

Figure A.4: Model details and solver control panels.

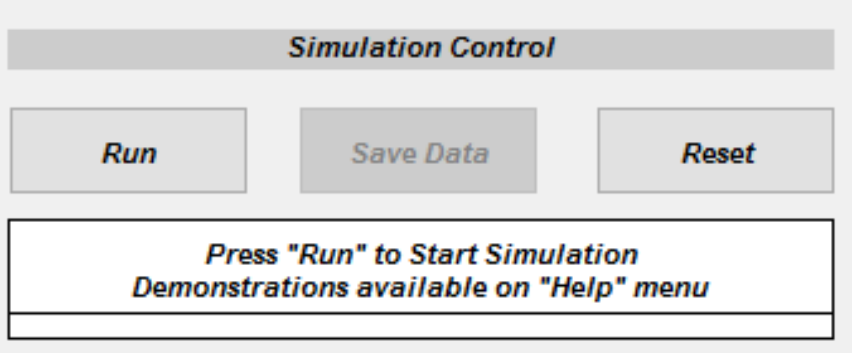

Figure A.5: Simulation progress.

results by clicking on the button *Load Data*. By clicking on the button *Mobile Phase Axial Concentration Profile*, figures with the internal concentration profiles throughout the entire SMB length at the end of each cycle are generated. The time-averaged outlet concentration profiles and purities are obtained by clicking on their respective buttons. The user can also generate a movie of the internal profiles varying along with the time by setting a value on the *Frames/Second* field. A pause between two switches can be set in the *Pause* field.

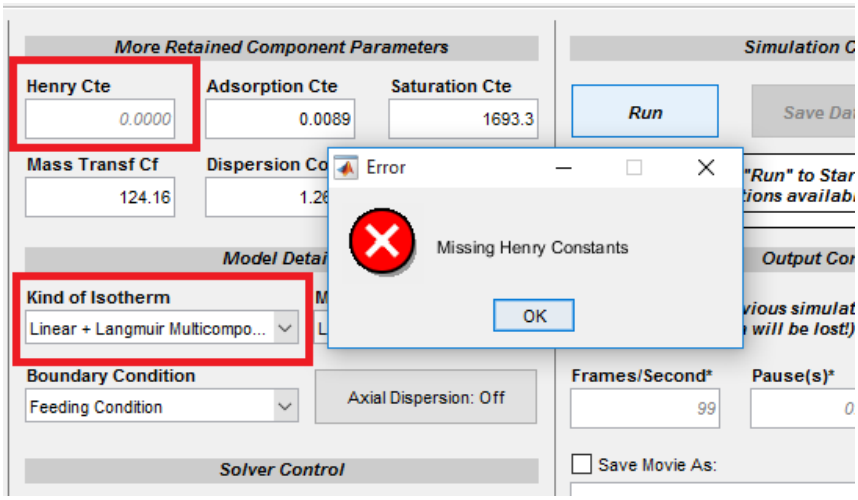

Figure A.6: Error message due to missing parameters (note that the linear + Langmuir isotherm is selected; in this isotherm, the Henry constants are necessary but the user did not provided them).

A.2 SiMoCon Application

In order to make anything in the control application, the user must first load a virtual plant by clicking on the big *Load Virtual Plant* button at the top of the GUI. This plant can be built with the modeling app, as explained before, and then saving the results. The results file is stored in a ".mat" file; that file is the virtual plant aforementioned. Once the plant is successfully loaded, the light bar at the bottom of the GUI change from red to yellow, that means that everything went properly and indicates that the controller is turned off. The *Plant Preview* button shows the time-averaged outlet purities of the selected plant in the chart at the right-hand side of the GUI.

In the *Controller Model* panel shown in Figure A.7, the user can configure the internal model of the controller. The perfect model case is selected by default, but the user can alter any feature in the tabs *Controller Model, LR Component Pars., MR Component Pars.*, or *Columns Pars.* by choosing the option *Plant-Model Mismatch* in the *Model Uncertainties* panel. In the tab *Solver Details* shown in Figure A.8, the user can set the optimization's algorithm and stopping criteria. Also the upper bound limits for the manipulated variables and the controller's objective function can be set in this tab.

In the *Controller Settings* panel (Figure A.9) the user can select the *Prediction Horizon*, the purity set points for the Raffinate and the Extract and the total number of cycles to simulate. Moreover, in the *Measured Disturbances* panel the instrumentation malfunction class of control problems can be carried out. The

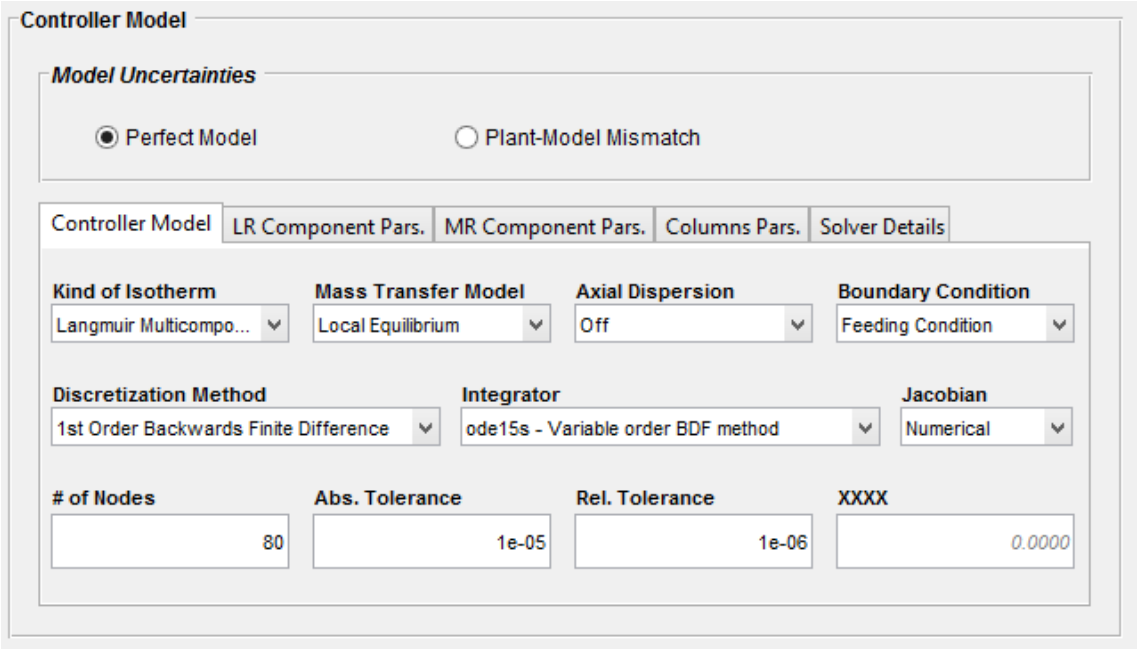

Figure A.7: Controller model panel of the SiMoCon application.

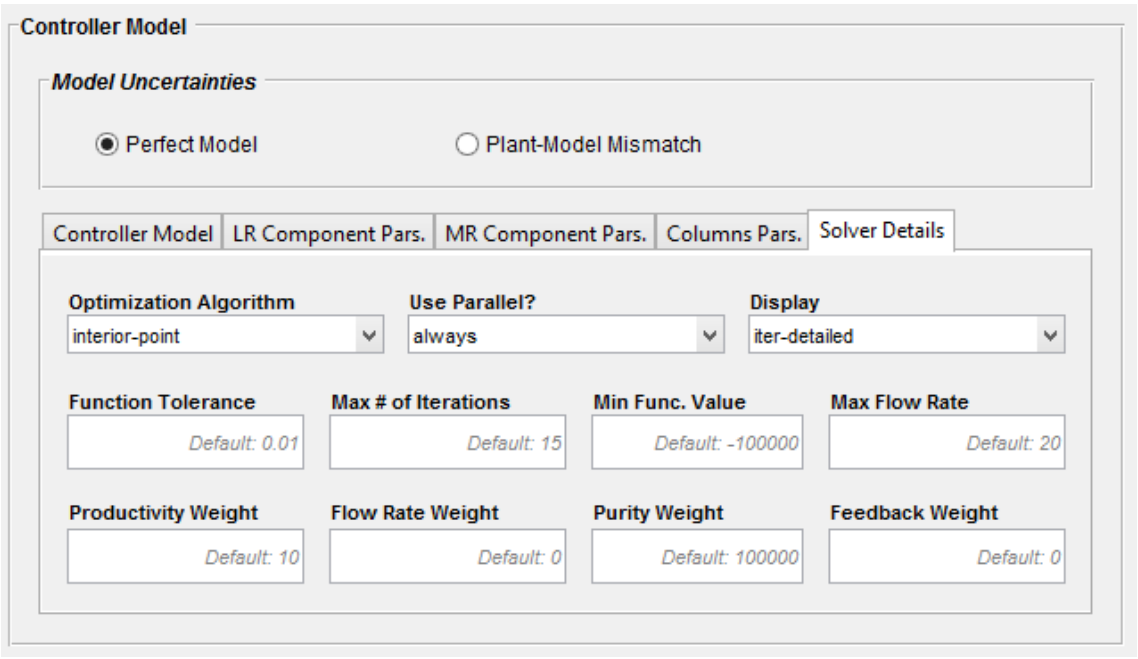

Figure A.8: Solver details tab of the SiMoCon application.

user can select any of the pumps or the switching valve to simulated a malfunction and set the new level desired in their respective fields. Only one pump can fail at time. If a set point tracking kind of problem is desired to be conducted, the user can select the *None* option.

By clicking on the *Start* button, the simulation starts from the final state of the loaded virtual plant. For this reason, it is recommended to use a virtual plant with a developed CSS. Any perturbation is applied after one cycle of operation.

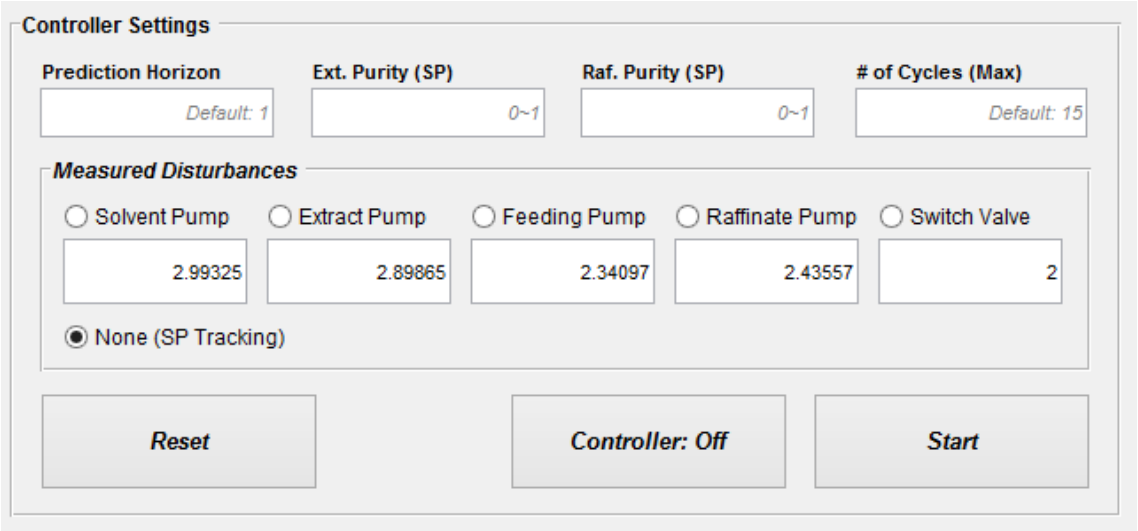

Figure A.9: Controller settings panel of the SiMoCon application.

The controller can be activate or deactivated at any time, before or after hitting the start button, by clicking on the *Controller* button. The light bar at the bottom of the GUI turns from yellow to green in order to signal the activation of the controller, and from green to yellow in order to signal its deactivation. When the simulation is finished, the light bar turns to blue (see Figures A.10 to A.12)

The simulation can be monitored through the seven charts at the right side of the GUI, which display: (i) the controlled variables response; (ii) the manipulated variables trajectory; (iii) the objective function value at each sampling period; (iv) the productivity; (v) the outlet concentrations; (vi) the internal flow rates trajectory; and (vii) the idle CPU time. The displaying charts can be alternated by clicking in their respective tabs at any time.

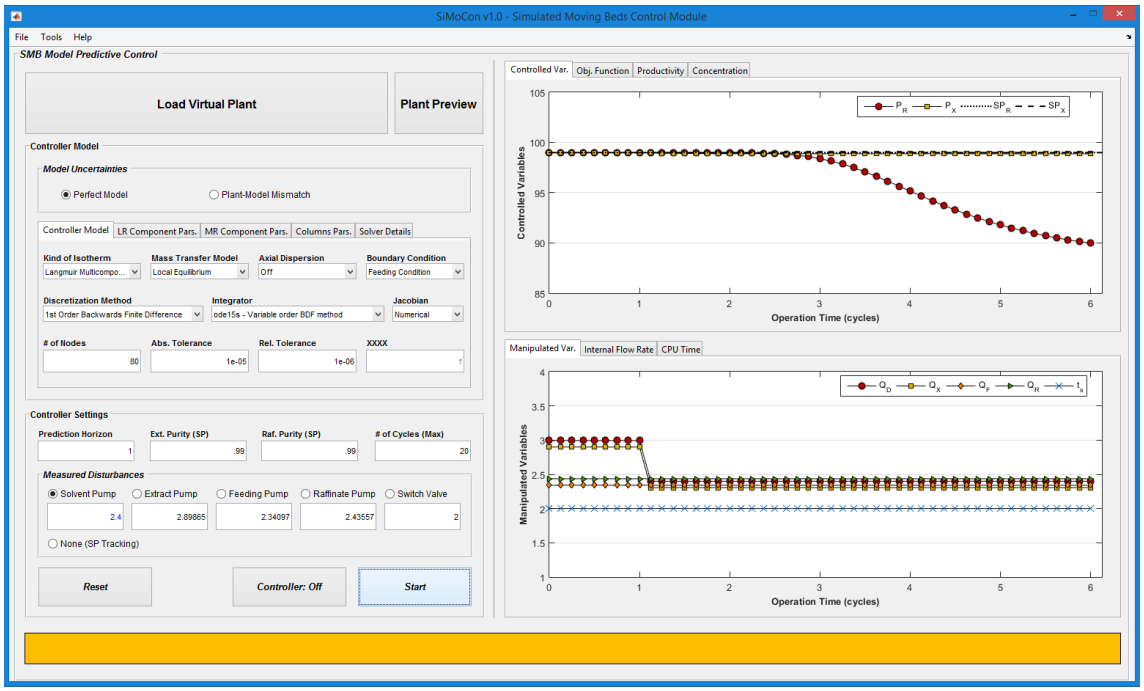

Figure A.10: SiMoCon application: controller off.

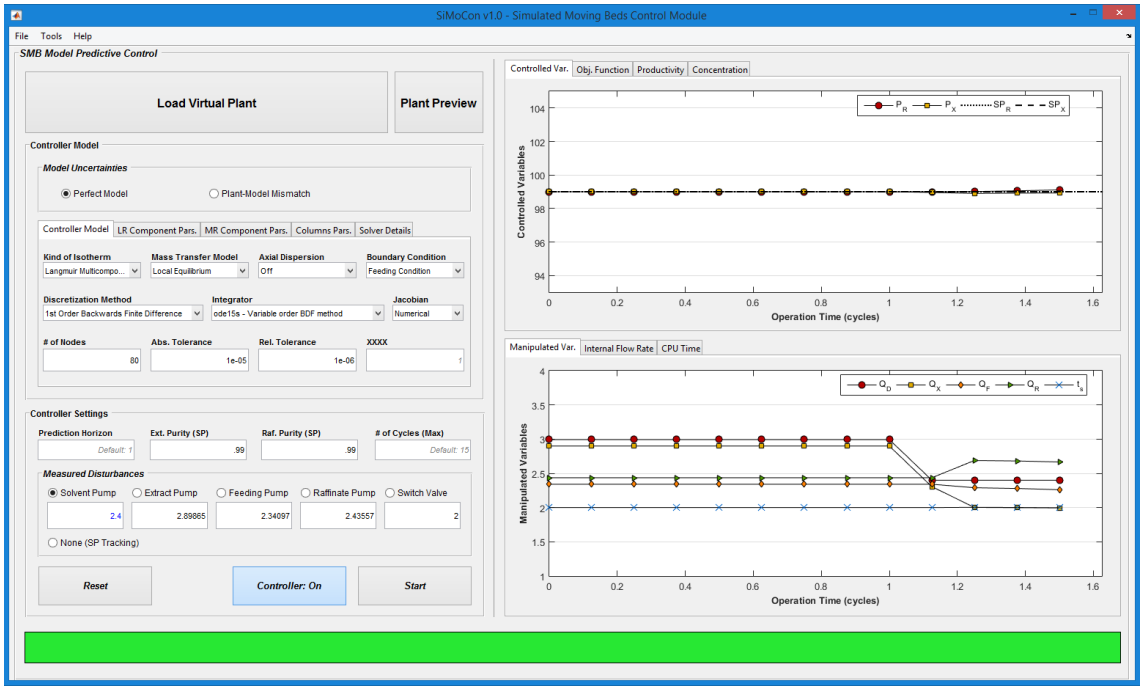

Figure A.11: SiMoCon application: controller on.

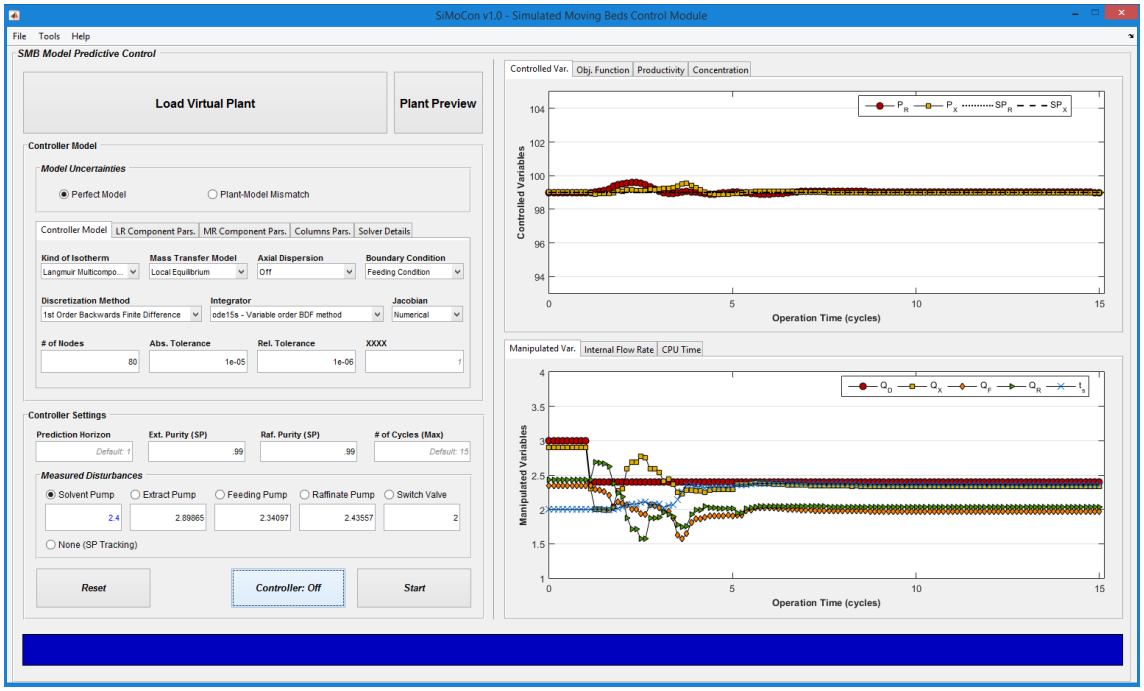

Figure A.12: SiMoCon application: simulation finished.

Appendix B

GPA Algorithms

```
function [A,B,x] = GPA_Matrices(n)
%GPA_Matrices calculates the first and second derivatives of the Lagrange's
%interpolation polynomial.
%
% Syntax:  [A,B,x] = GPA_Matrices(n)
%
%           Inputs:
%           n..................... Number of internal points
%
%           Outputs:
%           A..................... First derivative matrix
%           B..................... Second derivative matrix
%           x..................... Normalized collocation points
%                                  (the roots of the Legendre's orthogonal
%                                   polynomial)

N = n+2;
x = Legendre_roots(n);
v(N) = 0; A(N,N) = 0;
for i = 1:N
    p = 1;
    for j = 1: N
        fat = x(i) - x(j);
        v(i) = fat*v(i) + p;
        p = fat*p;
    end
end

for i = 1:N
    for j = 1:N
        if j~= i
            A(i,j) = v(i)/v(j)/(x(i)-x(j));
            A(i,i) = A(i,i) - A(i,j);
        end
    end
end
B = A^2;
end

```

```
40
41  %% Secondary functions
42
43  function r = Legendre_roots(n)
44  tol = 1e-12;
45  r(n+2) = 1;
46  x = 0;
47  y = Legendre_orth_poly(n,x);
48  while abs(y)>tol
49      x = x - y;
50      y = Legendre_orth_poly(n,x);
51  end
52  r(2) = x;
53  K = 2;
54  if n>=1
55      for k = 3:n+1
56          x = r(K)+1e-3;
57          F = Legendre_orth_poly(n,x);
58          y = F/(1-F*sum(1./(x-r(1:K))));
59          while abs(y)>tol
60              x = x-y;
61              F = Legendre_orth_poly(n,x);
62              y = F/(1-F*sum(1./(x-r(1:K))));
63          end
64          r(k) = x;
65          K = K+1;
66      end
67  end
68  end
69
70  function res = Legendre_orth_poly(n,x)
71  q = 1;
72  dq = 0;
73  p = x-0.5;
74  dp = 1;
75  dP=1;
76  if n>=1
77      for i = 2:n
78          h = (i-1)*(i+1)/4/(2*i+1)/(2*i-1);
79          P = (x - 0.5)*p-h*q;
80          dP = p+(x-0.5)*dp-h*dq;
81          q=p;
82          dq=dp;
83          p=P;
84          dp=dP;
85      end
86      res = p/dP;
87  end
88  end
```

Appendix C

Additional Control Problems

Switching valve malfunction +50%

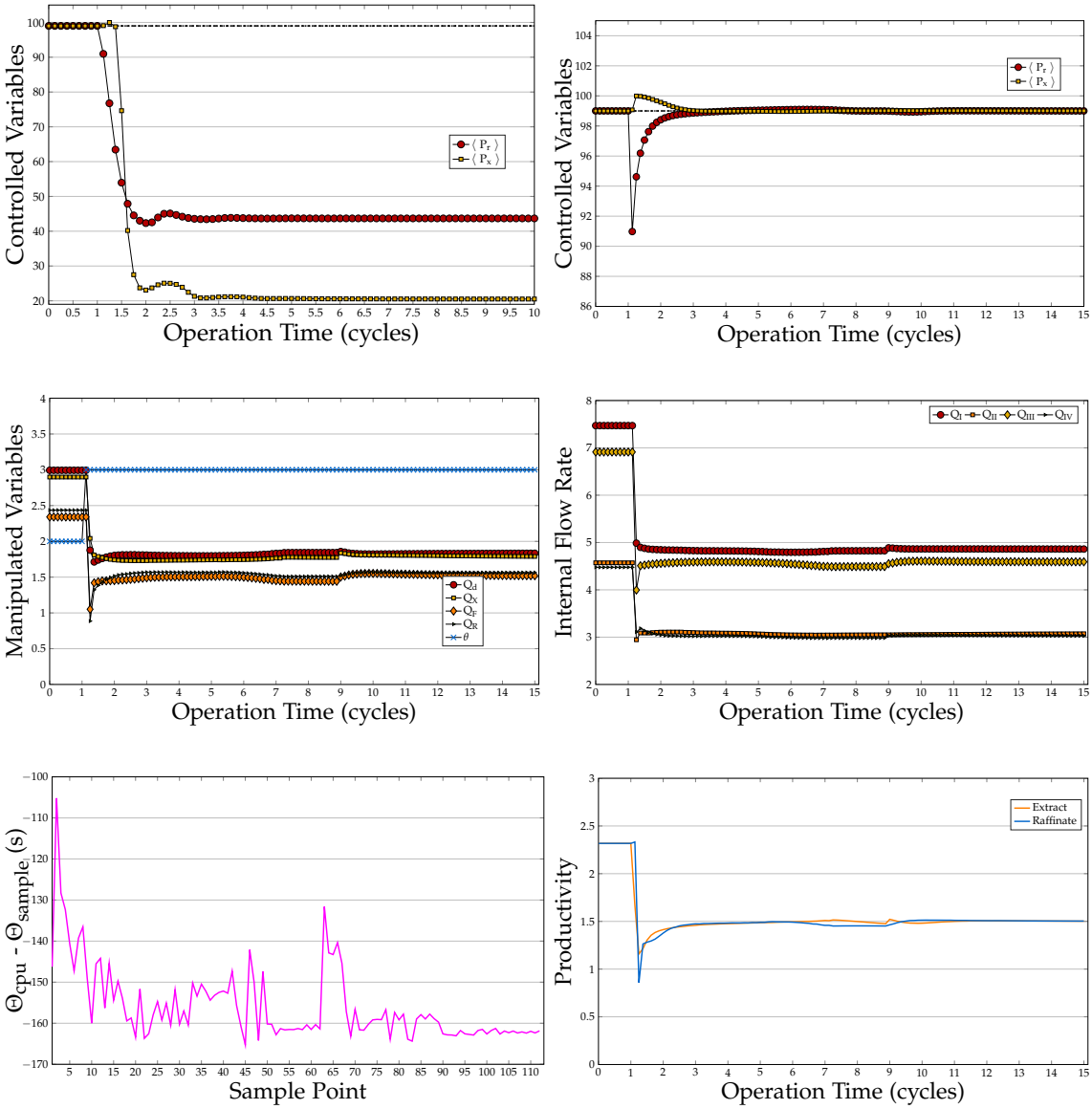

Figure C.1: Compilation of results for a perturbation of +50% in the switching valve.

Raffinate pump malfunction -20%

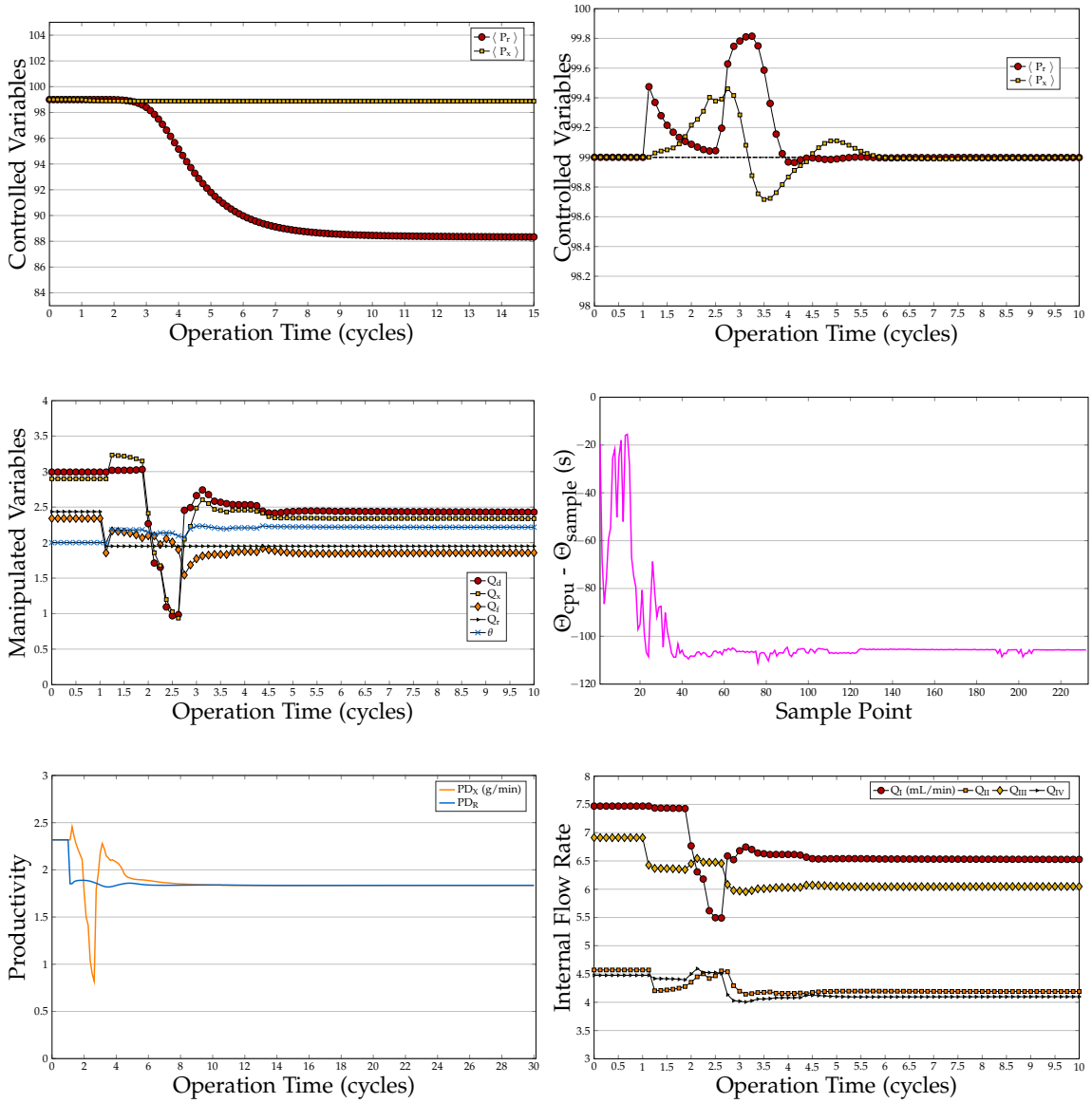

Figure C.2: Compilation of results for a perturbation of -20% in the raffinate pump.

Extract pump malfunction -20%

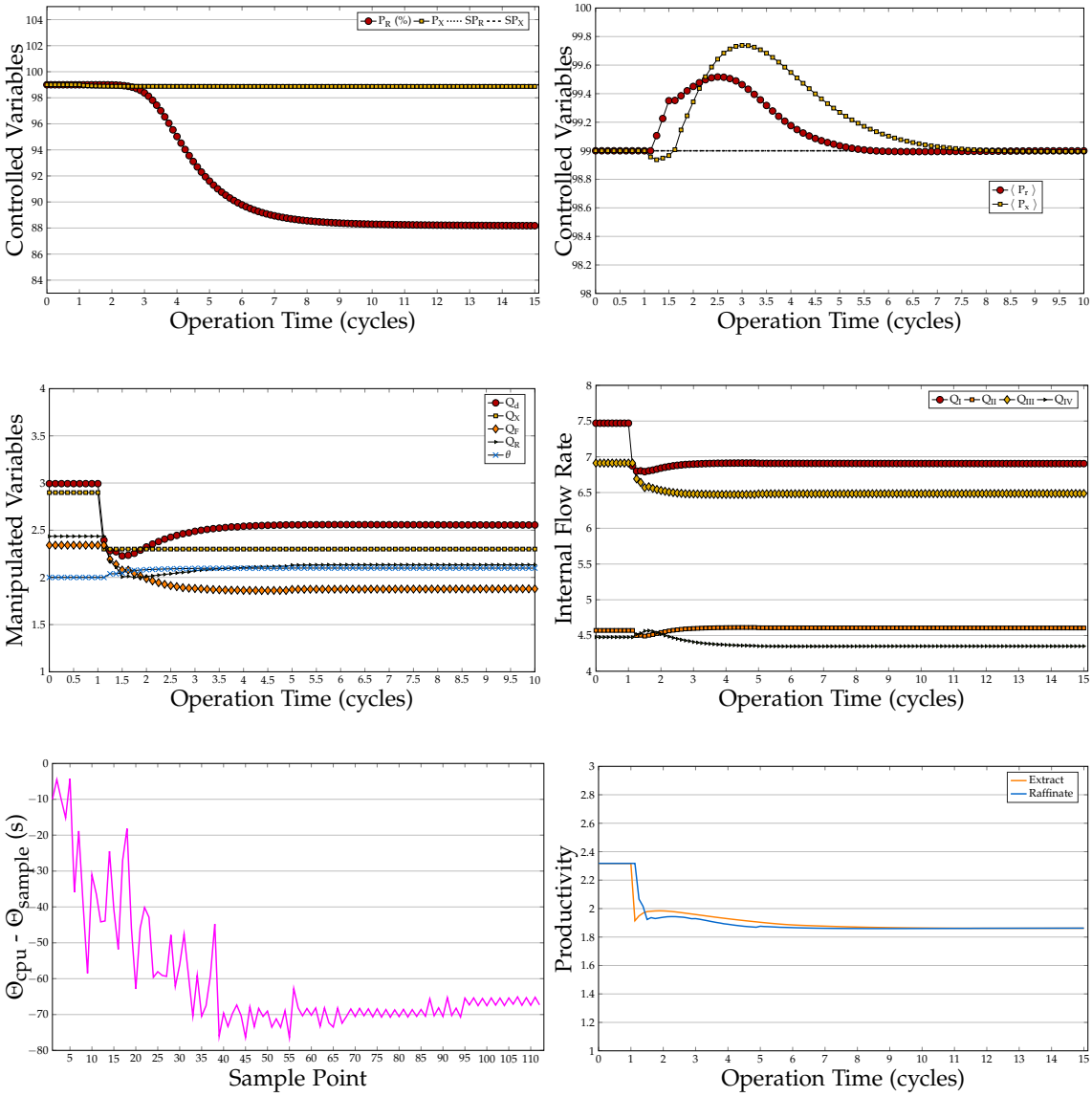

Figure C.3: Compilation of results for a perturbation of -20% in the extract pump.